COPPE
Instituto Alberto Luiz Coimbra de
Pós-Graduação e Pesquisa de Engenharia
UFRJ

INTEGRATED PRODUCTION MODELING TO ASSESS THE EFFECT OF SUBSEA WATER SEPARATION

Yuxi Wang

Tese de Doutorado apresentada ao Programa de Pós-graduação em Engenharia Oceânica, COPPE, da Universidade Federal do Rio de Janeiro, como parte dos requisitos necessários à obtenção do título de Doutor em Engenharia Oceânica.

Orientadores: Segen Farid Estefen
Marcelo Igor Lourenço de Souza

Rio de Janeiro
Novembro de 2019

INTEGRATED PRODUCTION MODELING TO ASSESS THE EFFECT OF SUBSEA WATER SEPARATION

Yuxi Wang

TESE SUBMETIDA AO CORPO DOCENTE DO INSTITUTO ALBERTO LUIZ COIMBRA DE PÓS-GRADUAÇÃO E PESQUISA DE ENGENHARIA (COPPE) DA UNIVERSIDADE FEDERAL DO RIO DE JANEIRO COMO PARTE DOS REQUISITOS NECESSÁRIOS PARA A OBTENÇÃO DO GRAU DE DOUTOR EM CIÊNCIAS EM ENGENHARIA OCEÂNICA.

Orientadores: Segen Farid Estefen
Marcelo Igor Lourenço de Souza

Aprovada por: Prof. Segen Farid Estefen
Prof. Ilson Paranhos Pasqualino
Prof. Celso Kazuyuki Morooka
Prof. José Luis Drummond Alves
Prof. Virgílio José Martins Ferreira Filho

RIO DE JANEIRO, RJ – BRASIL
NOVEMBRO DE 2019

Wang, Yuxi

Integrated Production Modeling to Assess the Effect of Subsea Water Separation/Yuxi Wang. – Rio de Janeiro: UFRJ/COPPE, 2019.

XX, 122 p.: il.; 29, 7cm.

Orientadores: Segen Farid Estefen

Marcelo Igor Lourenço de Souza

Tese (doutorado) – UFRJ/COPPE/Programa de Engenharia Oceânica, 2019.

Referência Bibliográfica: p. 103 – 114.

1. Integrated Production Modeling. 2. Subsea Water Separation. I. Estefen, Segen Farid *et al.* II. Universidade Federal do Rio de Janeiro, COPPE, Programa de Engenharia Oceânica. III. Título.

Dedico este trabalho a todos
aqueles que contribuíram para
minha formação acadêmica

Agradecimentos

First and foremost, I would like to extend my heartfelt gratitude to my supervisor, Professor Segen Farid Estefen, for his patience, critical suggestions, and constant encouragement. His endless passion and enthusiasm both on research and in daily life have inspired me to overcome every difficulty encountered along the way to successfully complete the doctoral study, as well as this thesis.

I would also like to express my sincere gratitude to Professor Marcelo Igor Lourenço de Souza, for his precious comments and help in many aspects of my study and research.

My wholehearted thanks also go to my friend and mentor Hong Cheng. I learned from his kindness, rational thinking, hard working, and problem-solving attitude, and I sincerely thank his encouragement, companionship, unconditional support, and unreserved help during the past 11 years.

Special thanks to Mr. Fidel Vladimir Chuchuca Aguilar, whose love and encouragement initiated this adventure. Special thanks to Professor Carlos Antonio Levi, whose conscientious academic spirit, kind encouragement during the course and every warm greeting are highly appreciated. I would also thank everyone that has lent their help, directly or indirectly, during my stay in Rio de Janeiro.

Finally, I am indebted to my parents for their trust and support in this long journey.

Resumo da Tese apresentada à COPPE/UFRJ como parte dos requisitos necessários para a obtenção do grau de Doutor em Ciências (D.Sc.)

MODELAGEM INTEGRADA DE PRODUÇÃO PARA AVALIAR O EFEITO DA SEPARAÇÃO SUBMARINA DE ÁGUA

Yuxi Wang

Novembro/2019

Orientadores: Segen Farid Estefen
Marcelo Igor Lourenço de Souza

Programa: Engenharia Oceânica

O processo convencional de projeto para o desenvolvimento de campos petrolíferos é baseado nos trabalhos isolados do departamento de reservatório e do departamento de engenharia de produção. Simulações realizadas separando o reservatório e o sistema de produção não podem capturar a interação entre as duas disciplinas. Particularmente, no desenvolvimento offshore, é imperativo integrar os dois domínios de engenharia na qualificação do potencial de uma nova tecnologia submarina porque qualquer novo elemento adicionado à arquitetura submarina afetará o desempenho de todo o sistema.

Apresenta-se, nesta tese, quatro modelos integrados de produção, dois dos quais são modelos totalmente implicitamente integrados, enquanto os outros dois são simulações acopladas entre um simulador de reservatório e um simulador de escoamento na rede de pipelines. Exemplos numéricos mostram que, em comparação com simulações fracamente acopladas, modelos de integração implícita são geralmente favoráveis em termos de tempo e estabilidade de computação.

Três estudos de caso demonstram a aplicação dos dois modelos implicitamente integrados para avaliar o efeito da separação submarina da água em três indicadores quantitativos: valor presente líquido, recuperação de óleo e índice parafina-livre. Os resultados mostram que a separação submarina da água tem o potencial de aumentar o valor presente líquido e a recuperação para um sistema de poços em cluster. Porém, sua aplicação em poços satélites tem vantagens limitadas devido à interferência negativa entre todos os poços no campo. Além disso, ao aplicar a separação submarina da água, haverá um risco de deposição de parafina maior para um sistema de poços satélites do que para um sistema de poços clusterizados.

Abstract of Thesis presented to COPPE/UFRJ as a partial fulfillment of the requirements for the degree of Doctor of Science (D.Sc.)

INTEGRATED PRODUCTION MODELING TO ASSESS THE EFFECT OF SUBSEA WATER SEPARATION

Yuxi Wang

November/2019

Advisors: Segen Farid Estefen
Marcelo Igor Lourenço de Souza

Department: Ocean Engineering

Conventional field development design and planning based on isolated work from the reservoir and the production engineering department can not capture the interaction between the two disciplines for long term production forecast. Particularly, in offshore development, it is imperative to integrate the two engineering domains in the qualification of a potential subsea technology because any new element added into the subsea architecture will impact the performance of the entire system. This thesis establishes models that integrate the reservoir and the subsea production system as a whole. The integrated approach is then applied to quantify the effect of a specific subsea technology: subsea water separation.

In this work, four integrated production models are presented and compared. Two of them are fully implicitly integrated models while the other two are coupled simulations between a reservoir simulator and a pipeline simulator. Numerical examples show that, compared to loosely-coupled simulations, implicitly integrated models are in general favorable in terms of computation time and stability.

Three case studies are presented to demonstrate the application of the two implicitly integrated models for evaluating the effect of subsea water separation on three quantitative indicators: NPV, recovery rate, and wax-free index. Results show that subsea water separation has the potential to increase NPV and recovery for a clustered well system by increasing production rates and reducing injection requirements. However, its application on individual satellite producers has limited advantages because of the negative interference among wells. What's more, when applying subsea water separation, there will be a higher risk of wax deposition for a satellite well system than for a clustered well system.

Contents

List of Figures

List of Tables

Nomenclature

Acronyms

AOF	absolute open-flow, page 40
CFD	computational fluid dynamics, page 16
DOF	digital oil field, page 2
EOR	enhanced oil recovery, page 10
ESP	electric submersible pump, page 13
FPS	floating production and storage, page 10
FPSO	floating, production, storage and offloading, page 48
GOR	gas oil ratio, page 18
HCPV	hydrocarbon pore volume, page 31
IAM	integrated asset modeling, page 2
ICV	inflow control valve, page 11
IFAM	integrated flow assurance modeling, page 20
IOR	improved oil recovery, page 14
IPM	integrated production modeling, page 2
IPR	inflow performance relationship, page 40
IPTC	International Petroleum Technology Conference, page 9
MPI	message passing interface, page 20
MRST	MATLAB reservoir simulation toolbox, page 3
NPV	net present value, page 3

OOIP	original oil in-place, page 75
OTC	Offshore Technology Conference, page 9
PDE	partial differential equation, page 53
PVM	parallel virtual machine, page 8
SSAO	separador submarino de água e óleo, page 16
SSBI	subsea separation, boosting and injection, page 14
SSWS	subsea water separation, page 4
VASPS	vertical annular separation and pumping system, page 13
VOF	volume of fluid, page 26

Greek Symbols

α	phase volume fraction, page 25
$\bar{\bar{\tau}}$	stress-strain tensor, page 25
κ	thermal conductivity, page 24
λ	friction factor, page 24
μ	fluid viscosity, page 33
ϕ	porosity, page 34
ψ	liquid holdup correction factor, page 37
θ	pipe inclination angle respecting to the horizontal line, page 37
ε	convergence criterion, page 30
Θ	source term, page 24

Roman Symbols

b_{g}	reciprocal of gas formation volume factor, page 32
b_{o}	reciprocal of oil formation volume factor, page 32
b_{w}	reciprocal of water formation volume factor, page 32
c_p	specific heat, page 38

c_r rock compressibility factor, page 32

e kinetic energy per unit mass, page 24

e^* total energy per unit mass, page 24

f_{g} inflow gas fraction, page 48

f_{w} inflow water fraction, page 48

h enthalpy per unit mass, page 24

h^* total enthalpy per unit mass, page 24

i internal energy per unit mass, page 24

k absolute, specific, or intrinsic permeability, page 32

k_{rg} gas relative permeability, page 33

k_{ro} oil relative permeability, page 33

k_{rw} water relative permeability, page 33

m ratio between initial gas cap and initial oil volume, page 32

q_{g} gas underground production rate (volumetric flow rate), page 32

q_{o} oil underground production rate (volumetric flow rate), page 32

q_{w} water underground production rate (volumetric flow rate), page 32

$q_{N\mathrm{g}}$ gas production rate under standard condition in the pipeline network, page 47

$q_{N\mathrm{o}}$ oil production rate under standard condition in the pipeline network, page 47

$q_{N\mathrm{w}}$ water production rate under standard condition in the pipeline network, page 47

$q_{W\mathrm{g}}$ gas production rate under standard condition in wells, page 54

$q_{W\mathrm{o}}$ oil production rate under standard condition in wells, page 54

$q_{W\mathrm{w}}$ water production rate under standard condition in wells, page 54

w mass flow rate, page 38

x gas, oil, or water phase, page 33

B_{g} gas formation volume factor, page 32

B_{o} oil formation volume factor, page 32

B_{w} water formation volume factor, page 32

D pipe internal diameter, page 36

E_l non-slip liquid holdup, page 37

G_m mixture mass flux rate, page 36

G_p cumulative production of gas, page 32

H reservoir effective thickness, page 40

H_l liquid holdup, page 36

J productivity index, page 40

L axial direction in one-dimensional pipe flow, page 34

N initial oil in place, stb, page 32

N_p cumulative production of oil, stb, page 32

N_{Fr} Froude number, page 37

P_{cgo} capillary pressure between gas and oil, page 33

P_{cow} capillary pressure between oil and water, page 33

P_{i} initial reservoir pressure, page 31

P_r reservoir pressure, page 31

P_{wf} bottomhole pressure, page 40

Q_{inj} maximum field water injection rate, page 79

$Q_{\mathrm{o\,max}}$ maximum field oil production rate, page 79

$Q_{\mathrm{w\,max}}$ maximum field water production rate, page 79

$Q_{\mathrm{w}t\,\mathrm{max}}$ maximum topside water production rate, page 79

R_p cumulative production gas-oil ratio, page 32

R_s solution gas oil ratio, page 32

R_{si} solution gas oil ratio under initial reservoir pressure, page 32

S_g gas saturation, page 32

S_{oi} initial oil saturation, page 81

S_o oil saturation, page 32

S_{wc} connate water saturation, page 32

S_w water saturation, page 32

T fluid temperature, page 38

T_{amb} ambient temperature, page 38

U overall heat-transfer coefficient, page 38

W_i cumulative injection of water, stb, page 32

W_p cumulative production of water, stb, page 32

$\mathcal{I}$ set of all the paths, page 47

$\mathcal{I}_{in}$ set of inlet paths, page 48

$\mathcal{N}_{in}$ set of inlet nodes, page 48

$\mathcal{N}_{nn}$ set of internal nodes, page 47

$\mathcal{N}_{out}$ set of outlet nodes, page 48

$\mathcal{S}_i$ set of segments in path i, page 47

$\mathcal{U}_n$ set of inlet and outlet path pairs at node n, page 47

$A^{n,i}$ $A^{n,i} = 1$ if node n is the inlet of path i; $A^{n,i} = -1$ if node n is the outlet of path i; $A^{n,i} = 0$ if node n is not connected with path i, page 47

$F_g^{n,j}$ the fraction of gas flowing into path j at node n, page 47

$F_o^{n,j}$ the fraction of oil flowing into path j at node n, page 47

$F_w^{n,j}$ the fraction of water flowing into path j at node n, page 47

Chapter 1

Introduction

1.1 Motivation

Traditionally, modeling of the reservoir and the production network has been isolated and predictions are performed in each domain with estimated boundary conditions such as wellhead pressure. It has been well recognized that this traditional approach which separates the two intrinsically interacting domains fails to provide reliable rates and pressure variations for long term production planning and may lead to suboptimal solutions in a production optimization task. Actually, any change in one domain influences the performance of the other, as well as the whole system. Therefore, integrated production modeling, which incorporates the reservoir and the production network in a single model, sets the foundation for more reliable predictions of the entire system, especially in the offshore context where different subsea architectures lay different controls on the reservoir and consequentially affect both the technical and economical feasibility of a project. In this work, different integrated production modeling techniques will be applied and compared serving as a basis for further applications of this approach.

Subsea water separation pilot test dates back to the Troll C pilot in the North Sea, in 2001. Discussions on this subsea technology have been active in the past years. One of the initial drivers for the research and development of this subsea equipment is to improve oil recovery for mature offshore fields. It bears the expectation of increasing production rate by lowering down back pressure on production wells and prolong the production life by debottlenecking topside water processing capacity. It may also reduce the risk of hydrate, scaling, and corrosion in terms of flow assurance. However, the high heat capacity of water keeps the fluid with higher temperature, reducing the risk of wax deposition and blockage in the flowlines. Also, for reservoirs developed under water injection, while lower back pressure impels higher production rates, injection rates may also need to be increased to balance out the

underground withdrawal. The combined effect of this subsea technology on the exploitation activity along the field life should be studied looking at the whole picture to determine whether it worths the credit. Applying the integrated production modeling approach, this study provides a more comprehensive understanding of the potential benefits and problems that subsea water separation may bring about.

1.2 Objective

The general objective of this study is to establish integrated production models that combine the reservoir and the production network as a whole and to apply this approach to quantify the effect of subsea water separation along the entire production life.

1.3 Scope of the study and methodology

The core concept behind this study is system analysis. A system is an entity with interrelated and interdependent parts. Changing one part of the system affects other parts as well as the whole system. The successful modeling of a complex system relies a lot on the development of computer technology. In the oil and gas industry, terms like integrated production modeling (IPM) and integrated asset modeling (IAM), together with the concept of digital oil field (DOF), started to gaining popularity after stepping into the 21st century. An IAM comprises a coupled system of reservoir simulation models with surface facility network models and perhaps other models, such as process facility and economics models, if available. At a minimum, models of the reservoir and production system, up to a separator, should be included so that the separator becomes a valid pressure boundary for the system. For this minimum version of IAM, the term IPM is more appropriate since the focus is more on production issues. In the offshore context, an integrated production system should couple the simulation from the reservoir through all the subsea infrastructures to the topside.

This study claims itself as IPM since modeling for the process plants is not considered. In consistency with the objective of the study, the scope of IPM is further narrowed down in two aspects: the components included and the purpose of modeling, described as follows.

First, the integrated production system in this work involves two subsystems, or two domains: the *reservoir domain*, which follows equations governing multiphase flow through porous media, and the *pipeline network domain*, which models multiphase flow in wellbores and pipelines, and through manifolds and subsea separators. Some subsea in-line devices and facilities, such as chokes and pumps, are currently

not included in the network model in order to eliminate distractions from these components when evaluating the effect of subsea water separation. However, the established programming framework is free to include these components in future studies. Net present value (NPV) calculations will be performed when assessing the effect of subsea water separation.

Second, in terms of the analysis of integrated systems, at least three kinds of system solutions are often pursued by engineers in industrial activities: *history matching*, *production prediction*, and *production optimization*. History matching is a quality control process usually carried out before any prediction or optimization task. It involves adjustment of model parameters to achieve minimum difference between model solution and the reference history, which is essentially an optimization problem with a least-square objective. In the production prediction mode, model solution is acquired under given operation parameters and boundary conditions, which involves the solution of equations that describe the system behavior. Production optimization is a higher level task than solely production prediction. In production optimization, operational components of the system, including boundary conditions and equipment operating parameters, are not fixed input, but variables with certain bounds or constraints. It is undoubted that production optimization should be built upon a sound and efficient production prediction model. Therefore, this thesis will focus on integrated production modeling for production prediction purpose rather than an aggressive pursue in higher level optimization task, although the established integrated model is inherently the base for production optimization and it is possible to reconstruct the problem with appropriate constraints to perform corresponding optimizations in the future.

Numerical simulation is the main method applied in integrated production modeling. In this study, mathematical equations and their solutions are programmed in MATLAB environment for implicit integration between a reservoir model and a network model. Data and different software are also processed and controlled through MATLAB scripts, such as the coupled simulations between the reservoir simulator MRST and the pipeline network simulator OLGA. The programs follow the object-oriented programming paradigm. Automatic differentiation is the main contributor in the linearization of nonlinear equations.

1.4 Anticipated contributions

In the thesis, four integrated production models with different coupling techniques and different levels of complexity will be presented and compared. The difference in production behavior with and without the application of subsea water separation will be demonstrated by case studies. A workflow for quantifying the effect of

subsea water separation will be established, which will enable feasibility assessment of this subsea processing technology for a given offshore field. Thus, the following contributions are expected through the study of the topic:

1. **A simple and a fully implicit integrated production model** applying the established network model named "NET", where both pressure and temperature calculations are considered.

2. **Automatic modeling and data processing** in NET and simulator OLGA, which enables automatic comparison among explicit, partially-implicit and fully-implicit modeling schemes.

3. **Quantitative assessment** of the effect of subsea water separation (SSWS) on NPV, oil recovery, and wax-free index, for different subsea configurations applying the IPM approach.

4. **A workflow for the estimation of the break-even price** for a new subsea technology to help make investment decisions.

1.5 Work organization

This thesis consists of two major parts:

1. development of IPM tools with four different approaches

2. application of IPM on evaluating the effect of subsea water separation

The main structure of the thesis is depicted in Figure 1.1 and the content of each chapter is briefly introduced below.

Chapter 1 presents the motivation and objective of the thesis, as well as the research scope and anticipated results.

Chapter 2 reviews the development and application of integrated production modeling and the current status of subsea water separation technology.

Chapter 3 gives the fundamental theorems and equations used in building the integrated production models, including the modeling in the reservoir domain and in the network domain, as well as coupling techniques.

Chapter 4 describes the discretization in the network domain and for the reservoir equations, followed by two fully integrated production models. One with simplified reservoir representation based on a zero-dimensional tank model. The other with a full-field three-dimensional reservoir model.

Chapter 5 describes both explicit and partially-implicit coupling between an open-source full-field reservoir simulator MRST, and a pipeline network simulator

OLGA. At the end of this chapter, comparison among explicit, partially-implicit and fully-implicit schemes is discussed.

Chapter 6 presents the application of fully integrated production models in quantifying the effect of subsea water separation. Three case studies are included to demonstrate the model application in different subsea configurations.

Chapter 7 lists the main conclusions and future work.

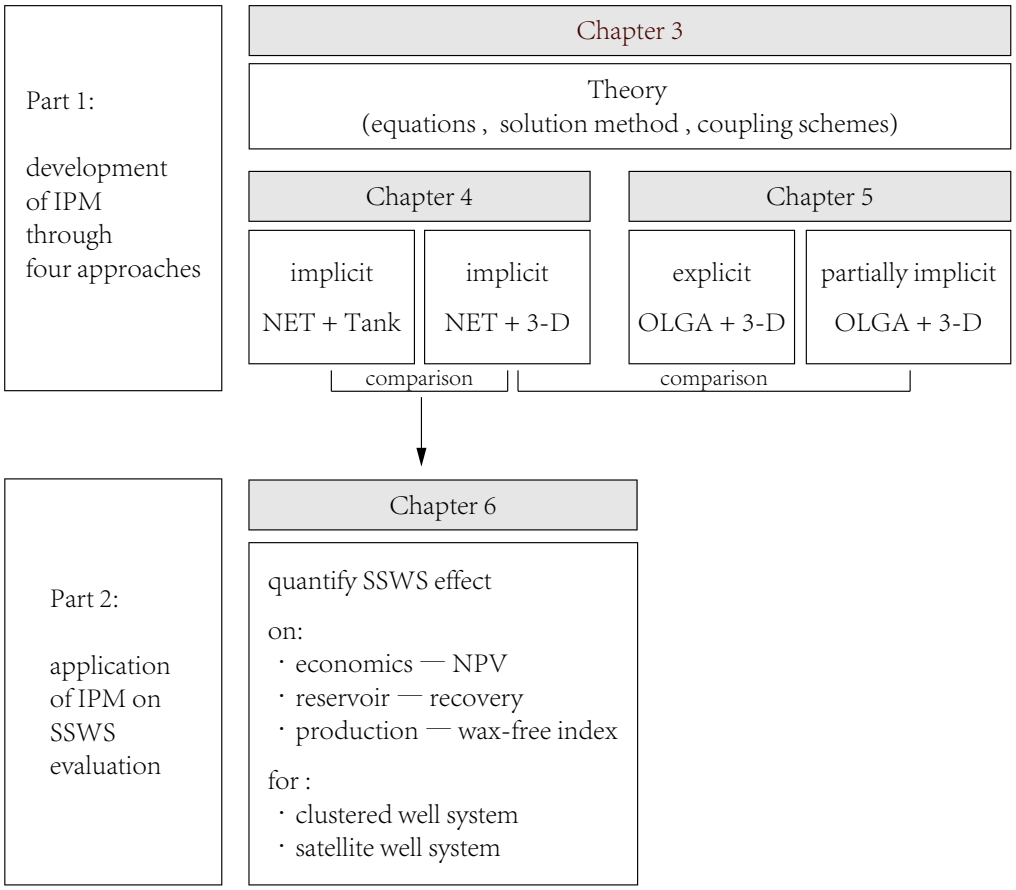

Figure 1.1: Thesis structure and relationships between the main chapters.

Chapter 2

Literature Review

2.1 Integrated production modeling (IPM)

Traditionally, reservoir engineers and production engineers perform isolated designs for the development of oil and gas fields. The reservoir models are executed in a stand-alone mode and results are passed to the production network models to see feasibility to manage the production in the optimum. The results from the network are then passed-on to facilities model to verify against available capacity [1].

In these stand-alone reservoir models, flow within the reservoir and between the reservoir and the wellbore, is decoupled from the rest of the production and injection facilities. This setup is sufficient for a history matching purpose. However, it is less accurate in prediction mode when hydraulic calculations are necessary to reflect the flow characteristics in pipeline network and facilities. What's more, when it comes to production optimization under all kinds of network and facility constraints, the results from conventional stand-alone reservoir models are prone to less realistic production predictions, which lead to suboptimal solutions when the network and facilities are present.

On the other hand, flow assurance engineers employ production profiles of early, mid and late field life to design surface networks. These production profiles may be obtained from reservoir simulations or simply estimated with uncertainty. This approach relies heavily on the assumption that these production profiles are reliable and in most cases the engineer does not contest how these profiles were obtained. However, production forecasted from stand-alone reservoir simulations using a bottomhole pressure constraint, for example, is highly inaccurate in the deep water area, or when many wells share the same surface network. Under these circumstances, rate-dependent back pressure lead to great variations on bottomhole pressure along the field life, making the production profiles generated from constant bottomhole pressure controlled reservoir simulations inaccurate for production network design.

OKAFOR [2] addressed the significance of integrated modeling for flow assurance engineers leading to savings of millions of dollars by reducing mis-design such as oversized or undersized pipelines and facilities.

The shortcoming of the above-mentioned conventional workflow is a reflection of one of the biggest challenges met by most industry, not only the oil and gas sector, the unautomation in data process [3]. Excessive use of human labor in exchanging information back and forth among different departments leads to errors and low efficiency. Integrating interdisciplinary knowledge into a shared system is one of the base transformations that need to be done for more efficient field management. With the rapid development of computer technology, faster and more complex simulations became realizable. After stepping into the 21st century, terms like integrated production modeling and integrated asset modeling started to be recognized, together with the popular concept of digital oil field [4].

An IAM comprises a coupled system of reservoir simulation models with surface facility network models and perhaps other models, such as process facility and economics models, if available [5]. At a minimum, models of the reservoir and production system, up to a separator, should be included so that the separator becomes a valid pressure boundary for the system. For this minimum version of IAM, the term IPM is more appropriate since the focus is more on production rates. More and more companies are becoming aware of the important role of integrated modeling approach, especially in the offshore sector, where both complex subsea architecture and high capital cost are involved. Simulation of the whole integrated system enables the communication among multi-disciplines and realizes oil and gas field management in a more effective and integral way.

The significance of integrated production modeling, or integrated asset modeling, has been addressed again and again by world-class oil and gas companies [6–8]. Some key benefits and value gains of the integrated approach include:

1. more accurate and reliable short-term/long-term production forecasts by having the reservoir, surface network, and process models integrated.

2. more realistic and proactive optimizations of the system taking all the reservoir, network and facilities constraints into consideration, which ensures asset integrity by operating in safe envelopes.

3. more effective decision making by breaking down the barrier between different departments and involving people from reservoir, production and process engineering.

2.1.1 History of IPM

Beginning with the pioneering work of DEMPSEY *et al.* [9], where a coupled gas–water two-phase system for gas field deliverability analysis was first presented, many researchers and companies pursued the integration between reservoir and pipeline network for gas field application in the last two decades of the 1900s. Chevron [10–12] firstly extended the application for oil field development. Since then, several major companies, such as Shell [13, 14] and BP [15, 16], began to develop their proprietary integrated reservoir/surface solution, and/or have integrated their proprietary reservoir simulator with a commercial network software. Researchers also developed acceleration techniques to improve computation efficiencies [17–19].

With the emergence of message passing libraries like parallel virtual machine (PVM), explicitly coupling two commercial software through an interface becomes efficient. HEPGULER *et al.* [20] coupled the reservoir simulator ECLIPSE with the network simulator and optimizer NETOPT at the timestep level using PVM interface, where the network simulator acted as the master program sending and receiving messages. TRICK [21] coupled the reservoir simulator ECLIPSE to a surface model called FORGAS for gas deliverability forcasting at the iteration level.

Petroleum Experts (PETEX) released its first commercial IPM suit in the year 2006. After several years, it got a consolidate share in the market and has been adopted as a corporate standard by some major international companies. It is from then a bloom of publications on utilizing IPM tools for field design and management is witnessed [22–32]. The IPM suite from PETEX provides the users with both a material balance toolkit for reservoir modeling called MBAL and a full-field numerical reservoir modeling tool called REVEAL. It also includes a module named PROSPER for well modeling and nodal analysis, and a multiphase network modeling and optimization module called GAP. An interface called RESOLVE provides explicit coupling between the reservoir and the network simulators.

The IAM tool *Maximus*™[33] from FEESA Ltd. (acquired by KBC, a wholly-owned subsidiary of Yokogawa Electric Corporation, in the year 2014) highlights its ability in flow assurance analysis in the pipeline network domain so that the description of reservoir dynamics is simplified by modeling the reservoir as a tank or from a lookup table. The IAM tool emphasizes its rigorous thermal-hydraulic calculation for flows through wells, flowlines, and risers with physical properties and phase behaviors modeled using accurate black oil and compositional methods without the need for introducing simplifying assumptions, such as PVT lookup tables.

The surface–subsurface integrated next-generation reservoir simulator *Nexus*®Suite from Landmark (a Halliburton business line) applies the fully-

implicit method in solving the surface facilities and the reservoir, which provides a rigorous solution of the compositional properties, and offers benefit of larger and more stable timesteps [34, 35].

2.1.2 IPM applications and lessons learned

There is a growing trend in the oil and gas industry to apply integrated reservoir/network models in field planning, forecasting, surveillance, and optimization. Many field application cases are reported in international conferences every year, such as the International Petroleum Technology Conference (IPTC), Offshore Technology Conference (OTC), etc. Some of them employ commercial software, while others have been active in developing proprietary software packages. This section reviews the applications of IPM in various situations.

Firstly, comparative studies between IPM and stand-alone simulation reveal that there are large differences in production rates and it is the accuracy of the boundary condition that affects the gap between an integrated model and a stand-alone one. HATVIK *et al.* [36] compared the performance of three types of models, a stand-alone dynamic reservoir model, a stand-alone flow network model, and a fully coupled reservoir-network model. The dynamic reservoir model was run on its own without taking into account pressure drop in the production system, which over-predicts or underpredicts the recovery in accordance with the boundary condition settings. The stand-alone network model used the production profile generated from the reservoir model and cuts back production rate when lifting pressure is not sufficient. The more cut-backs, the more under-prediction of recovery is observed. Only the fully coupled simulation model reflects the integrated behavior of the whole system, which reduces the uncertainty of the forecast in early phase. Nevertheless, while the integrated approach acts as a cement between different disciplines to ensure consistency between production profiles and base of design, it does not mean to substitute the detailed engineering studies performed by the different departments. Many more advanced stand-alone studies are still needed to be performed to further assess specific technical points [37].

An IPM tool is especially advantageous in production prediction and/or optimization for offshore developments where multiple fields/reservoirs/wells with different properties are connected to a shared production/injection system. ARIAS *et al.* [22] reported applying the IPM suite in evaluating the possibility of reconfiguring a Gulf of Mexico offshore field named Na Kika, to stimulate production from the subfield Kepler whose production was suppressed by the high back pressure from its shared flowline loop with another field called Arial. With the help of IAM, the operability and flow assurance risks involved with the reconfiguration were evalu-

ated, and an incremental production gain of 5% with a cumulative production gain of nearly 2 million barrels oil equivalent in the sequent two years are predicted and validated. MARIR *et al.* [38] presented the application of IPM on a green field located in offshore Abu Dhabi, which is currently being developed by combining the production from six distinct carbonate reservoirs. The fully integrated model provides value in gas recycling optimization and management, avoiding the tedious iterative approach used previously. SIFUENTES *et al.* [1] reported the application of IAM on selecting and evaluating enhanced oil recovery (EOR) strategies for the 35-year-old Samarang field located offshore Sabah, Malaysia, which involves fifteen stacked sandstone sequences with different levels of aquifer suppports and pressure decline trends. Under the IAM framework, more accurate and reliable forecasts are obtained, and increased collaboration and reduced communication time between different disciplines are achieved to enhance the decision-making process from an integrated management perspective. ALAIGBA *et al.* [30] reported using the IPM suite to predict full-field performance of the Duke field, a condensate field in the gulf of Guinea, offshore Nigeria, under different scenarios. It integrates the five developed Duke reservoirs (modeled with MBAL), wells and subsea network to optimize water injection allocation with the objective of achieving the highest net present value for the whole field. [39] and [40] reported applying the implicitly coupled simulation model developed in reservoir simulator Nexus to provide more accurate forecasts by consistently allocating injection volumes to two subfields located offshore Abu Dhabi, which will serve in identifying necessary network upgrades to accommodate the long-term development plan. GONG *et al.* [32] reported the application of IPM in the Who Dat field, located in Mississippi Canyon under 3,100 ft of water. The field consists of 11 productive horizons, 26 reservoirs, and is developed by one privately owned semisubmersible FPS. The history-matched IPM model is used to assist field development planning, including the optimization of production rate, definition of new drilling, water flood and artificial lift method.

When it comes to concept selection for a green field development, an IPM study helps the operator identify project potential and feasibility in synergy with surrounding assets. Deepwater satellites are usually marginal fields that may not produce enough net income to make it worth developing and requires careful development design to unlock their potentials. MARMIER *et al.* [41] reported the application of IPM on unlocking three sandstone marginal deepwater fields development at the conceptual selection phase, where three development concepts are evaluated, namely a short tie-back, a long tie-back, and a stand-alone development of the three fields. The use of an integrated model allows comparing the production profiles of the different development concepts while ensuring consistent implementation and computation of constraints. The final selection of development concepts is a compromise

between costs and total production. Results show that a stand-alone concept has the highest production per well as the equipment would be sized to fit the field's potential, but at the highest cost per barrel due to high cost on the new production facilities. The short tie-back concept shows the lowest production per well but also the lowest cost per barrel, making it an attractive solution.

The IPM approach also provides a more comprehensive way in evaluating performance of new technologies. Reference [42] reported the way to model intelligent wells by an IPM tool, where the impact of intelligent control components, such as inflow control valves (ICVs), is essential in evaluating well performance. The approach involves the combination of well inflow performance from MBAL, stand-alone well models built in PROSPER and the intelligent components modeled in GAP. In terms of the application of IPM in evaluating subsea separation performance, COSTA *et al.* [43] presented a relevant work of Total where the working envelope of their gas–liquid two-phase subsea separator in Pazflor project was studied by coupling a pipeline multiphase flow dynamic software OLGA with a process dynamic software D-SPICE. It was a first to apply coupled simulation to investigate the effect of subsea separation in the production system. But the approach didn't go down to the reservoir level. Another work [44] applied the IPM suite to evaluate the possible advantages of using subsea gas–liquid separation as the main artificial lift method for a reservoir in Brazil, in comparison with conventional gas lift method. Their study gave a positive answer to the increment of oil production by gas–liquid separation. GALVAN *et al.* [45] applied IPM to forecast production rates together with fluid properties across the whole production system in Perdido project, where two-phase caisson separator is applied. However, the evaluation of subsea water separation by IPM has not yet been found in the literature.

2.2 Subsea water separation

Water injection has long been used as a means of improving the recovery of oil in both onshore and offshore fields. Injecting water into the reservoir maintains reservoir pressure and sweeps oil towards the producers. As reservoirs mature, continuing producing oil out of the reservoirs entails more water production as well, which affects the economics of field exploitation activities in a number of areas like corrosion, crude quality, disposal, separation, and metering. Oil and gas companies must view water as a strategic component of their value chain. [46]

2.2.1 Technology drivers and expected earns

One of the challenges posed by subsea production is how to reduce wellhead pressure to allow effective recovery of hydrocarbon resources. Subsea water separation became a possible option for fields facing high water cut in late production life. Optimists commonly state that subsea water separation is a promising technology for deepwater development as it is able to increase production rate by lowering down back pressure on production wells, to prolong the production life by debottlenecking topside water processing capacity, and to reduce the risk of hydrate, scaling and corrosion [47–49]. However, there are also voices doubting each of the mentioned expected earns and other related issues, such as emulsion, sand production, and separated water treatment [50].

Subsea separation has been applied in all the four major global offshore oil and gas clusters: the North Sea, Gulf of Mexico, West Africa deepwater and Brazilian pre-salt [51]. Large oil and gas companies, including Shell, Statoil (Equinor), Total, and Petrobras, are active in the campaign for developing new subsea processing technologies and each of them has applied subsea separation, two-phase or three-phase, to enable economic development of deeper offshore green fields, or to extend production life of brownfields and improve oil recovery.

Subsea water separation VS. subsea gas–liquid separation

The competition between subsea water separation and subsea gas–liquid separation is essentially wrestling between subsea separation technology and subsea boosting technology. The primary problem faced by subsea boosting is the gas volume at the suck-in of a subsea pump. One reasonable and immediate solution is to separate gas from the liquid phase and then boost only the liquid phase. However, the drawback of separating gas out of oil is to increase fluid density and viscosity which may overuse the pump. On the contrary, if water, the heaviest phase in the fluid stream, is separated from the hydrocarbon phase, lower lifting pressure is required which may even cut off the need for subsea boosting.

A short summary of commercial installations of different subsea separation projects are provided in Tables 2.1 to 2.3.

Table 2.1: Summary of commercial installations of subsea separation stations

System	Project	Type	Mechanism	Weight	Size	Capacity
gas–liquid separation	Perdido	caisson	cyclone	169 t	D=35 in, L=100 m	25,000 bopd
	Pazflor	vertical	gravity	870 t	D=3.5 m, H=9 m	110,000 bopd
gas–oil–water separation	Marlim	inline	gravity	392 t	$10.8\times29\times8.4$ m^3	22,000 bopd
	Tordis	horizontal	gravity	900 t	D=2.1 m, L=17 m	50,000 bopd 100,000 bwpd

Generally, gas–liquid two-phase subsea separation and gas–oil–water three-phase subsea separation pilot installation happened in the same year. In 2001, while three-phase subsea separation, the Troll pilot [52], was put on stream in the North Sea, the vertical annular separation and pumping system (VASPS) for two-phase separation was first employed at Marimbá field [53], offshore Brazil. However, the pilot test at Marimbá encountered some failure related to ESP control system in its first operation year. After replacement and updates, the system was finally decommissioned after 3 years and 8 months of continuous work [54]. Subsea separators installed in Tordis [55] and Pazflor [56] are large separation vessels employing similar separator configurations as those used on the topside. However, the overall cost of subsea processing station can be significantly reduced by the use of compact separator design. This is one of the reasons that projects in deeper water, such as Perdido [57] and Parque das Conchas [58], have selected caisson separator, and Marlim pilot has embraced inline pipe-type separator.

Table 2.2: Summary of subsea gas–oil–water separation projects

Project	Location	Year	Waterdepth	Type	Topside	Operator
Troll pilot	North sea	2001	340 m	horizontal	semi	Statoil
Tordis	North sea	2007	210 m	horizontal	semi	Statoil
Marlim pilot	Brazil	2011	876 m	inline	FPSO	Petrobras

Table 2.3: Summary of subsea gas–liquid separation projects

Project	Location	Year	Waterdepth	Type	Topside	Operator
BC-10	Brazil	2009	2000 m	caisson	FPSO	Shell
Perdido	GoM	2010	2438 m	caisson	SPAR	Shell
Pazflor	Angola	2011	800 m	vertical	FPSO	Total

2.2.2 State of the art

Theoretically, subsea oil–water separation can be designed to be handled at two places, either downhole or on the seafloor. A downhole unit would separate the water from the oil using a hydrocyclone and the separated water would be reinjected into a lower zone for reservoir pressure support using a submersible pump. A seafloor unit would comprise of a separator, gravity or cyclone based, and two separate lines, one for the hydrocarbon stream, and the other for separated water. The produced water may be re-injected after treatment in a facility installed on the seafloor.[59]

Downhole oil–water separation

Downhole oil–water separation is not a new concept. It was first patented in the late 90s [60]. However, installation is rare. Cao Fei Dian oilfield, located in the Bohai bay in China with a water depth of 25 m, has installed one pilot test [61]. But the test did not expand to field-scale application because of failure after one-year's trial. The selection criterion for candidate wells is so strict that the application of downhole separation is extremely restricted and therefore downhole oil–water separation is currently not taken as an available technology for either onshore or offshore application.

Seafloor oil–water separation

The other option for oil–water separation is to install a separation station on the seafloor, which may receive fluids from a single well, or from a commingled fluid stream.

The first subsea water separation pilot test is the Troll C pilot in the North Sea, on stream in August 2001. The Troll oil field is located west of the giant Troll gas field. Norsk Hydro, as the operator, has developed this field with subsea wells producing back to a semisubmersible processing platform named Troll C, at a water depth of 350 m. Fluids produced from 4 subsea wells come into the subsea separation station. The stream is separated in a horizontal gravity separator with diameter of 2.8 m and length of 9 m. The separator provides 7.5 min of retention time for water, and 4.5 min for oil. Separated oil is mixed with pre-separated gas at the separator outlet and sent back to Troll C in one flowline, while free water separated from the oil is reinjected into the aquifer below the oil layer in the Troll reservoir [62, 63].

After the Troll C pilot, Tordis IOR project realized the first commercial full scale subsea separation installation in the world, in 2007 [64–76]. The Tordis field is a mature field, which has been producing since 1994. It is a subsea development at 200 m water depth with tie-in of the production to Gullfaks C platform. As the field produces quite large amount of water, there was not enough capacity on the platform to treat this excessive water production. Installation of the subsea separation, boosting and injection (SSBI) system removes water on the seafloor. Statoil expected to improve the recovery factor from 49 % to 55 % and to extract 35 million barrels of additional oil from the field by the full-scale commercial installation of the SSBI system [55]. The subsea separator installed in Tordis is almost twice the size of Troll Pilot. They have similar structures. The major difference lies in sand handling capacity. The Troll Pilot is designed for negligible sand production, while the de-sanding capacity for Tordis is up to 500 kg per day. The separation station

is illustrated in Figures 2.1 and 2.2.

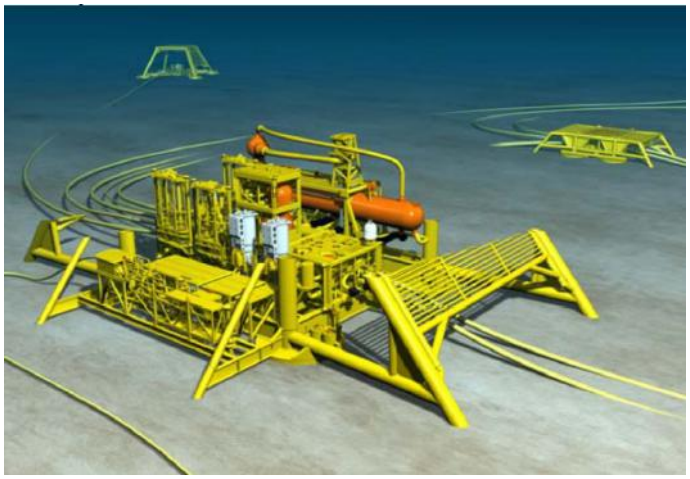

Figure 2.1: Illustration of the subsea separation, boosting and injection (SSBI) station in the Tordis field. Separator and desander vessels are illustrated in orange. The multiphase and water injection pumps and leakage detectors are shown in white. Figure from reference [55].

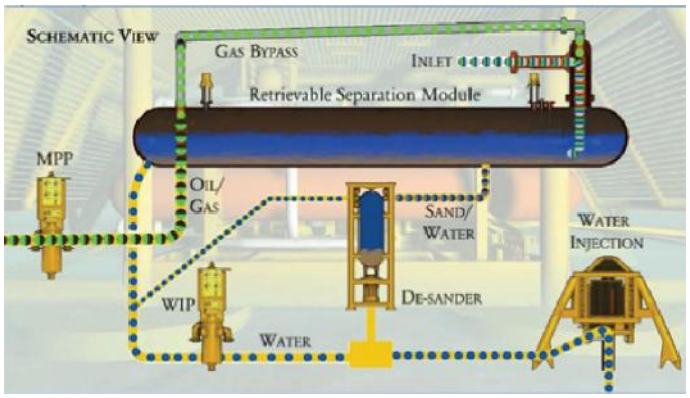

Figure 2.2: Simplified schematic of the separation process of Tordis SSBI station. Figure from reference [55].

Pilot installation of another type of subsea separator, a pipe-type separator, was in Marlim field [77, 78]. The Marlim field locates at the northeastern part of Campos Basin, Brazil, 110 km offshore the state of Rio de Janeiro. The water depth of the field is 650 m to 1,050 m. Marlim field got its first oil in March 1991. As it approaches the end of production life, extensive water production restricts further development. To debottleneck water processing capacity on the host, a pilot subsea separation station with 29 m of length, 10.8 m of width, 8.4 m of height and overall assembly weight in-air of 392 ton was installed at a water depth of 870 m for the pilot well MRL-141, in 2011. The subsea separation station performs three-phase separation and water reinjection. The production stream firstly goes through an inline multiphase sand remover that removes the bulk part of produced solids.

Downstream the multiphase sand remover, gas is separated from liquid through a set of vertically arranged pipes, named as the *harp*. Right downstream of it, there is a pipe separator of around 60 m long to perform oil–water separation. At the very end of the pipe separator loop, oil is recombined with separated gas and flows free in a multiphase stream to the topside stationary production unit, while separated water with oil content above limits for reservoir reinjection is routed to a polishment system, which comprises another inline sand remover and two stages of hydrocyclones. The hydrocyclones reduce the amount of oil in water to acceptable levels for reinjection. Furthermore, water reinjection is realized using centrifugal pumps. The separation station is illustrated in Figure 2.3 and 2.4.

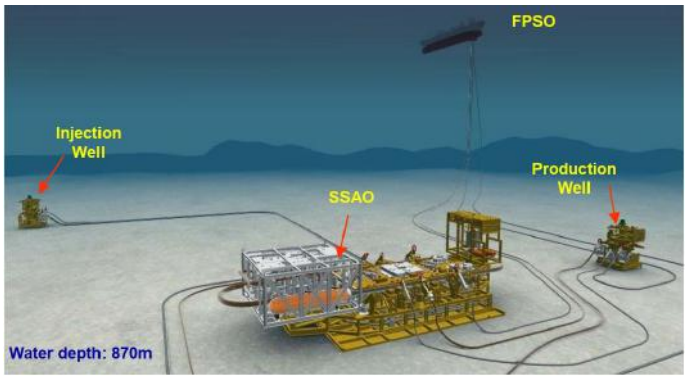

Figure 2.3: Artistic view of oil–water subsea separation system (SSAO) of Marlim. Figure from reference [78].

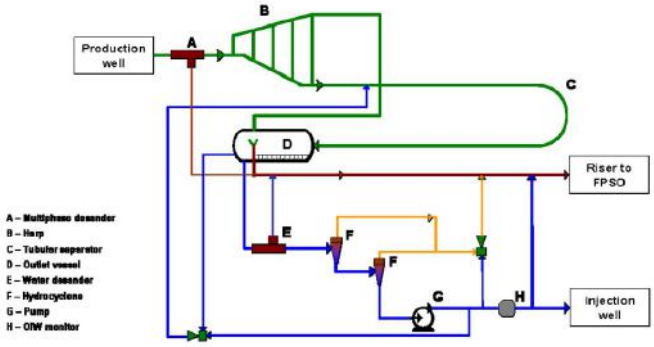

Figure 2.4: Flow diagram of Marlim SSAO station. Figure from reference [78].

Many other concept designs for pipe-type subsea separator have been reported in the literature. However, their studies are yet mainly based on CFD (computational fluid dynamics) simulations. Experimental verifications are rarely reported. Separation based on hydrocyclone and electrostatic force are two areas of research interest, but not yet verified on large scales. Also, the qualification standard of novel technologies itself is ambiguous to some extent. The industry needs more efficient and reliable separation technology for all water depths.

Chapter 3

Theoretical Background

"*Rigorous exact solutions in engineering are essentially non existent. In all engineering problems one has to resort to some kind of approximations in which the physics of the problem is approximated and formulated in a format tractable by analytical or numerical means. This kind of approximation is termed modeling.*" [79]

In the quest for a more accurate and reliable answer to an engineering problem, appropriate modeling consideration is of utmost importance. In petroleum field development, integrated production modeling is unquestionably an interdisciplinary problem involving at least the modeling of the reservoir and the production pipeline network. The identification of system components, as well as the modeling method in each domain is fundamental. In this chapter, it is firstly introduced the key components for integrated production modeling, then, theoretical fundamentals for modeling in each domain are recalled.

3.1 Key components of integrated production modeling

An integrated reservoir-pipeline network model consists of: 1) models describing multiphase flow through porous media in the reservoir domain, 2) models for multiphase flow in wells, pipelines, risers, devices and processing equipment in the network domain, and 3) a global coupling scheme to realize interaction and synchronization between these two domains. Thus, three main issues must be addressed when building an integrated production model:

- Modeling of reservoir dynamics
- Modeling of flow in the production network
- Reservoir–network coupling scheme

In spite that IPM aims at the integration between the reservoir and pipeline network domain, emphasis on either domain may dominate. Several levels of models can be selected in each domain taking into consideration factors such as limitations on simulation time, the storage capacity of computers, etc. A matrix of the possible options for modeling each domain is shown in Figure 3.1. The size of each box indicates the number of variables involved in the model and the color indicates the difficulty of integrating the system. Detailed discussions of each of these options are presented below.

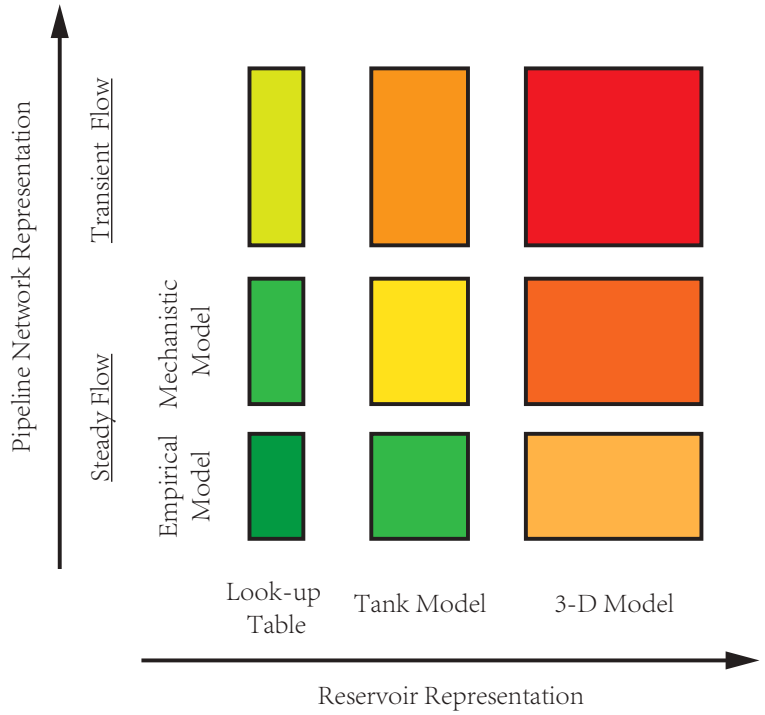

Figure 3.1: Reservoir and network models for integrated production modeling.

Reservoir modeling methods

In representing the reservoir dynamics, three modeling techniques with progressive complexity are available, namely look-up table, tank model and full-field numerical reservoir simulation model [80]:

1. **Look-up table**. The look-up table comprises the relationship among cumulative rate, water cut, GOR, reservoir pressure, and productivity index[33]. Normally this table is created from analog-reservoir models, full-reservoir simulation output, decline curve analysis, or material balance tools. The impact of the production system on reservoir recovery cannot be evaluated with this approach since it is implied that a fixed volume is to be produced by each well irrespective of how it is produced. However, production acceleration can be

quantified, such as the amount of production accelerated by applying artificial lift in comparison to natural production. Therefore, such an approach is somewhat helpful in sizing and selecting equipment.

2. **Tank model**. The basis of tank model analysis is material balance, or, the principle of the conservation of mass. Either a one-cell or a multi-layer tank model can be applied to capture the reservoir dynamics. The material balance equation is zero-dimensional, meaning that it does not take into account the geometry of the reservoir, the drainage areas, the position and orientation of the wells, etc [81]. It is not necessary to enter the reservoir production history to run a production prediction, however, it is highly recommended to tune the model when any history data is available because it will by no means provide a convincing prediction when the model parameters are not reliable.

3. **Full-field numerical reservoir simulation model (3-D model)**. Classical reservoir simulation sets its foundation on mass conservations and the simple momentum conservation law in the form of Darcy's equation. The resulting set of partial differential equations describes single phase or multiphase flow in porous media. By solving these partial differential equations, reservoir states and production variations are obtained. Recent developments in numerical reservoir simulation include more advanced models for unconventional resources. It is the most complex modeling technique to capture reservoir dynamics and is believed to be the most reliable one if the reservoir model is well tuned through history matching.

The level of detailedness and the requirement of input data vary among the above-mentioned models. The selection of the type of model to be applied depends on the duration and scope of the study, in addition to what data are available. In IPM, the main task of a reservoir model is to provide boundary conditions to the network model in each simulation time step and to respond to the changing network back pressure. In some collaborative projects, due to the limitation on data sharing among operators and suppliers, a look-up table approach may be firstly applied for conceptual selection and design [80].

Network modeling

As for modeling the pipeline network, it is fundamental to distinguish between steady-state flow model and transient flow model:

1. **Steady-state flow model**. The behavior of multiphase flow in wells and networks is described by steady-state pressure and temperature calculations.

Empirical correlations and mechanistic models are options for these calculations. A simplification is to use lookup tables, where water cut, GOR, and outlet pressure are listed with inlet pressure. The integrated reservoir to surface modeling widely used within the oil and gas industry has been relying on steady-state flow through wells and networks.

2. **Transient flow model**. Integrated models with steady-state well and network flow simulations are not able to properly describe flow assurance issues such as slugging, liquid loading, shut-down, depressurizations, ramp-up, pigging, start-up, etc. One of the main difficulties in coupling dynamic flow simulations with reservoir simulations relates to the timescale difference. Reservoir simulations are most often performed with mid-to-long time steps from weeks to months for years, while dynamic well and network simulations are performed with short time steps from seconds to minutes for hours. That is, it is not realistic to perform a 20-year production profile with time steps of seconds. Reference [82] reported an approach where the steady-state integrated asset model is paused routinely, or when a flow assurance check or investigation is deemed necessary, to evoke the dynamic simulation in software LedaFlow to capture the impact of transient flow and feedback to the integrated model. For example, the feature of slug flow in the vertical riser is modeled in more details by the dynamic flow simulator when the steady-state flow correlation detects a slug flow regime. Another example where flow assurance and dynamics in the network is emphasized is presented in [83]. They stated the concept of integrated flow assurance modeling (IFAM) where transient operations like turn-down, shut-down, restart, start-up, ramp-up, pigging, should be simulated. The coupling routine is realized through the interface RESOLVE in the IPM suite from PETEX.

Reservoir–network integration techniques

Integration between reservoir and pipeline network may take either an explicit form or an implicit form. In explicit coupling, the two independent programs are communicated through an interface. Data exchange between the two domains can be realized with file manipulation or through message passing libraries such as PVM or MPI . Usually, the interface is implemented in the surface simulator, leaving the reservoir simulator a slave process. Another coupling method, which is commonly referred to as "fully integrated solution", assembles equations that describe both domains and seek for simultaneous solutions.

1. **Explicit Coupling.** In explicit coupling scheme, the reservoir and the network models are solved independently and alternatively, only boundary con-

ditions are interchanged. Usually the information interchange between the reservoir and the network module is carried out by a message passing open interface such as PVM or MPI, eliminating the necessity for file exchange [8]. The main advantage of this coupling scheme is its simplicity and flexibility in software choice. The main disadvantage is that the reservoir simulator may require more Newton iterations to converge its time step. There are basically three key issues involved in explicit coupling: data consistency, coupling location, and equilibration frequency and definition of timestep convergence.

- Data consistency includes many aspects, including the consistency of fluid properties, well names, reference depth, etc. The key to the accurate prediction in the integrated system is the calculation of reliable and consistent physical properties and phase behavior. This is an aspect that is often overlooked. Black oil model is often adopted by both simulators, however, it is important to make sure that they generate consistent results. When different fluid models are assumed, such as a black oil reservoir simulator coupled to a network simulator using fluid property based on compositional model, appropriate delumping techniques should be used to minimize discrepancy. A naming convention has to be established in order to have consistency in all wells declared in the reservoir simulator and those defined in the network model. The number of strings and reference depth have to be checked as well to be consistent in both models, to avoid pressure response discrepancy due to pressures referenced at different potentials.
- The coupling location, or coupling point, basically corresponds to a nodal analysis point, typically the bottomhole or wellhead. Regardless of the coupling location, as long as the models used are consistent, the results should be equally representative [5]. BARROUX *et al.* [84] discussed three possible configurations where the reservoir and the network may be coupled: wellhead level, reservoir level with IPR overlap, and reservoir level with tubing performance and IPR overlap.
- In each simulation time step, network simulator and reservoir simulator are called alternatively from the controlling interface. Equilibration level and frequency of equilibration (the frequency for calling the surface network resolution) have great impact on computation time. A coupling method is called explicit if equilibration is performed at the timestep level and partially-implicit if coupled at the iteration level [85].

2. **Implicit Coupling.** Implicitly coupled reservoir–network simulation is also named **fully integrated** since equations describing multiphase flow in the

reservoir, the well inflow relationship, flow in tubing and the pipeline network model are solved simultaneously. The complete system of equations is linearized and the resulting linear system is solved to obtain the updated values of the solution variables at each Newton iteration. Thus additional derivatives need to be computed and accommodated in the Jacobian matrix of the reservoir simulator. Compared to the flexibility and the simplicity of an explicit coupling scheme, the implicit mode offers improved convergence and higher stability during the simulation run. However, it requires the assembly of a coefficient matrix for both the reservoir and the network. Although an implicit coupling might provide better convergence when solving the non-linear system of equations, it suffers from a lack of flexibility when it comes to software choice. Furthermore, coupling several reservoir models to a shared surface facility is not feasible, inefficient and difficult to maintain presenting a large number of grid blocks [86].

The quality of each model component is the most critical part for the integrated production modeling. It is, therefore, necessary to make sure that each component that is added to an IPM framework is properly history matched and up-to-date, to represent the reservoir and field conditions as close as possible.

3.2 Computational fluid dynamics basis

The naturally occurring petroleum deposits are composed of a variety of organic chemicals with widely different characteristics [87]. A typical crude oil may contain thousands of different chemical compounds. Some of them, mainly those of small molecules, are gas under standard condition, while others are liquid with different appearances. The properties of petroleum fluid depend heavily on its composition, however, the flow process from the reservoir, through wells and pipelines, to the processing host, is governed by the same basic conservation laws. The mathematical statement of these physical relationships forms a set of governing equations, which are the fundamentals of fluid dynamics. Both reservoir simulation and pipe flow modeling are built upon the basic theories of computational fluid dynamics.

In this section, a brief retrospect of the governing equations for single-phase flow is presented first, followed by those for multiphase flow. The relationship between single and multiphase flow, as well as the linking between the general multiphase flow models and the reservoir-network models, are introduced along the context. Detailed theory and derivation of the governing equations can be found in classic textbooks of computational fluid dynamics and multiphase flows, including but not limited to those listed in the bibliography [88] [89].

3.2.1 Conservation laws for single phase flow

In fluid dynamics, the fluid is regarded as a continuum and all fluid properties are functions of space and time. For example, density, pressure, temperature and the velocity vector should be expressed as $\rho(x, y, z, t)$, $P(x, y, z, t)$, $T(x, y, z, t)$, and $\boldsymbol{u}(x, y, z, t)$, respectively. To avoid unduly cumbersome notation, the dependence on space co-ordinates and time will not be expressed explicitly in the following text.

For the analysis of fluid flows at macroscopic length scales, the molecular structure of matter and molecular motions may be ignored. A fluid particle or point in a fluid is then the smallest possible element of fluid whose macroscopic properties are not influenced by individual molecules. We consider such a small element of fluid with sides δx, δy and δz. Figure 3.2 (a) shows the representation of some kind of flux through each cell face, and Figure 3.2 (b) illustrates the surface forces on the fluid element.

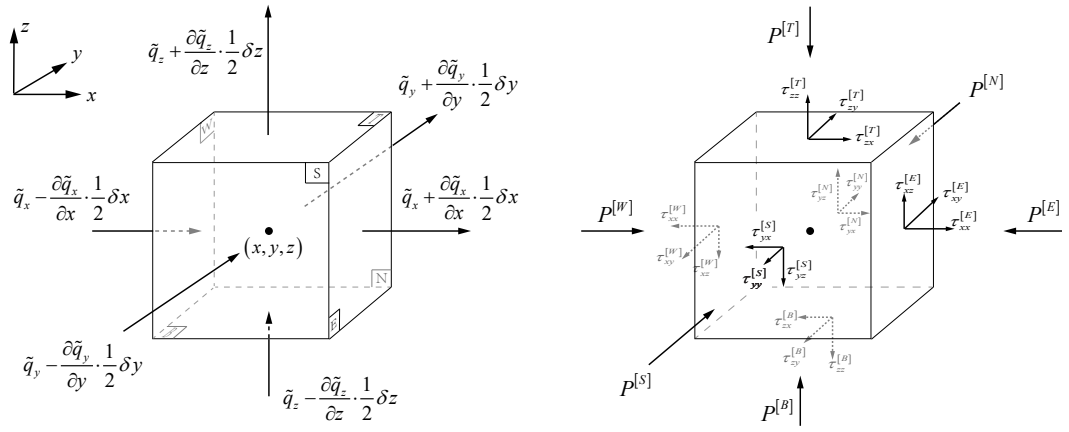

Figure 3.2: Illustration of a fluid element. $\tilde{q}$ represents a type of flux through a side face, e.g. mass flux, heat flux.

Currently, there are two approaches to consider the behavior of the fluid continuum, termed the Lagrangian approach and the Euler approach. The Lagrangian approach aims at tracking the motion of a particular particle or collections of fluid particles while the Euler approach focuses on the change in a spatial stationary position. Generally, the Lagrangian approach is only practical when the dispersed phase fraction is relatively low.

Under the Euler framework, we express the three basic conservation laws of physics for a fluid element as conservation of mass, conservation of momentum (Newton's second law) and conservation of energy (first law of thermodynamics):

Conservation of Mass

the rate of increase of mass in a fluid element	=	the net rate of flow of mass into the fluid element

Conservation of Momentum

the rate of change of momentum of a fluid element	=	the sum of the forces acting on the fluid element

Conservation of Energy

the rate of change of internal energy of a fluid element	=	the sum of the rate of heat addition to and the rate of work done on the fluid element

The left hand side of the three conservation laws take similar forms since the rate of increase of a conserved property Ψ for a fluid particle equals the rate of increase of Ψ per unit volume plus the net flow of Ψ out of the fluid element per unit volume, which can be expressed as

$$\frac{\partial(\rho\Psi)}{\partial t} + \nabla\cdot(\rho\Psi\boldsymbol{u}) \tag{3.1}$$

The corresponding quantities of Ψ for the conservation of mass, momentum, and energy are 1, $\boldsymbol{u}$ and i, respectively. Thus, the conservative form of the three basic conservation equations can be written as Eq. 3.2, 3.3 and 3.8, respectively. Conservation laws expressed by other quantities, such as kinetic energy (e), enthalpy (h), etc., can be derived from the three basic conservation equations and are also listed in Table 3.1. ∂_t in the equations denotes differentiation in time. In practice, one may choose the set of conservation equations expressed by the quantities that are most available for certain calculation purposes.

Integral of the partial differential equations for an arbitrary control volume Ω generates the following generic form of governing equations:

$$\iiint_{\Omega} \frac{\partial(\rho\Psi)}{\partial t}\mathrm{d}\Omega + \oiint_{\partial\Omega} \rho\Psi\boldsymbol{u}\cdot\boldsymbol{n}\mathrm{d}S = \oiint_{\partial\Omega} \Gamma\nabla\Psi\cdot\boldsymbol{n}\mathrm{d}S + \iiint_{\Omega} \Theta_{\Psi}\mathrm{d}\Omega \tag{3.12}$$

The second term on the left side of the equation is the convection term, and the first term on the right is the diffusion term. Γ is called the diffusion coefficient. Finite volume method is commonly used for numerical solution of Eq. 3.12.

During early production stages of a gas reservoir or an undersaturated oil reservoir, single-phase flow in the formation occurs. To model this situation in the reservoir domain, the mathematical representation of a single fluid flow suffices. However, most of the time, one has to deal with mixed flow of oil, gas, and water along the production life, which naturally leads to the modeling of multiphase flow.

Table 3.1: Conservative form of the governing equations for the flow of a compressible Newtonian fluid

Mass	$\partial_t(\rho) + \nabla\cdot(\rho\boldsymbol{u}) = \Theta_c$	(3.2)
Momentum	$\partial_t(\rho\boldsymbol{u}) + \nabla\cdot(\rho\boldsymbol{u}\boldsymbol{u}) = \nabla\cdot[\mu(\nabla\boldsymbol{u} + \nabla\boldsymbol{u}^\intercal)] - \nabla P + \boldsymbol{\Theta}_M$	(3.3)
x-momentum	$\partial_t(\rho u_x) + \nabla\cdot(\rho u_x\boldsymbol{u}) = \nabla\cdot(\mu\nabla u_x) - \partial_x P + \Theta_{Mx}$	(3.4)
y-momentum	$\partial_t(\rho u_y) + \nabla\cdot(\rho u_y\boldsymbol{u}) = \nabla\cdot(\mu\nabla u_y) - \partial_y P + \Theta_{My}$	(3.5)
z-momentum	$\partial_t(\rho u_z) + \nabla\cdot(\rho u_z\boldsymbol{u}) = \nabla\cdot(\mu\nabla u_z) - \partial_z P + \Theta_{Mz}$	(3.6)
Kinetic energy	$\partial_t(\rho e) + \nabla\cdot(\rho e\boldsymbol{u}) = -\boldsymbol{u}\cdot\nabla P + \Phi_e + \boldsymbol{u}\cdot\boldsymbol{\Theta}_M$	(3.7)
Internal energy	$\partial_t(\rho i) + \nabla\cdot(\rho i\boldsymbol{u}) = \nabla\cdot(\kappa\nabla T) - P\nabla\cdot\boldsymbol{u} + \Phi_i + \Theta_i$	(3.8)
Enthalpy	$\partial_t(\rho h) + \nabla\cdot(\rho h\boldsymbol{u}) = \nabla\cdot(\kappa\nabla T) + \partial_t P + \boldsymbol{u}\cdot\nabla P + \Phi_i + \Theta_i$	(3.9)
Total energy	$\partial_t(\rho e^*) + \nabla\cdot(\rho e^*\boldsymbol{u}) = \nabla\cdot(\kappa\nabla T) - \nabla\cdot(P\boldsymbol{u}) + \Phi_i + \Phi_e + \Theta_{e^*}$	(3.10)
Total enthalpy	$\partial_t(\rho h^*) + \nabla\cdot(\rho h^*\boldsymbol{u}) = \nabla\cdot(\kappa\nabla T) + \partial_t P + \Phi_i + \Phi_e + \Theta_{h^*}$	(3.11)

3.2.2 Modeling multiphase flow

The significant difficulty in modeling multiphase flow compared with single fluid flow lies in the fact that there may exist different levels of interchange of mass, momentum, and energy between different fluid phases under different flow conditions. A persistent theme throughout the study of multiphase flows is the need to model and predict the detailed behavior of those flows and the phenomena that they manifest. Conservation laws need to be modified due to the presence of multiple phases. Generally, the conservation equations for an individual phase n can be written as those listed in Table 3.2.

Compared to single-phase flow, an extra primary variable is added into the multiphase flow models, i.e. the volume fraction of each phase. In multiphase flow, the concept of volume fraction of component n, denoted by α_n, plays an important role in relating models of multiphase flows with single-phase flows. $\boldsymbol{u}_n$, the component velocity, equals the phase volumetric flow rate divided by its flowing cross-sectional area. However, since the laboratory measurable is the total cross-sectional area, rather than the flowing area for each individual phase, extensive use of superficial velocities are observed when studying multiphase flow. The superficial component velocity $\boldsymbol{v}_n$ is related to real component velocity $\boldsymbol{u}_n$ through the volume fraction α_n, and $\boldsymbol{v}_n = \alpha_n\boldsymbol{u}_n$. Without further declaration, this notation convention for phase velocity is reserved throughout this thesis.

The possibility of coding the Navier-Stokes equations for each of the phases or

Table 3.2: Governing equations for phase n in multiphase flow

Conservation of mass

$$\partial_t(\alpha_n\rho_n) + \nabla\cdot(\alpha_n\rho_n\boldsymbol{u}_n) = \sum_k(\dot{m}_{kn} - \dot{m}_{nk}) + \Theta_{cn} \tag{3.13}$$

Conservation of momentum

$$\partial_t(\alpha_n\rho_n\boldsymbol{u}_n) + \nabla\cdot(\alpha_n\rho_n\boldsymbol{u}_n\boldsymbol{u}_n) = \nabla\cdot\bar{\bar{\tau}}_n - \alpha_n\nabla P + \sum_k(\boldsymbol{F}_{kn} + \dot{m}_{kn}\boldsymbol{u}_{kn} - \dot{m}_{nk}\boldsymbol{u}_{nk}) + \boldsymbol{\Theta}_{Mn} \tag{3.14}$$

Conservation of energy

$$\partial_t(\alpha_n\rho_n h_n^*) + \nabla\cdot(\alpha_n\rho_n h_n^*\boldsymbol{u}_n) = -\nabla\cdot\boldsymbol{Q}_n + \alpha_n\partial_t P + \sum_k(\boldsymbol{Q}_{kn} + \dot{m}_{kn}h_{kn} - \dot{m}_{nk}h_{nk}) + \Theta_h \tag{3.15}$$

components and computer every detail of a multiphase flow, the motion of all the fluid around and inside every particle or drop, the position of every interface, requires high power and speed computers. When one or both of the phases becomes turbulent (as often happens), the magnitude of the challenge becomes truly astronomical. Therefore, reasonable simplifications of the governing equations based on amenable assumptions are crucial in the establishment of tractable models for most multiphase flows. Experimental correlations are also substitutes or supplements for the exact solution of the conservation equations.

In order to build appropriate models for different multiphase flow phenomena, the first and foremost task is to classify different flow situations. Two basic types of flows can be distinguished, namely separated flows and disperse flows[89]. Separated flows consist of two or more continuous streams of different fluids separated by interfaces, while disperse flows are involved with finite particles, drops or bubbles (the disperse phase) distributed in a connected volume of the continuous phase. The different content and mixing level of different phases lead to significant difference in flow behaviors. Therefore, different flow should be modeled by different assumptions and simplifications of the general conservation equations in Table 3.2. Or, stated the other way around, different modeling approaches are only applicable for certain flow conditions. The essential difference among multiphase flow models is the way that the momentum equations are treated.

In separated flows, the phases are considered immiscible and not interpenetrating. The position of the interface between the fluids is of interest. The simplest way to model this situation is to assume that the velocity is shared among all the phases and thusly a single momentum equation should be solved throughout the domain. The VOF (volume of fluid) model [90] is such an approach to track the fraction of

each phase in each computational cell, which indicates whether the cell is full of a specific phase, or contains the interface between two or more phases. The variables and properties in any given cell are either purely representative of one of the phases, or volume-averaged values of a mixture of the phases. Potential applications of the VOF model includes stratified flows, free-surface flows, and the steady or transient tracking of any liquid-gas interface. The main limitation of this approximation is that it cannot reflect large velocity differences between the phases.

In disperse flows, on the contrary, the fluids are interpenetrating and the disperse phase is treated as a second continuous phase intermingled and interacting with the continuous phase. In such situations, either an Euler-Lagrange or an Euler-Euler approach may be applied according to the dispersed-phase volume fraction. Generally speaking, to model flows in which dispersed-phase volume fractions exceed 10%, one should consider using the Euler-Euler approach. Flows in which the dispersed-phase volume fractions are less than or equal to 10% can be modeled using the Euler-Lagrangian approach. In an Euler-Lagrange approach, the fluid phase is treated as a continuum by solving the Navier-Stokes equations, while the trajectories of the dispersed phase, particles, bubbles, or droplets, are computed. The dispersed phase can exchange momentum, mass, and energy with the continuous phase. This approach is made considerably simpler when particle–particle interactions can be neglected, which requires that the dispersed second phase occupies a low volume fraction, making it inappropriate for the modeling of liquid–liquid mixtures or any application where the volume fraction of the second phase cannot be neglected. In an Euler-Euler approach, two types of models are applicable: Mixture model and Eulerian model. The main difference between them is how the momentum equations are treated. The essential idea behind the Mixture model, which solves for a mixture momentum equation for the multphase fluid, is the concept of drift velocity. The Mixture model reduces to homogeneous multiphase flow assumption when the relative velocities for the dispersed phase is not accounted for. It is applicable in bubbly flows, sedimentation, and cyclone separators. In the Eulerian model, the momentum equation for each phase is included, resulting in the most complex model of multiphase flow. The application of the Eulerian multiphase is generally wider. However, computational time should be taken into consideration.

The technical key points of each above-mentioned multiphase flow models are summarized in Table 3.3.

Now, coming back to the context of petroleum field production, the fluids under consideration should at least include three phases: gas, oil, and water. The classic modeling approach for the flows of the three-phase mixture in both the reservoir and the pipeline network, as applied in industrial standard commercial software, is Eulerian model, where momentum equations are written for each phase.

Table 3.3: Summary of multiphase flow models

Model	Key notes
VOF model	shared momentum equation, shared velocity among all the phases
Trajectory model	non-conservative form of conservation equations, discrete phase trajectory tracked
Mixture model	single mixture momentum equation, phase velocity calculated from drift velocity models
Eulerian model	momentum equation for each phase

The classic black oil assumption is one contributor to the simplification of the Eulerian model. It is based on the assumption that the various chemical species can be lumped together to form two components at surface conditions, a heavy hydrocarbon component called "oil" and a light hydrocarbon component called "gas". At reservoir conditions, the two components can be partially or completely dissolved in each other depending on pressure and temperature, forming either one or two phases, a liquid oleic phase, and a gaseous phase. This assumption simplifies the treatment regarding the unknown terms $\dot{m}$ in Eq. 3.15, since the phase mass transfer between gas and oil is represented by the single parameter named dissolved gas-oil ratio, which is a function of pressure.

In the reservoir domain, another contributor in simplifying the Eulerian model is the Darcy's law (section 3.3.2), which is indeed a momentum equation that states explicitly the relationship between phase velocity and phase pressure.

In the pipeline network domain, the simplification relies on the fact that it is usually sufficient to represent flows through pipe-like structures as one-dimensional. The conservation equations can be significantly simplified (section 3.4) so that the main concern comes to the calculation of variables like liquid holdup for different flow patterns. Empirical correlations based on physical experiments usually provide satisfactory results within the range of experimental conditions, while mechanistic models, or two-fluid models, solve the momentum equation for each phase, such as the model used in software OLGA [91]. Modeling the flow in a pipeline network is essentially a pressure bounded problem where the reservoir pressure and the reception facilities pressure are fixed at a given instant in time and the production rate adjusts accordingly. [92]

Section 3.3 and 3.4 present how the basic conservation equations are modified and applied in modeling flows in the reservoir and the network, respectively. To set up a well-posed model, constitutive laws, initial conditions, as well as boundary conditions are also required. For example, rock compressibility expressed as a function of fluid pressure is required to model a compressible reservoir formation. Other

auxiliary equations will be presented along the text when necessary. Correlations for black oil property calculation are presented in Appendix A.

3.2.3 Numerical solution of flow models

In seeking for numerical solutions for fluid flow models, two types of solvers are optional, namely the pressure-based solver and the density-based solver. In both methods, the velocity field is obtained from the momentum equations. In the density-based approach, the continuity equation is used to obtain the density field while the pressure field is determined from the equation of state. In the pressure-based approach, the pressure field is extracted by solving a pressure or pressure correction equation by manipulating continuity and momentum equations [90].

Using either method, one has to solve the governing equations of mass and momentum conservation, and for energy and other scalars such as turbulence and chemical species, in the generic form of Eq. 3.12. A control-volume-based technique is used that consists of

1. Divide or discretize the computational domain into finite control volumes using structured cells or grids;

2. Construct algebraic equations (usually nonlinear) by either integrating numerically the governing equations on each control volume (finite-volume method) or using differences to replace derivatives (finite-difference method);

3. Solve the nonlinear equation system by some iteration algorithm such as the Newton-Raphson method.

For transient simulation, the governing equations are time-dependent and must be discretized in both space and time. The generic time evolution of a variable Ψ can be expressed as

$$\frac{\partial \Psi}{\partial t} = f(\Psi) \tag{3.16}$$

Different evaluation of $f(\Psi)$ leads to different temporal integral schemes. The method is called *explicit* if $f(\Psi)$ is evaluated using current information:

$$\Psi^{t+1} = \Psi^t + f(\Psi^t)\delta t \tag{3.17}$$

The method is *implicit* if $f(\Psi)$ is evaluated at the future such that

$$\Psi^{t+1} = \Psi^t + f(\Psi^{t+1})\delta t \tag{3.18}$$

The advantage of the implicit temporal integration scheme is that it is unconditionally stable with respect to time step size, while in explicit scheme, the time step δt

is restricted to the stability limit of the underlying solver (Courant-Friedrichs-Lewy condition).

Notice that the explicit and implicit time integration schemes discussed here have nothing to do with the aforementioned reservoir–network coupling scheme. In this work, the implicit time integration scheme is always adopted, and in the rest of this thesis, the terms "implicit" and "explicit" are only used for coupling schemes between the reservoir and the network domain.

All the algebraic equations in the form of Eq. 3.18 make up a set of nonlinear equations that can be expressed in a generic residual form: $\mathbf{R}(\mathbf{\Psi}) = 0$. The superscript $t + 1$ has been dropped for simplicity. The Newton-Raphson method for solving the equations includes the formulation of an iterate at iteration k by

$$\mathbf{\Psi}^{k+1} = \mathbf{\Psi}^k - \mathbf{R}(\mathbf{\Psi}^k)/\mathbf{J}(\mathbf{\Psi}^k) \tag{3.19}$$

and a convergence criterion.

$$\|\mathbf{\Psi}^{k+1} - \mathbf{\Psi}^k\| \leq \varepsilon \tag{3.20}$$

The basic concepts in fluid flow modeling and solution methods retrospected in this section are the fundamentals for specific models applied in the petroleum industry, as will be presented in the following sections.

3.3 Reservoir model

The essence of reservoir modeling is multiphase flow through porous media. In this section, it is firstly introduced the zero-dimensional reservoir model, also known as the tank model, or material balance analysis. Then, the classic 3-D black oil numerical model is presented.

3.3.1 Tank model

A tank model, or material balance analysis, assumes that the reservoir is a single cell with an average reservoir pressure and phase saturations. It applies the mass conservation law for zero-dimensional space and in a time integral form, which is often termed material balance analysis.

The mass conservation law states that the rate of increase of mass in a fluid element equals the net rate mass flow into the fluid element. If the overall volume of a reservoir is taken as the only "element", and we restate the mass conservation in the means of decrease of mass since we are extracting hydrocarbon phases out of the reservoir, we get the following statement for the so-called tank model, or material balance: *The rate of decrease of mass in the reservoir equals the net rate of*

underground production. Or, more commonly stated in a cumulative (time integral) sense:

the decrease of HCPV in the reservoir (compared to the original HCPV)	=	the net cumulative underground withdrawal

A typical reservoir tank is illustrated in Figure 3.3. Initially, the porous formation rock is filled with oil, cap gas and connate water, which is the water trapped in the pores of a rock during the formation of the rock. Along the production, water is injected into the reservoir cell to displace reservoir fluids into production wells. Reservoir pressure and hydrocarbon pore volume (HCPV) change according to the relationships between injected and produced volume.

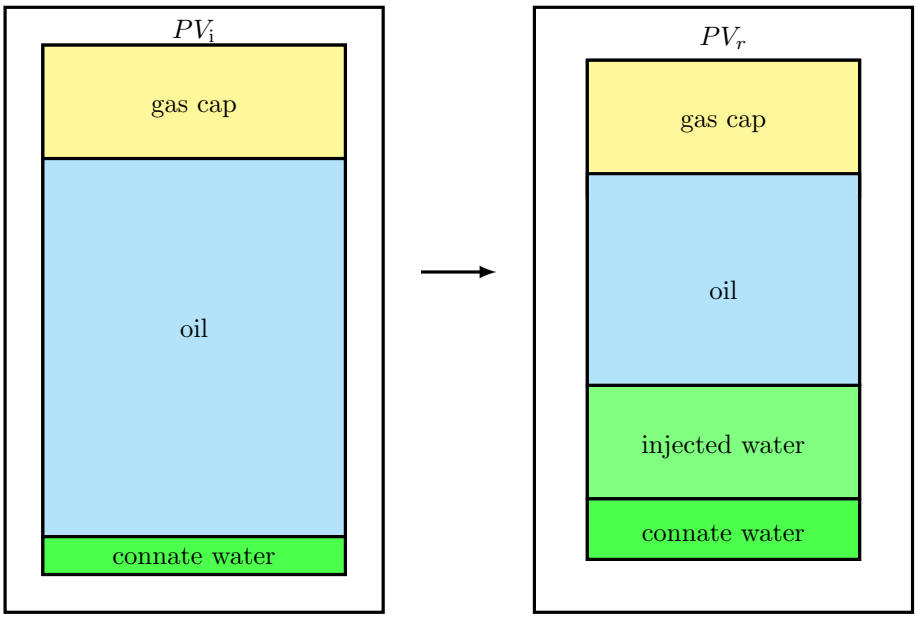

Figure 3.3: Illustration of the reservoir cell from the initial reservoir pressure P_{i} (left) to a depleted pressure P_r (right).

The decrease of HCPV, evaluated at a pressure P_r lower than initial pressure P_{i}, includes the increase due to expansion of the oil plus originally dissolved gas, the expansion of the initial gascap gas, and the decrease in HCPV due to the combined effects of the expansion of the connate water and reduction in reservoir pore volume. The net cumulative underground withdrawal for a reservoir under water injection, is made up of the cumulative production of oil (from the oil zone), gas (from the gas cap, liberated gas from the produced oil, and liberated gas in the oil zone when reservoir pressure drops below bubble point pressure), and the net cumulative production of water (cumulative water production minus cumulative water injection).

This results in the following equation:

$$N_p\big[B_\mathrm{o} + B_\mathrm{g}(R_p - R_s)\big] = NB_\mathrm{oi}\Bigg\{\frac{B_\mathrm{o} - B_\mathrm{oi} + (R_\mathrm{si} - R_s)B_\mathrm{g}}{B_\mathrm{oi}} + m\left(\frac{B_\mathrm{g}}{B_\mathrm{gi}} - 1\right) + (1+m)\left[\frac{c_\mathrm{w}S_\mathrm{wc} + c_r}{1 - S_\mathrm{wc}}(P_\mathrm{i} - P_r)\right]\Bigg\} + (W_i - W_p)B_\mathrm{w} \tag{3.21}$$

3.3.2 3-D reservoir model

A full-scale three-dimensional numerical reservoir model includes mass conservation equations in porous media for each phase, Darcy's law, constitutive laws, and other auxiliary equations.

Conservation of Mass. Black oil model assumes that the oil phase consists of only two components: the dissolved (solution) gas and the residual black oil that remains when solution gas is liberated. No phase transfer occurs between water and oil or between water and gas. Taken the oil phase as an example, the oil mass conservation equation per reservoir rock volume V, evaluated at surface condition, is expressed as:

$$\partial_t(\phi S_\mathrm{o} b_\mathrm{o}\rho_{ost}) + \nabla\cdot(b_\mathrm{o}\rho_{ost}\boldsymbol{v}_\mathrm{o}) = b_\mathrm{o}\rho_{ost}q_\mathrm{o}/V \qquad [kg/s/m^3] \tag{3.22}$$

which is consistent with Eq. 3.13 and the mass transfer term is eliminated by using the concept of formation volume factor (or precisely, its reciprocal b_o in the equation). $\boldsymbol{v}_\mathrm{o}$ is the phase Darcy velocity, or the superficial velocity of oil, as mentioned in section 3.2.2. By eliminating ρ_{ost}, Eq. 3.22 is equivalent to

$$\partial_t(\phi S_\mathrm{o} b_\mathrm{o}) + \nabla\cdot(b_\mathrm{o}\boldsymbol{v}_\mathrm{o}) = b_\mathrm{o}q_\mathrm{o}/V \qquad [s^{-1}] \tag{3.23}$$

Finally, the conservations of water, oil, and gas phase are written as:

$$\partial_t\left(\phi b_\mathrm{w}S_\mathrm{w}\right) + \nabla\cdot\left(b_\mathrm{w}\boldsymbol{v}_\mathrm{w}\right) - b_\mathrm{w}q_\mathrm{w}/V = 0 \tag{3.24}$$

$$\partial_t\left(\phi b_\mathrm{o}S_\mathrm{o}\right) + \nabla\cdot\left(b_\mathrm{o}\boldsymbol{v}_\mathrm{o}\right) - b_\mathrm{o}q_\mathrm{o}/V = 0 \tag{3.25}$$

$$\partial_t\big[\phi(b_\mathrm{g}S_\mathrm{g} + R_s b_\mathrm{o}S_\mathrm{o})\big] + \nabla\cdot\left(b_\mathrm{g}\boldsymbol{v}_\mathrm{g} + R_s b_\mathrm{o}\boldsymbol{v}_\mathrm{o}\right) - \left(b_\mathrm{g}q_\mathrm{g} + R_s b_\mathrm{o}q_\mathrm{o}\right)/V = 0 \tag{3.26}$$

Conservation of Momentum (Darcy's law). The french hydrologist Henry Darcy first observed the proportionality between flow velocity and pressure gradient in 1856 when studying flow of water through beds of sand:

$$\boldsymbol{v} = -\frac{k}{\mu}\,\nabla P \tag{3.27}$$

where, the proportionality factor k is called absolute permeability and the relationship is known as the Darcy's law. Permeability is the basic flow property of a porous medium that measures its ability to transmit a single fluid when the void space is completely filled with this fluid. Conventional reservoirs typically have permeabilities ranging from 0.1 mD to 20 D for liquid flow and down to 10 mD for gases [93]. In recent years, however, there has been an increasing interest in unconventional resources, like shale gas and shale oil, which are trapped within extraordinarily impermeable and hard rocks.

When more than one phase is present in the pore space, each phase has an effective permeability, or relative permeability, which is less than the absolute permeability. Since the presence of another phase is an additional obstacle to flow, the sum of all the effective phase permeabilities will generally be less than one. The relative permeabilities are regarded as nonlinear functions of phase saturations and the relative permeability curves are obtained through laboratory experiments. Simple analytic models can also be used to calculate relative permeabilities. One of such models is the power-law relationship, or, the Corey-type relative permeability [94]:

$$k_{\mathrm{rx}} = k_{\mathrm{rxm}} \left(\frac{S_{\mathrm{x}} - S_{\mathrm{xr}}}{S_{\mathrm{xm}} - S_{\mathrm{xr}}} \right)^{n_{\mathrm{x}}} \tag{3.28}$$

where, the subscript x represents gas, oil, or water phase. Considering the relative permeability and phase pressure, the momentum equation for each phase reads:

$$\boldsymbol{v}_{\mathrm{w}} = -\frac{k k_{\mathrm{rw}}}{\mu_{\mathrm{w}}} \big(\nabla P_{\mathrm{w}} - \gamma_{\mathrm{w}} \nabla Z \big) \tag{3.29}$$

$$\boldsymbol{v}_{\mathrm{o}} = -\frac{k k_{\mathrm{ro}}}{\mu_{\mathrm{o}}} \big(\nabla P_{\mathrm{o}} - \gamma_{\mathrm{o}} \nabla Z \big) \tag{3.30}$$

$$\boldsymbol{v}_{\mathrm{g}} = -\frac{k k_{\mathrm{rg}}}{\mu_{\mathrm{g}}} \big(\nabla P_{\mathrm{g}} - \gamma_{\mathrm{g}} \nabla Z \big) \tag{3.31}$$

Saturations. The pore volume is always to be completely filled, with one or more phases, so that

$$\sum_{\mathrm{x}} S_{\mathrm{x}} = 1 \tag{3.32}$$

Capillary Pressure. Because of the existence of surface tension, the equilibrium pressure in two phases separated by a curved interface will generally be different. The difference in phase pressures is called capillary pressure:

$$P_{\mathrm{cow}}(S_{\mathrm{w}}, S_{\mathrm{o}}) = P_{\mathrm{o}} - P_{\mathrm{w}} \tag{3.33}$$

$$P_{\mathrm{cgo}}(S_{\mathrm{o}}, S_{\mathrm{g}}) = P_{\mathrm{g}} - P_{\mathrm{o}} \tag{3.34}$$

Capillary pressures are functions of saturation and the required functional forms

are normally obtained from a combination of physical experiments, small-scale numerical simulations, or analytical modeling based on bundle-of-tubes arguments.

Porosity. Rock porosity can be modeled as a pressure-dependent parameter, which is also stated as the rock is *compressible*. Rock compressibility is defined by

$$c_r = \frac{1}{\phi}\frac{d\phi}{dP} = \frac{d\ln\phi}{dP} \tag{3.35}$$

For a rock with constant compressibility, 3.35 can be integrated into

$$\phi(p) = \phi_0 e^{c_r(P-P_0)} \tag{3.36}$$

where, ϕ_0 is a reference porosity at pressure P_0. For simplified models, it is common to use a linearization so that:

$$\phi = \phi_0[1 + c_r(P - P_0)] \tag{3.37}$$

Other pressure-dependent properties like density ρ, viscosity μ, reciprocal of the formation volume factor b, solution gas oil ratio R_s, should also be calculated or provided in PVT tables. Black oil correlations such as those provided in Appendix A are some choices for calculation.

3.4 Pipeline network model

A pipeline network consists of flowpaths like tubings, flowlines, and risers, as well as nodes, or junctions, where two or several flowpaths are interconnected. Study on multiphase flow through pipe-like structures has a long tradition by simplifying the process as one-dimensional. Predicting pressure and temperature variations along the flowpath requires information on fluid properties, which in turn are normally functions of pressure and temperature. Great efforts have been made by researchers in conducting experiments and developing models to interpret the fluid behavior in a more universal way. This section briefly presents the network equations for fluid flow in flowpaths and at junctions.

3.4.1 Pressure calculation in pipes

Pressure distribution along a flowpath follows the conservation of momentum, or equivalently, the conservation of kinetic energy. Applying the momentum conservation equation for single-phase flow (Eq. 3.3) to steady-state one-dimensional form results in:

$$\frac{dP}{dL} = -\rho g \sin\theta - \rho u\frac{du}{dL} - \frac{d\tau}{dL} \tag{3.38}$$

Eq. 3.38 indicates that three forms of head loss contribute to the total pressure drop along a flowpath, namely, frictional loss, gravitational loss and acceleration loss:

total head loss ΔP	=	gravitational head loss ΔP_{el}	+	acceleration head loss ΔP_{ac}	+	friction head loss ΔP_{fr}

In most practical cases, the acceleration pressure drop is often neglected due to its small contribution on total pressure drop (less than 10%). Frictional pressure loss is the dominant term for horizontal flow, while in vertical flow, gravitational pressure loss dominates.

Gas–liquid two-phase pressure drop calculation in pipes has been a research subject for almost a century and is still an important topic nowadays. Extensive models and methods have been developed seeking for solutions with higher accuracy and wider application range. Some of the classic and widely applied models are listed in Table 3.4. In the early days of the research, attempts were made on developing generic correlations that are independent of flow regimes or weaken the necessity of calculating different forms of pressure loss [95, 96]. More recent investigations barely avoid discussions on flow patterns and the mechanisms behind them. There is still no such a perfect model that can give satisfactory prediction under every condition. Most of them only work well within the range of their original experimental setup, such as pipe diameter and fluid type. Many researchers have compared the performance of different models based on large experimental database. ARYA and GOULD [97] compared two-phase liquid holdup and pressure drop correlations for horizontal and inclined pipes and concluded that Beggs-Brill correlation shows good performance. MEKISSO [98] compared 42 two-phase frictional pressure drop correlations using 2429 data points of experimental pressure drop measured from eleven different sources and suggested that Beggs-Brill method is one of the best in predicting pressure drop for air-oil system in moderate pipe diameter. AHMED and AYOUB [99] compared nine pressure drop correlations for vertical flow and also recommended Beggs-Brill method. YAHAYA *et al.* [100] compared several methods for vertical multiphase flow and concluded Ansari and Beggs-Brill method predicts best.

While mechanistic models solve the conservation equations for each individual phase, empirical models apply single-phase flow conservation equations on the mixture and correlate mixture properties with weighted individual phase properties, where Eq. 3.38 is rewritten as:

$$\frac{dP}{dL} = -\rho_m g \sin\theta - \rho_m u_m \frac{du_m}{dL} - \frac{d\tau_m}{dL} \tag{3.39}$$

Table 3.4: Summary of pressure drop calculation methods

Author	Year	Type	Flow	Flow patterns identification
Duns Ros[101]	1963	empirical	vertical	Region I, II, III
Hagedorn-Brown[96]	1964	empirical	vertical	(not relevant)
Eaton[95]	1967	empirical	horizontal	(not relevant)
Orkiszewski[102]	1967	empirical	vertical	bubble, slug, transition, mist
Aziz[103]	1972	drift flux	vertical	bubble, slug, (froth, annular not calculation method)
Beggs-Brill[104]	1973	empirical	all angles	segregated, intermittent, distributed
Hasan Kabir[105]	1988	mechanistic	vertical	bubbly, slug, churn, annular
Ansari[106]	1990	mechanistic	vertical	dispersed bubble, bubbly, developed slug, developing slug, annular
Gomez[107]	1999	mechanistic	all angles	stratified, nonstratified, slug, bubble, annular

Therefore, the determination of mixture density and velocity are crucial. In this work, the Beggs-Brill Method is applied to calculate pressure drop through a flow-path, which is introduced as follows.

Beggs-Brill Method

Eq. 3.39 is reformulated in the following form:

$$-\frac{dP}{dL} = \frac{[\rho_l H_l + \rho_g(1-H_l)]\, g \sin\theta + \frac{\lambda G_m u_m}{2DA}}{1 - [\rho_l H_l + \rho_g(1-H_l)] u_m u_g / P} \tag{3.40}$$

where, G_m is the mixture mass flux rate, u_g is gas superficial velocity, and u_m is the mixture superficial velocity. The calculation of liquid holdup H_l and friction factor λ depend on flow pattern, pipeline inclination, as well as flow direction.

Flow pattern. Based on their experiments, different flow patterns are identified according to the relationship between the Froude number N_{Fr} and non-slip liquid holdup E_l. The division criteria are given in Table 3.5:

Table 3.5: Flow pattern and division criteria in Beggs-Brill method

Flow pattern	Criteria
Segregated flow	$N_{Fr} < 316E_l^{0.302}$, $N_{Fr} < 92.52 \times 10^{-5} E_l^{-2.4684}$
Transient flow	$92.52 \times 10^{-5} E_l^{-2.4684} < N_{Fr} < 0.1E_l^{-1.4516}$
Intermittent flow	$N_{Fr} < 316E_l^{0.302}$, $N_{Fr} < 0.5E_l^{-6.733}$, $N_{Fr} > 0.1E_l^{-1.4516}$
Distributed flow	$N_{Fr} > 316E_l^{0.302}$, or, $N_{Fr} > 0.5E_l^{-6.733}$

Froude number N_{Fr} is a dimensionless parameter defined as

$$N_{Fr} = \frac{u_m^2}{gD} \tag{3.41}$$

Non-slip liquid holdup E_l is the inflow liquid content:

$$E_l = \frac{Q_l}{Q_l + Q_g} \tag{3.42}$$

In the case of gas-oil-water flow, $Q_l = Q_o + Q_w$.

Liquid Holdup $H_l(\theta)$. Liquid holdup in a inclined pipe is calculated by correcting the liquid holdup of horizontal flow:

$$H_l(\theta) = H_l(0)\psi \tag{3.43}$$

where, θ is the pipe inclination angle respecting to horizontal direction, and ψ is the correction factor. Liquid hold up in horizontal flow $H_l(0)$ is calculated by

$$H_l(0) = \frac{aE_l^b}{N_{Fr}^c} \tag{3.44}$$

and ψ is calculated by

$$\psi = 1 + C\left[\sin(1.8\theta) - \frac{1}{3}\sin^3(1.8\theta)\right] \tag{3.45}$$

$$C = (1 - E_L)\ln\left[d\ E_L^e\ N_{vl}^f\ N_{Fr}^g\right] \tag{3.46}$$

In Eq. 3.44 and 3.46, a, b, c, d, e, f and g are correlation coefficients depending on flow pattern and flow direction, as listed in Table 3.6

Table 3.6: Coefficients in Eq. 3.44 and 3.46

	stratified	intermittent	distributed
a	0.98	0.845	1.065
b	0.4846	0.5351	0.5929
c	0.0868	0.0173	0.0609
	upward		downward
	stratified	intermittent	all patterns
d	0.011	2.96	4.7
e	-3.768	0.305	-0.3692
f	3.539	-0.4473	0.1244
g	-1.614	0.0978	-0.5056

Friction Factor λ. Friction factor λ is correlated to non-slip friction factor λ' by:

$$\lambda = \lambda' \exp(s) \tag{3.47}$$

where, s is related to E_l and $H_l(\theta)$:

$$s = \frac{\ln y}{-0.0523 + 3.18 \ln y - 0.8725(\ln y)^2 + 0.01853(\ln y)^4} \tag{3.48}$$

$$y = \frac{E_l}{[H_l(\theta)]^2} \tag{3.49}$$

For $1 < y < 1.2$, $s = \ln(2.2y - 1.2)$. The non-slip friction factor λ' can be determined by Moody diagram using two-phase Reynolds number.

3.4.2 Temperature calculation in pipes

The steady-state one-dimensional form of energy conservation equation for single phase flow (Eq. 3.9), without mass source or heat source and neglecting viscous term, reduces to

$$\frac{dh}{dL} = -g \sin\theta - u\frac{du}{dL} - \frac{U\pi D(T - T_{\text{amb}})}{w} \tag{3.50}$$

The relationship in thermodynamics reads:

$$dh = \left[\frac{dh}{dT}\right]_P dT + \left[\frac{dh}{dP}\right]_T dP = c_p dT - \eta c_p dP \tag{3.51}$$

where, η is the Joule-Thomson coefficient:

$$\eta = \left[\frac{dT}{dP}\right]_h = -\frac{1}{c_p}\left\{T\left[\frac{\partial}{\partial T}\left(\frac{1}{\rho}\right)\right]_P - \frac{1}{\rho}\right\} \tag{3.52}$$

Therefore,

$$\frac{dh}{dL} = c_p\frac{dT}{dL} - \eta c_p\frac{dP}{dL} \tag{3.53}$$

Eq. 3.50 and 3.53 lead to:

$$\frac{dT}{dL} + \frac{U\pi D}{wc_p}T = \frac{U\pi D}{wc_p}T_{\text{amb}} + \frac{1}{c_p}\left(\eta c_p\frac{dP}{dL} - g\sin\theta - u\frac{du}{dL}\right) \tag{3.54}$$

Assuming constant ambient temperature in the calculating pipe segment, Eq. 3.54 is integrated into:

$$T_{\text{out}} = T_{\text{amb}} + (T_{\text{in}} - T_{\text{amb}})\exp(-L/A) + \Delta T_{JT} \tag{3.55}$$

where, ΔT_{JT} is the Joule-Thomson effect,

$$\Delta T_{JT} = A\big[1 - \exp(-L/A)\big]\left[\eta c_p \frac{dP}{dL} - g\sin\theta - u\frac{du}{dL}\right] \tag{3.56}$$

and

$$A = \frac{wc_p}{U\pi D} \tag{3.57}$$

For gas-oil-water three-phase flow, mixture heat capacity and Joule-Thomson coefficient are calculated by weighted phase values $c_{p\mathrm{w}}$, $c_{p\mathrm{o}}$,$c_{p\mathrm{g}}$, η_{w}, η_{o}, and η_{g}, referring to [108],

3.4.3 Continuity at pipe junctions

The continuity at a node or junction includes mass continuity, pressure balance and energy conservation. Mass continuity of phase x at a pipe junction can be expressed as:

$$\sum_{i\in\{\mathrm{in}\}} q_{\mathrm{x}}^i = \sum_{j\in\{\mathrm{out}\}} q_{\mathrm{x}}^j \tag{3.58}$$

where, {in} and {out} represent the set of inflow and outflow flowpaths at a node, respectively.

For a junction where equipment like pump or compressor is absent, simple pressure continuity holds:

$$P^i = P^j, \quad \forall i \in \{\mathrm{in}\}, \forall j \in \{\mathrm{out}\} \tag{3.59}$$

Energy conservation at a junction is an appropriate assumption when the fluids mix quickly and the heat loss to the surrounding environment is negligible. For a node where fluids coming from different flowpaths commingle, the temperature after mixing is calculated by

$$T^j = \frac{\sum_{i\in\{\mathrm{in}\}} w^i c_p^i T^i}{\sum_{i\in\{\mathrm{in}\}} w^i c_p^i}, \quad \forall j \in \{\mathrm{out}\} \tag{3.60}$$

3.5 Coupling techniques

As mentioned in section 3.1, there are two distinct coupling schemes for integrated production modeling: explicit and implicit. The former *couples* a reservoir simulator with a pipeline network simulator through some interface for data exchange, while the latter *integrates* reservoir and network equations for simultaneous solutions in both domains. The term "coupled" and "integrated" are interchangeable regarding terms like "uncoupled" or "stand-alone". In the thesis, when the focus is to compare

among different coupling schemes, "couple" is used especially for explicit scheme and "integrate" for implicit. Otherwise, a simulation may be named as "uncoupled" or "coupled" when more emphasis is on whether an IPM approach is used.

The key element connecting the reservoir domain and the pipeline network domain is the well. The well either works under constant mass flux, which is a Neumann boundary condition, or constant flowing bottomhole pressure, which is a Dirichlet boundary condition. In the course of a simulation, a rate or Neumann condition may exist for a certain period of time where the desired production continues at some fixed rate. After the flowing bottomhole pressure reaches a limit value, a Dirichlet condition becomes effective where the well produces the maximum rate possible at constant bottomhole pressure.

A well is commonly modeled by an inflow performance relationship (IPR). IPR and its normalization are briefly presented in this section.

3.5.1 Well inflow performance

An IPR curve relates well production rate with pressure drawdown between the reservoir and the bottomhole. For a vertical well in an undersaturated reservoir, where oil is the only phase in the reservoir, linear IPR is applicable:

$$q_{\mathrm{o}} = J(P_r - P_{wf}) \tag{3.61}$$

where, the productivity index J should be obtained from well tests, or be approximated by

$$J = \frac{2\pi kH}{B_{\mathrm{o}}\mu_{\mathrm{o}}\left[\ln\left(\frac{r_{eq}}{r_w}\right) - \frac{1}{2} + S\right]} \tag{3.62}$$

where, r_{eq} is the reservoir equivalent radius, and S is the skin factor.

When reservoir pressure is below the bubble point pressure, gas comes out of the oil phase and two phases coexist in the reservoir. In this case, oil productivity index is no longer constant due to the existence of the gas phase. The IPR for such a situation can be calculated with VOGEL model [109],

$$\frac{q_{\mathrm{o}}}{q_{\mathrm{o\,max}}} = 1 - 0.2\left(\frac{P_{wf}}{P_r}\right) - 0.8\left(\frac{P_{wf}}{P_r}\right)^2 \tag{3.63}$$

where, $q_{\mathrm{o\,max}}$ is called the absolute open-flow capacity (AOF).

For gas-oil-water three-phase flow, a composite IPR is applied, which is a method proposed by Petrobras [110]:

$$q_l = (1 - f_{\mathrm{w}})q_{\mathrm{o}} + f_{\mathrm{w}}q_{\mathrm{w}} \tag{3.64}$$

where, q_o is calculated from Eq. 3.61 or Eq. 3.63 depending on the reservoir condition, and q_w is calculated from the linear IPR for the water phase.

3.5.2 Normalization of IPR

The well models presented above are usually used with a tank reservoir model and in a pipeline network model where near-well conditions are ambiguous. In such situations, reservoir pressure is the average value in the single reservoir cell, hence, well production rate is computable given its productivity index and bottomhole pressure. As for a full-field 3-D reservoir model, a well always penetrates a group of cells, and the total well production rate is the sum of the production from each perforated cell, as illustrated in Figure 3.4.

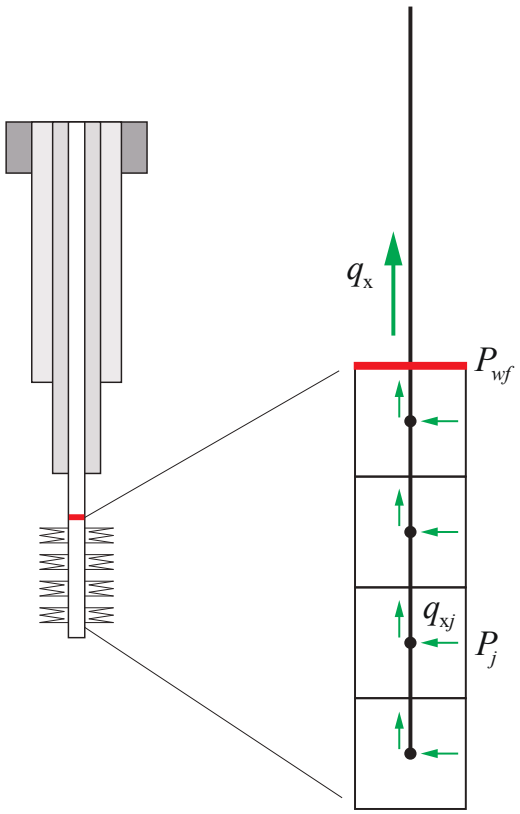

Figure 3.4: Illustration of the well model.

Peaceman equation is applied to calculate the well inflow performance in each perforated cell. Peaceman equivalent radius reads [111]:

$$r_e = 0.28 \frac{\left(\sqrt{k_y/k_x}\delta x^2 + \sqrt{k_x/k_y}\delta y^2\right)^{1/2}}{(k_y/k_x)^{1/4} + (k_x/k_y)^{1/4}} \tag{3.65}$$

By including gravity forces in the well and assuming hydrostatic equilibrium, the

production rate for phase x from a perforation numbered j is:

$$q_{\mathrm{x}j} = WI_j M_{\mathrm{x}j}(P_j - P_{wf} - \delta P_j) \tag{3.66}$$

where, WI is well index:

$$WI = \frac{H\sqrt{k_x k_y}}{\ln(r_e/r_w) + S} \tag{3.67}$$

M_{x} is phase mobility:

$$M_{\mathrm{x}} = \frac{k_{\mathrm{rx}}}{B_{\mathrm{x}}\mu_{\mathrm{x}}} \tag{3.68}$$

and δP_j is the effective hydrostatic pressure difference for phase x at perforation j:

$$\delta P_j = \rho_{\mathrm{x}} g(Z_j - Z_{wf}) \tag{3.69}$$

where, Z_j is the vertical depth of grid j and Z_{wf} is bottomhole depth.

To couple or integrate a 3-D numerical reservoir model with a pipeline network model in which the well is also included, the well equations used in both domains should be the same to ensure model consistency, which is commonly referred to as IPR overlap. Comparing Eq. 3.66 with Eq. 3.61, normalization of IPR should be performed so that the well total production rate calculated in the numerical reservoir model, which is the sum of the production from all the perforated cells, equals that calculated in the network domain.

$$q_{\mathrm{x}} = \sum_{j\in\mathrm{nPerf}} b_{\mathrm{x}j} q_{\mathrm{x}j} = \sum_{j\in\mathrm{nPerf}} b_{\mathrm{x}j} WI_j M_{\mathrm{x}j}(P_j - P_{wf} - \delta P_j) \tag{3.70}$$

Therefore, the normalized well inflow performance reads

$$q_{\mathrm{x}} = \hat{J}(\hat{P}_r - P_{wf}) \tag{3.71}$$

$$\hat{P}_r = \frac{\sum_{j\in\mathrm{nPerf}} b_{\mathrm{x}j} WI_j M_{\mathrm{x}j}(P_j - \delta P_j)}{\sum_{j\in\mathrm{nPerf}} b_{\mathrm{x}j} WI_j M_{\mathrm{x}j}} \tag{3.72}$$

$$\hat{J} = \sum_{j\in\mathrm{nPerf}} b_{\mathrm{x}j} WI_j M_{\mathrm{x}j} \tag{3.73}$$

where, $\hat{P}_r$ and $\hat{J}$ are the equivalent or normalized reservoir pressure and well productivity index, respectively. The IPR normalization is applied in the explicit coupling between a reservoir simulator and a network simulator in chapter 5.

Chapter 4

Fully Integrated Reservoir–Pipeline Network Modeling

The fully integrated reservoir–network simulation follows an *equation-oriented* approach where a set of equations describing the behavior of a system is formulated and solved. Such an approach is flexible in declaring unknown variables for different design purposes. For example, a designer may specify the pressure and temperature changes along a pipeline and the flow rate, and solve for the required diameter and insulation thickness, or he/she can specify the pipeline diameter and insulation to do the pressure and temperature calculation instead. In this work, the focus is on the latter case.

In this chapter, the pipeline network model is first constructed. The equations are then combined with a tank model and a 3-D full-scale reservoir model described in chapter 3, respectively, to form two fully integrated models.

4.1 Development of a simple integrated model with tank reservoir model

A simple integrated production model is established by combining steady-state network flow equations with dynamic reservoir performance predicted by a tank model.

4.1.1 Discretization of network equations

A network consists of paths and nodes and is specified by their interconnections. Basic conservation equations of mass, momentum, and energy, hold for the entire network: along each flow path and at each node. Primary variables of the network include the distribution of flow rate q_{x} for each phase x, pressure P and temperature T. Pressure and temperature fields in the network are shared for all the phases.

Considering the relationships between flow rate and pressure/temperature, staggered definition of unknown variables is convenient for the discretization of the differential equations. One can either define pressure and temperature unknowns at the nodes and flow rate in the flowpaths, or define flow rate at each node and pressure and temperature in the middle of each path, as in software OLGA. In this work, we adopt the former configuration because momentum and energy conservations imply pressure/temperature discontinuity at junctions.

An original network, such as the one depicted in Figure 4.1 (a), includes the minimum information needed to construct a network model. The network presents 4 pressure, 4 temperature, and 9 rate variables (3 for each phase). However, the temperature balance at the internal node n actually leads to two more imaginary temperature variables. Also, the length of each path may be too long to be assumed with uniform fluid properties. Therefore, to set up a well-posed set of equations, the original network is augmented in two senses:

1. to include imaginary nodes at the original internal junctions
2. to discrete the original paths into smaller segments

As illustrated in Figure 4.1 (b), each node in the augmented network is either an inlet or an outlet for a certain path and the paths in the augmented network are bounded by non-repeating nodes.

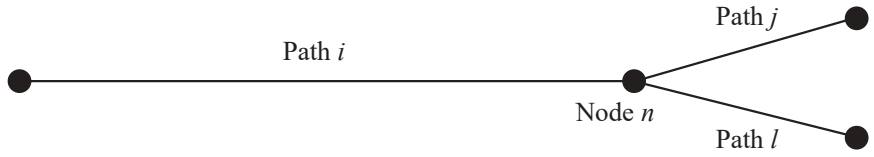

(a) Simplified Path-Node representation

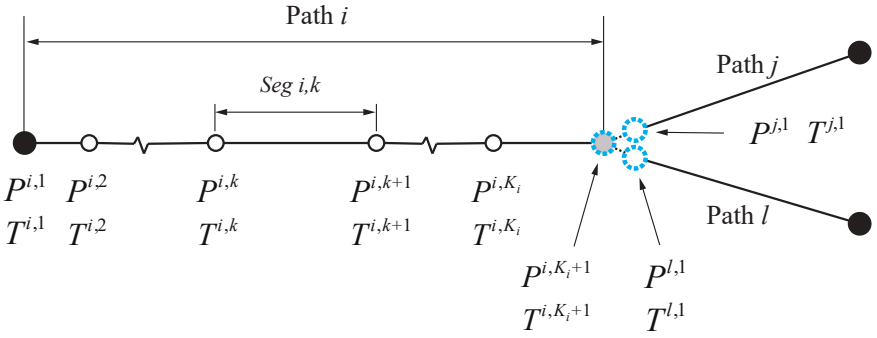

(b) Augmented Path-Node representation

Figure 4.1: Original and augmented network representation.

Under the augmented network framework, the definition of manifold and separator is consistent. As shown in Figure 4.1, the conjunction node n is a *manifold* if the flow direction is from right to left. In other words, fluids coming from path j and path l commingle at node n and flow into path i. In this case, the augmented nodes serve as the outlet of the inflow paths. The number of inflow paths that commingle at the manifold is the number of slots of the manifold. On the contrary, when the flow direction is reverted, the original node n is a *separator* where the fluid from path i is separated at the node n and different components of the inflow fluid may flow into different downstream flowpaths, i.e. path j and path l. Thus the augmented nodes serve as the inlet of the outflow paths.

Under the augmented network framework, the pressure equation for segment k in path i refers to the hydraulics relationship between the head and tail pressure for the segment and the flow within it, which is expressed as

$$P^{i,k} = P^{i,k+1} + (dP/dL)^{i,k} L^{i,k} \tag{4.1}$$

where, $(dP/dL)^{i,k}$ is calculated by Eq. 3.40.

Similarly, the temperature equation for the segment k in path i is expressed as

$$T^{i,k} = T^{i,k+1} + (dT/dL)^{i,k} L^{i,k} \tag{4.2}$$

where, $(dT/dL)^{i,k}$ is calculated by Eq. 3.54.

Each segment in the augmented network is assigned a segment type, representing the type of segment equations that should be used. The current program distinguishes four types of segment: *pipe*, *well*, *pump*, *valve*. A "pipe" segment applies the hydraulics and temperature relationships of Eq. 4.1 and 4.2. A "well" segment substitutes the pressure equation with the well inflow relationship of Eq. 3.64 and assumes isothermal inflow from the reservoir to bottomhole. The "pump" and "valve" segments are not relevant in this work.

The established augmented network framework is named the "NET" model in the rest of the thesis.

4.1.2 Closure of the problem

The NET model is steady-state, meaning that it calculates the pressure/temperature/rate distribution under certain stationary reservoir conditions. To simulate the life-long production variation, a dynamic reservoir model should be combined with it. The simple integrated model is to include a tank model for reservoir dynamic prediction. Since the reservoir is simplified as a single cell, reservoir pressure is nothing more than an inlet node in the network.

Consider a pipeline network without loop. The original network consists of N nodes, in which the number of inlets, outlets, manifolds and separators are N_{in}, N_{out}, N_{m} and N_{s}, respectively. For simplicity, assuming the number of slots of each manifold in the network is the same, denoted by m, and all the separators in the network are s phase separators. Thus the topology of the network gives

$$N = N_{\text{in}} + N_{\text{out}} + N_{\text{m}} + N_{\text{s}} \tag{4.3}$$

$$N_{\text{out}} = N_{\text{in}} - (m-1)N_{\text{m}} + (s-1)N_{\text{s}} \tag{4.4}$$

After augmenting the original network, the total number of augmented nodes and segments are denoted by N_a and N_b, respectively. The new topology gives

$$N_a = N_b + mN_{\text{m}} + sN_{\text{s}} + 1 \tag{4.5}$$

The number of equations for each augmented segments and augmented nodes are listed in Table 4.1.

Table 4.1: Number of equations in a network without loop

equation type	number of equations
augmented segment	$2N_b$
manifold	$(4+m)N_{\text{m}}$
separator	$5sN_{\text{s}}$

Given the relationships in Eqs. 4.3, 4.4 and 4.5, the difference between the total number of unknowns and total number of equations is

$$\left[3N - 1 + 2N_a\right] - \left[2N_b + (4+m)N_{\text{m}} + 5sN_{\text{s}}\right] = 4N_{\text{in}} + 1 \tag{4.6}$$

Therefore, to close the system, $4N_{\text{in}}+1$ equations should be provided, of which $4N_{\text{in}}$ are related with the reservoir model and the last one is the outlet pressure boundary condition.

4.1.3 A simple integrated model applying tank model

Combining the tank model in section 3.3.1 with the NET model, a simple integrated reservoir–network model is established. As shown in the previous section, to form a well-posed problem, the reservoir equations should provide appropriate boundaries for the network. The evolution of the boundary conditions, i.e. reservoir pressure and saturation, makes the possibility of prediction along the production life.

The unknown vector for the reservoir and pipeline network system is

$$\mathbf{U} = \left[q_{N\mathrm{w}}, q_{N\mathrm{o}}, q_{N\mathrm{g}}, P, T, S_{\mathrm{w}}, S_{\mathrm{g}}\right]^{\intercal} \tag{4.7}$$

The residual vector for the simple integrated model is

$$\mathbf{R} = \left[R_P, R_T, R_{\mathrm{w}}, R_{\mathrm{o}}, R_{\mathrm{g}}, R_{MB}, R_{S_{\mathrm{w}}}, R_{S_{\mathrm{g}}}, R_{bc}\right]^{\intercal} \tag{4.8}$$

Each component in the residual vector is explained as follows.

Mass conservation for each phase directly leads to the residuals of node mass conservation equations.

For water:

$$R_{\mathrm{w}} = q^j_{N\mathrm{w}} + F^{n,j}_{\mathrm{w}} \textstyle\sum_i A^{n,i} q^i_{N\mathrm{w}}, \quad \forall (i,j) \in \mathcal{U}_n, \forall n \in \mathcal{N}_{\mathrm{nn}} \tag{4.9}$$

For oil:

$$R_{\mathrm{o}} = q^j_{N\mathrm{o}} + F^{n,j}_{\mathrm{o}} \textstyle\sum_i A^{n,i} q^i_{N\mathrm{o}}, \quad \forall (i,j) \in \mathcal{U}_n, \forall n \in \mathcal{N}_{\mathrm{nn}} \tag{4.10}$$

For gas:

$$R_{\mathrm{g}} = q^j_{N\mathrm{g}} + F^{n,j}_{\mathrm{g}} \textstyle\sum_i A^{n,i} q^i_{N\mathrm{g}} + (F^{n,j}_{\mathrm{o}} - F^{n,j}_{\mathrm{g}}) \sum_i A^{n,i} R^n_s q^i_{N\mathrm{o}}, \forall (i,j) \in \mathcal{U}_n, n \in \mathcal{N}_{\mathrm{nn}} \tag{4.11}$$

The pressure-related residuals include residual of segment pressure drop equation (momentum equation) and node pressure continuity:

$$\begin{aligned}
R_P &= \left[R_{Ps}, R_{Pn}\right] \\
R_{Ps} &= P^{i,k} - P^{i,k+1} + \Delta P^{i,k}, \quad \forall i \in \mathcal{I}, \forall k \in \mathcal{S}_i && (4.12) \\
R_{Pn} &= A^{n,i} P^{i,K_i+1} - A^{n,j} P^{j,1}, \quad \forall (i,j) \in \mathcal{U}_n, \forall n \in \mathcal{N}_{\mathrm{nn}} && (4.13)
\end{aligned}$$

Correspondingly, the temperature-related residuals (energy equations) include residuals of the segment temperature drop equation and node temperature mixing relationship:

$$\begin{aligned}
R_T &= \left[R_{Ts}, R_{Tn}\right] \\
R_{Ts} &= T^{i,k} - T^{i,k+1} + \Delta T^{i,k}, \quad \forall i \in \mathcal{I}, k \in \mathcal{S}_i && (4.14) \\
R_{Tn} &= A^{n,j} T^{j,1} - \frac{\sum_i A^{n,i} w^i c_p^{K_i} T^{i,K_i+1}}{\sum_i A^{n,i} w^i c_p^{K_i}}, \quad \forall (i,j) \in \mathcal{U}_n, \forall n \in \mathcal{N}_{\mathrm{nn}} && (4.15)
\end{aligned}$$

Residual of the tank material balance equation (see Eq. 3.21):

$$R_{MB} = \Delta PV - c_r \Delta P_r \tag{4.16}$$

Residual of the tank water saturation equation:

$$R_{S_w} = S_{\mathrm{w}} - V_{\mathrm{w}}/PV \tag{4.17}$$

Residual of the tank gas saturation equation:

$$R_{S_g} = S_{\mathrm{g}} - V_{\mathrm{g}}/PV \tag{4.18}$$

Boundary conditions include inflow stream gas-oil-ratio and watercut, reservoir pressure and temperature, and topside separator pressure (outlet pressure), which are the $4N_{\mathrm{in}}+1$ equations needed to close the system (section 4.1.2). When applying a tank model, the reservoir pressure is replaced by the material balance equation to capture the reservoir dynamic. Thus, the boundary conditions include:

$$\begin{aligned}
R_{bc} &= \left[R_{fg}, R_{fw}, R_{Tr}, R_{Pout}\right] \\
R_{fg} &= q^i_{N\mathrm{g}} - q^i_{N\mathrm{o}}(f_{\mathrm{g}} + R_{swf}), && \forall i \in \mathcal{I}_{\mathrm{in}} && (4.19)\\
R_{fw} &= q^i_{N\mathrm{w}} - q^i_{N\mathrm{o}} f_{\mathrm{w}}, && \forall i \in \mathcal{I}_{\mathrm{in}} && (4.20)\\
R_{Tr} &= A^{n,i} T^{i,1} - T^n_{\mathrm{in}}, && \forall n \in \mathcal{N}_{\mathrm{in}} && (4.21)\\
R_{Pout} &= A^{n,i} P^{i,K_i+1} + P^n_{\mathrm{out}}, && \forall n \in \mathcal{N}_{\mathrm{out}} && (4.22)
\end{aligned}$$

Eqs. 4.9 to 4.22 form the simple integrated model. It is solved using the Newton-Raphson method. In each iteration, a set of linearized equations in the form of $\mathbf{J}\Delta\mathbf{U} = -\mathbf{R}$ is solved. Figure 4.3 provides a glimpse on the Jacobian matrix $\mathbf{J}$ for the test example 1 presented below.

4.1.4 Test example 1

To test and verify the performance of the simple IPM tool established above, a simple one-well system is modeled. Simulation results from the model are compared with those from industrial standard software OLGA to verify the developed program in MATLAB environment.

The example reservoir lies 5000 m below sea level, with 2000 m of water depth in the field region. Initial reservoir pressure and temperature are 550 bar and 80 °C, respectively. One producer is placed in the reservoir tank, which is tied to the FPSO with 6000 m of subsea flowline, as illustrated in Figure 4.2. Well production string and the riser are simplified as vertical straight lines and the seabed is considered flat. The reservoir is developed by water injection. Since the focus is on production, the injection well is not shown in the sketch, but the injection rate is calculated in the simulation. Well productivity is 20 Sm^3/day/bar. The diameter of the entire flowpath including tubing, subsea flowline, and riser, is 4 inch with insulation to a

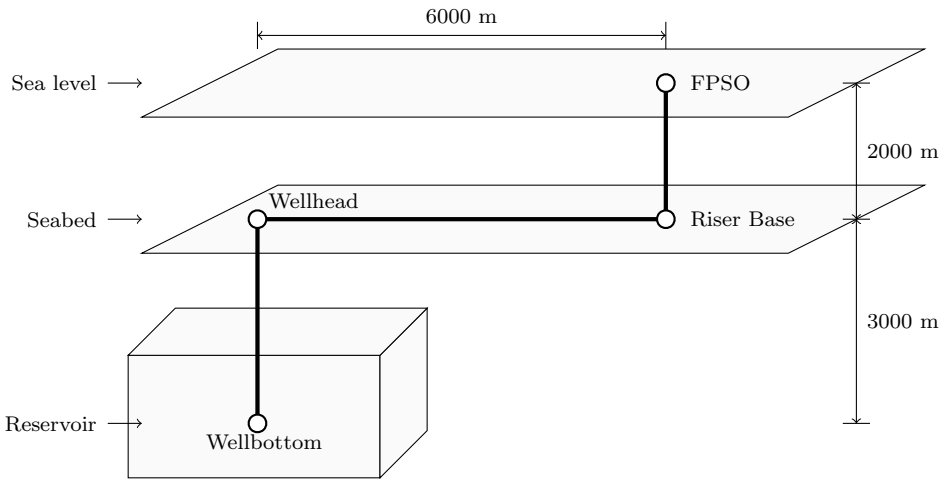

Figure 4.2: Sketch of the integrated model for test example 1.

U-value of 4.5 W/m^2-C. System outlet pressure, i.e. the separator pressure on the FPSO, is 20 bar. Fluid properties are listed in Table 4.2 and black oil correlations are used.

Table 4.2: Fluid property, test example 1

Oil API	24.5
GOR, Sm^3/Sm^3	135.5
Gas specific gravity	0.92
Bubble point, bar	305.7

It is obligated to provide an injection plan for material balance calculation. In this test example, the following strategy is applied. Initially, the injector injects at most 8000 stb/day, allowing the reservoir pressure to reduce and production comes from pressure depletion. When the reservoir pressure reduces to a level that is insufficient to deliver any flow to the topside, the injection rate is increased to balance out the production rate and maintain the reservoir pressure at constant. With further development, watercut gradually increases and consequently, the increase of liquid density makes the reservoir pressure insufficient to deliver any flow. The injection rate is again increased to recover reservoir pressure for production. In practice, this development strategy is commonly adopted.

The example model contains 453 equations, as well as 453 unknown variables. The Jacobian matrix takes the banded form as shown in Figure 4.3, with dimension of 453×453 and 3112 non-zeros.

Simulation results are shown in Figure 4.4. The model results are compared with the solutions from the industrial standard software OLGA, which is also combined with the same tank model for reservoir dynamics prediction. The cross plot comparison verifies the coded NET model, as shown in 4.5.

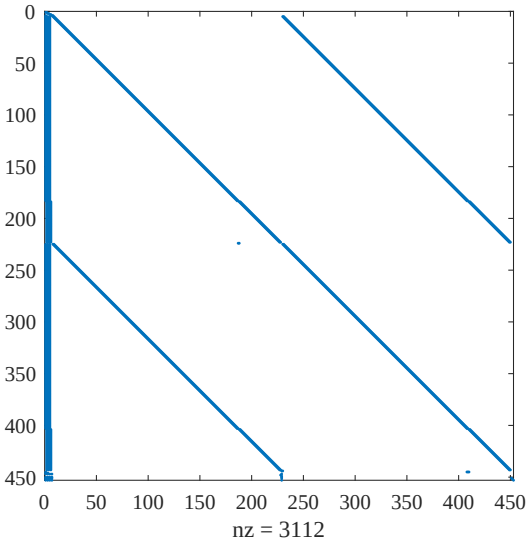

Figure 4.3: Jacobian matrix of the simple integrated model, test example 1.

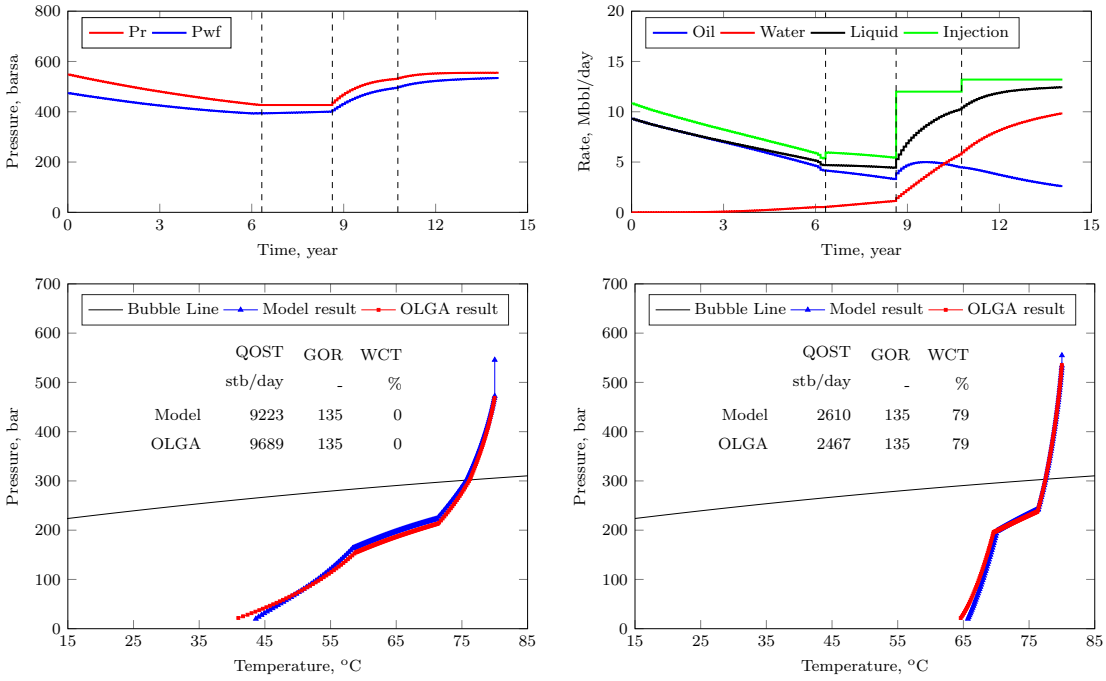

Figure 4.4: Simulation results for test example 1. Upper left: reservoir pressure and well bottomhole pressure; upper right: production and injection rates; lower left: pressure–temperature route at the first simulation step; lower right: pressure–temperature route at the last simulation step.

It is shown in Figure 4.5 that the relative differences between the NET code and OLGA on temperature, pressure, and flow rates are within ±10%. The main difference is related to the liquid holdup calculation. Liquid holdup calculated by the Beggs-Brill method is higher than that calculated from OLGA, especially in low holdup level (lower than 0.5).

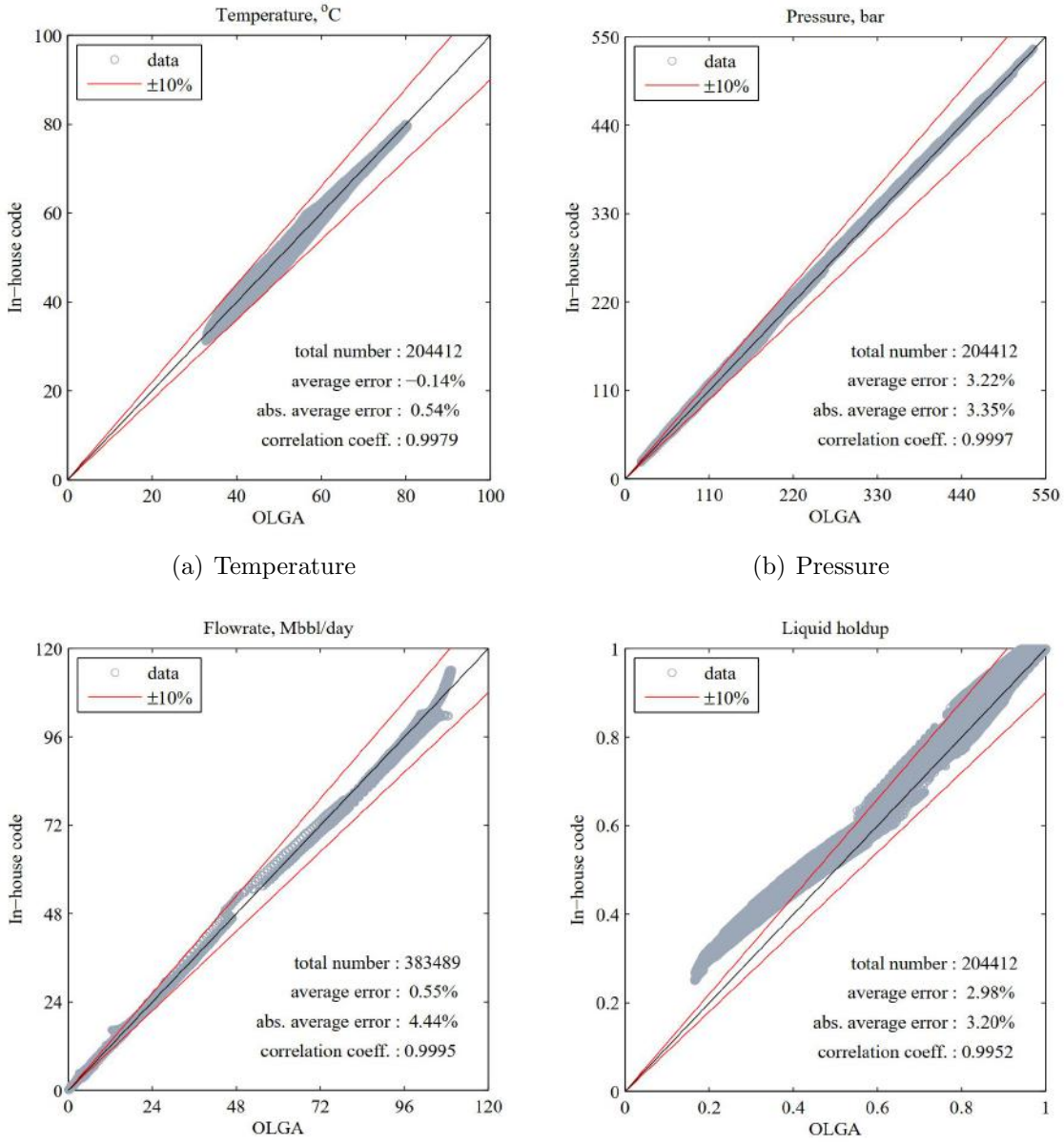

(a) Temperature

(b) Pressure

(c) Oil/water flowrate

(d) Liquid holdup

Figure 4.5: Cross plot of results from in-house code network model NET and commercial software OLGA.

4.2 Development of a fully integrated model with 3-D reservoir model

This section presents a more comprehensive model combining the augmented network framework presented in section 4.1 with a 3-D numerical reservoir model.

4.2.1 Discretization of reservoir equations

Applying Darcy's law (Eq. 3.29–3.31) and capillary pressure (Eq. 3.33 and 3.34) to Eq. 3.24–3.26, the following governing equations are obtained:
conservation of water phase:

$$\partial_t\big(\phi b_{\mathrm{w}} S_{\mathrm{w}}\big) + \nabla\Big[- \lambda_{\mathrm{w}}\big(\nabla P_{\mathrm{o}} - \nabla P_{\mathrm{cow}} - \gamma_{\mathrm{w}}\nabla Z\big)\Big] = b_{\mathrm{w}} q_{\mathrm{w}}/V \tag{4.23}$$

conservation of oil phase:

$$\partial_t\big(\phi b_{\mathrm{o}} S_{\mathrm{o}}\big) + \nabla\Big[- \lambda_{\mathrm{o}}\big(\nabla P_{\mathrm{o}} - \gamma_{\mathrm{o}}\nabla Z\big)\Big] = b_{\mathrm{o}} q_{\mathrm{o}}/V \tag{4.24}$$

conservation of gas phase:

$$\begin{aligned}\partial_t\big[\phi(b_{\mathrm{g}} S_{\mathrm{g}} + R_s b_{\mathrm{o}} S_{\mathrm{o}})\big] + \nabla\Big[- \lambda_{\mathrm{g}}\big(\nabla P_{\mathrm{o}} + \nabla P_{\mathrm{cgo}} - \gamma_{\mathrm{g}}\nabla Z\big) - R_s\lambda_{\mathrm{o}}\big(\nabla P_{\mathrm{o}} - \gamma_{\mathrm{o}}\nabla Z\big)\Big] \\ = (b_{\mathrm{g}} q_{\mathrm{g}} + R_s b_{\mathrm{o}} q_{\mathrm{o}})/V\end{aligned} \tag{4.25}$$

where,

$$\lambda_{\mathrm{w}} = \frac{b_{\mathrm{w}} k k_{\mathrm{rw}}}{\mu_{\mathrm{w}}}, \quad \lambda_{\mathrm{o}} = \frac{b_{\mathrm{o}} k k_{\mathrm{ro}}}{\mu_{\mathrm{o}}}, \quad \lambda_{\mathrm{g}} = \frac{b_{\mathrm{g}} k k_{\mathrm{rg}}}{\mu_{\mathrm{g}}}$$

Taken the oil mass conservation equation (3.22) as an example. The implicit time integral scheme results in the following algebraic equation for a computation timestep t with timestep length Δt^t:

$$\frac{(\phi b_{\mathrm{o}} S_{\mathrm{o}})^{t+1} - (\phi b_{\mathrm{o}} S_{\mathrm{o}})^t}{\Delta t^t} + \nabla\Big[- \lambda_{\mathrm{o}}^{t+1}(\nabla P_{\mathrm{o}}^{t+1} - \gamma_{\mathrm{o}}^{t+1}\nabla Z)\Big] = q_{Wo}^{t+1}/V \tag{4.26}$$

To keep a concise notation, the subscript $t+1$ is dropped and the notation t is rewritten as 0:

$$\frac{\phi b_o S_o - (\phi b_o S_o)^0}{\Delta t^0} + \nabla\Big[- \lambda_{\mathrm{o}}(\nabla P_{\mathrm{o}} - \gamma_{\mathrm{o}}\nabla Z)\Big] = q_{Wo}/V \tag{4.27}$$

Research on the numerical solution of the Laplace/Poisson equation has a long tradition, and there exist a large number of different finite-difference and finite-volume methods, as well as finite-element methods, which all have their merits. In

classical finite-difference methods, partial differential equations are approximated by replacing the derivatives with appropriate divided differences between point-values on a discrete set of points in the domain. In finite-volume methods, on the other hand, the unknown functions are represented in terms of average values over a set of finite-volumes, over which the PDE model is required to hold in an averaged sense. Although finite-difference and finite-volume methods have fundamentally different interpretations and derivations, for certain lower-order methods, the discrete equations derived for the cell-centered values by both methods are identical [93].

To discretize the convection term in a 3-D cell-centered Cartesian grid system by finite difference, transmissibilities of each phase at the faces between neighboring cells are defined by:

$$
\begin{aligned}
T_{\mathrm{w}x} &= \frac{\delta y \delta z}{\delta x}\lambda_{\mathrm{w}}, \quad T_{\mathrm{o}x} = \frac{\delta y \delta z}{\delta x}\lambda_{\mathrm{o}}, \quad T_{\mathrm{g}x} = \frac{\delta y \delta z}{\delta x}\lambda_{\mathrm{g}}, \quad T_{\mathrm{gd}x} = \frac{\delta y \delta z}{\delta x}R_s\lambda_{\mathrm{o}} \\
T_{\mathrm{w}y} &= \frac{\delta x \delta z}{\delta y}\lambda_{\mathrm{w}}, \quad T_{\mathrm{o}y} = \frac{\delta x \delta z}{\delta y}\lambda_{\mathrm{o}}, \quad T_{\mathrm{g}y} = \frac{\delta x \delta z}{\delta y}\lambda_{\mathrm{g}}, \quad T_{\mathrm{gd}y} = \frac{\delta x \delta z}{\delta y}R_s\lambda_{\mathrm{o}} \\
T_{\mathrm{w}z} &= \frac{\delta x \delta y}{\delta z}\lambda_{\mathrm{w}}, \quad T_{\mathrm{o}z} = \frac{\delta x \delta y}{\delta z}\lambda_{\mathrm{o}}, \quad T_{\mathrm{g}z} = \frac{\delta x \delta y}{\delta z}\lambda_{\mathrm{g}}, \quad T_{\mathrm{gd}z} = \frac{\delta x \delta y}{\delta z}R_s\lambda_{\mathrm{o}}
\end{aligned}
$$

Taking again the oil phase as an example, the transmissbilities at the six faces of a reservoir cell numbered (i, j, k) include:

$$
\begin{aligned}
\left[T_x\right]^{i+\frac{1}{2},j,k} &= \frac{\delta y_j \delta z_k}{\delta x_{i+\frac{1}{2}}}\lambda^{i+\frac{1}{2},j,k}, & \left[T_x\right]^{i-\frac{1}{2},j,k} &= \frac{\delta y_j \delta z_k}{\delta x_{i-\frac{1}{2}}}\lambda^{i-\frac{1}{2},j,k} \\
\left[T_y\right]^{i,j+\frac{1}{2},k} &= \frac{\delta x_j \delta z_k}{\delta y_{j+\frac{1}{2}}}\lambda^{i,j+\frac{1}{2},k}, & \left[T_y\right]^{i,j-\frac{1}{2},k} &= \frac{\delta x_j \delta z_k}{\delta y_{j-\frac{1}{2}}}\lambda^{i,j-\frac{1}{2},k} \\
\left[T_z\right]^{i,j,k+\frac{1}{2}} &= \frac{\delta x_j \delta y_j}{\delta z_{k+\frac{1}{2}}}\lambda^{i,j,k+\frac{1}{2}}, & \left[T_z\right]^{i,j,k-\frac{1}{2}} &= \frac{\delta x_j \delta y_j}{\delta z_{k-\frac{1}{2}}}\lambda^{i,j,k-\frac{1}{2}}
\end{aligned}
$$

where, the subscript o for T_x, T_y, T_z and λ is omitted. Furthermore, the operator Δ is defined as the finite difference in three-dimensional system, specifically:

$$
\begin{aligned}
\Delta T \Delta P \quad &= \Delta_x T_x \Delta_x P + \Delta_y T_y \Delta_y P + \Delta_z T_z \Delta_z P \qquad (4.28) \\
\Delta_x T_x \Delta_x P &= \left[T_x\right]^{i+\frac{1}{2},j,k}\left[P^{i+1,j,k} - P^{i,j,k}\right] + \left[T_x\right]^{i-\frac{1}{2},j,k}\left[P^{i-1,j,k} - P^{i,j,k}\right] \\
\Delta_y T_y \Delta_y P &= \left[T_y\right]^{i,j+\frac{1}{2},k}\left[P^{i,j+1,k} - P^{i,j,k}\right] + \left[T_y\right]^{i,j-\frac{1}{2},k}\left[P^{i,j-1,k} - P^{i,j,k}\right] \\
\Delta_z T_z \Delta_z P &= \left[T_z\right]^{i,j,k+\frac{1}{2}}\left[P^{i,j,k+1} - P^{i,j,k}\right] + \left[T_z\right]^{i,j,k-\frac{1}{2}}\left[P^{i,j,k-1} - P^{i,j,k}\right]
\end{aligned}
$$

$$
\begin{aligned}
\Delta T\gamma\Delta Z \quad &= \Delta_x T_x\gamma\Delta_x Z + \Delta_y T_y\gamma\Delta_y Z + \Delta_z T_z\gamma\Delta_z Z \qquad (4.29)\\
\Delta_x T_x\gamma\Delta_x Z &= \big[T_x\gamma\big]^{i+\frac{1}{2},j,k}\big[Z^{i+1,j,k} - Z^{i,j,k}\big] + \big[T_x\gamma\big]^{i-\frac{1}{2},j,k}\big[Z^{i-1,j,k} - Z^{i,j,k}\big]\\
\Delta_y T_y\gamma\Delta_y Z &= \big[T_y\gamma\big]^{i,j+\frac{1}{2},k}\big[Z^{i,j+1,k} - Z^{i,j,k}\big] + \big[T_y\gamma\big]^{i,j-\frac{1}{2},k}\big[Z^{i,j-1,k} - Z^{i,j,k}\big]\\
\Delta_z T_z\gamma\Delta_z Z &= \big[T_z\gamma\big]^{i,j,k+\frac{1}{2}}\big[Z^{i,j,k+1} - Z^{i,j,k}\big] + \big[T_z\gamma\big]^{i,j,k-\frac{1}{2}}\big[Z^{i,j,k-1} - Z^{i,j,k}\big]
\end{aligned}
$$

Finally, the convection term in Eq. 4.27 is discretized as:

$$
\nabla\big[-\lambda_{\mathrm{o}}(\nabla P_{\mathrm{o}} - \gamma_{\mathrm{o}}\nabla Z)\big] = -\big[\Delta T_{\mathrm{o}}\Delta P_{\mathrm{o}} - \Delta T_{\mathrm{o}}\gamma_{\mathrm{o}}\Delta Z\big]/\delta x\delta y\delta z \qquad (4.30)
$$

The discretization of the conversion term in water equation results in:

$$
\begin{aligned}
&\nabla\Big[-\lambda_{\mathrm{w}}\big(\nabla P_{\mathrm{o}} - \nabla P_{\mathrm{cow}} - \gamma_{\mathrm{w}}\nabla Z\big)\Big]\\
&\qquad = -\big[\Delta T_{\mathrm{w}}\Delta P_{\mathrm{o}} - \Delta T_{\mathrm{w}}\Delta P_{\mathrm{cow}} - \Delta T_{\mathrm{w}}\gamma_{\mathrm{w}}\Delta Z\big]/\delta x\delta y\delta z \qquad (4.31)
\end{aligned}
$$

and for gas equation:

$$
\begin{aligned}
&\nabla\Big[-\lambda_{\mathrm{g}}\big(\nabla P_{\mathrm{o}} + \nabla P_{\mathrm{cgo}} - \gamma_{\mathrm{g}}\nabla Z\big) - R_s\lambda_{\mathrm{o}}\big(\nabla P_{\mathrm{o}} - \gamma_{\mathrm{o}}\nabla Z\big)\Big]\\
&= -\big[(\Delta T_{\mathrm{g}} + \Delta T_{\mathrm{gd}})\Delta P_{\mathrm{o}} + \Delta T_{\mathrm{g}}\Delta P_{\mathrm{cgo}} - \Delta T_{\mathrm{g}}\gamma_{\mathrm{g}}\Delta Z - \Delta T_{\mathrm{gd}}\gamma_{\mathrm{o}}\Delta Z\big]/\delta x\delta y\delta z \qquad (4.32)
\end{aligned}
$$

4.2.2 A fully integrated model applying 3-D reservoir model

Combining the 3-D numerical reservoir model with the augmented network framework presented in section 4.1, a fully integrated model is established.

The unknown vectors for reservoir and pipeline network system are respectively,

$$
\mathbf{U}_{res} = \big[P_R, S_{\mathrm{w}}, X_{\mathrm{g}}, q_{W\mathrm{w}}, q_{W\mathrm{o}}, q_{W\mathrm{g}}, P_{wf}\big]^{\intercal} \qquad (4.33)
$$

$$
\mathbf{U}_{net} = \big[P_N, T_N, q_{N\mathrm{w}}, q_{N\mathrm{o}}, q_{N\mathrm{g}}\big]^{\intercal} \qquad (4.34)
$$

The residual vectors for the fully integrated model are

$$
\mathbf{R}_{res} = \big[R_{Rw}, R_{Ro}, R_{Rg}, R_{Ww}, R_{Wo}, R_{Wg}, R_{BHP}\big]^{\intercal} \qquad (4.35)
$$

$$
\mathbf{R}_{net} = \big[R_{NP}, R_{NT}, R_{Nw}, R_{No}, R_{Ng}, R_{bc}\big]^{\intercal} \qquad (4.36)
$$

The residuals R_{Nw}, R_{No}, R_{Ng}, R_{NP}, and R_{NT}, correspond to the ones applied in the simple model (Eq. 4.9–4.15). The extra subscript N is used to distinguish them from the residuals for the reservoir domain. Each component in the residual vectors is as follows.

Residual of water conservation equation:

$$R_{Rw}= (\delta x\delta y\delta z/\delta t)\big[\phi b_{\mathrm{w}}S_{\mathrm{w}} - \phi^0 b^0_{\mathrm{w}}S^0_{\mathrm{w}}\big] \\ -\big[\Delta T_{\mathrm{w}}\Delta P_R - \Delta T_{\mathrm{w}}\Delta P_{\mathrm{cow}} - \Delta T_{\mathrm{w}}\gamma_{\mathrm{w}}\Delta Z\big] - q_{W\mathrm{w}} \tag{4.37}$$

Residual of oil conservation equation:

$$R_{Ro}= (\delta x\delta y\delta z/\delta t)\big[\phi b_{\mathrm{o}}S_{\mathrm{o}} - \phi^0 b^0_{\mathrm{o}}S^0_{\mathrm{o}}\big] - \big[\Delta T_{\mathrm{o}}\Delta P_R - \Delta T_{\mathrm{o}}\gamma_{\mathrm{o}}\Delta Z\big] - q_{W\mathrm{o}} \tag{4.38}$$

Residual of gas conservation equation:

$$R_{Ro}= (\delta x\delta y\delta z/\delta t)\big[\phi(b_{\mathrm{g}}S_{\mathrm{g}} + R_s b_{\mathrm{o}}S_{\mathrm{o}}) - \phi^0(b^0_{\mathrm{g}}S^0_{\mathrm{g}} + R_s b^0_{\mathrm{o}}S^0_{\mathrm{o}})\big] \\ -\big[(\Delta T_{\mathrm{g}} + \Delta T_{\mathrm{gd}})\Delta P_R + \Delta T_{\mathrm{g}}\Delta P_{\mathrm{cgo}} - \Delta T_{\mathrm{g}}\gamma_{\mathrm{g}}\Delta Z - \Delta T_{\mathrm{gd}}\gamma_{\mathrm{o}}\Delta Z\big] - q_{W\mathrm{g}} \tag{4.39}$$

Residual of well water flow equation:

$$R_{Ww} = q_{W\mathrm{w}} - \sum_{n\in perf} WI^n M^n_{\mathrm{w}}(P^n_R - P_{Rwf} - \delta P^n_R) \tag{4.40}$$

Residual of well oil flow equation:

$$R_{Wo} = q_{W\mathrm{o}} - \sum_{n\in perf} WI^n M^n_{\mathrm{o}}(P^n_R - P_{Rwf} - \delta P^n_R) \tag{4.41}$$

Residual of well gas flow equation:

$$R_{Wg} = q_{W\mathrm{g}} - \sum_{n\in perf} WI^n (M^n_{\mathrm{g}} + R_s M^n_{\mathrm{o}})(P^n_R - P_{Rwf} - \delta P^n_R) \tag{4.42}$$

Residual of network water equation:

$$R_{Nw}= q^j_{N\mathrm{w}} + F^{n,j}_{\mathrm{w}} \textstyle\sum_i A^{n,i} q^i_{N\mathrm{w}}, \quad \forall (i,j)\in \mathcal{U}_n, \forall n \in \mathcal{N}_{\mathrm{nn}} \tag{4.43}$$

Residual of network oil equation:

$$R_{No}= q^j_{N\mathrm{o}} + F^{n,j}_{\mathrm{o}} \textstyle\sum_i A^{n,i} q^i_{N\mathrm{o}}, \quad \forall (i,j)\in \mathcal{U}_n, \forall n \in \mathcal{N}_{\mathrm{nn}} \tag{4.44}$$

Residual of network gas equation:

$$R_{Ng}= q^j_{N\mathrm{g}} + F^{n,j}_{\mathrm{g}} \textstyle\sum_i A^{n,i} q^i_{N\mathrm{g}} + (F^{n,j}_{\mathrm{o}} - F^{n,j}_{\mathrm{g}}) \sum_i A^{n,i} R^n_s q^i_{N\mathrm{o}}, \forall (i,j)\in \mathcal{U}_n, n\in \mathcal{N}_{\mathrm{nn}} \tag{4.45}$$

Residual of network pressure-related residuals:

$$
\begin{aligned}
R_{NP} &= \left[R_{Ps}, R_{Pn}\right] \\
R_{Ps} &= P_N^{i,k} - P_N^{i,k+1} + \Delta P_N^{i,k}, \quad \forall i \in \mathcal{I}, \forall k \in \mathcal{S}_i && (4.46) \\
R_{Pn} &= A^{n,i} P_N^{i,K_i+1} - A^{n,j} P_N^{j,1}, \quad \forall (i,j) \in \mathcal{U}_n, \forall n \in \mathcal{N}_{\text{nn}} && (4.47)
\end{aligned}
$$

Residual of network temperature-related residuals:

$$
\begin{aligned}
R_{NT} &= \left[R_{Ts}, R_{Tn}\right] \\
R_{Ts} &= T_N^{i,k} - T_N^{i,k+1} + \Delta T_N^{i,k}, \quad \forall i \in \mathcal{I}, k \in \mathcal{S}_i && (4.48) \\
R_{Tn} &= A^{n,j} T_N^{j,1} - \frac{\sum_i A^{n,i} w^i c_p^{K_i} T_N^{i,K_i+1}}{\sum_i A^{n,i} w^i c_p^{K_i}}, \quad \forall (i,j) \in \mathcal{U}_n, \forall n \in \mathcal{N}_{\text{nn}} && (4.49)
\end{aligned}
$$

Residual of reservoir–network bottomhole equilibrium:

$$
R_{BHP} = P_{Rwf} - P_{Nwf} \tag{4.50}
$$

Residual of boundary conditions, including the outlet pressure on the topside, and reservoir temperature:

$$
\begin{aligned}
R_{bc} &= \left[R_{Tr}, R_{Pout}\right] \\
R_{Tr} &= A^{n,i} T_N^{i,1} - T_{\text{in}}^n, \quad \forall n \in \mathcal{N}_{\text{in}} && (4.51) \\
R_{Pout} &= A^{n,i} P_N^{i,K_i+1} + P_{\text{out}}^n, \quad \forall n \in \mathcal{N}_{\text{out}} && (4.52)
\end{aligned}
$$

Eqs. 4.9 to 4.22 form the fully integrated model. It is solved using the Newton-Raphson method, as shown by the pseudo code in Algorithm 1. The reservoir equations in MRST black oil module and the embedded solution algorithm are modified and applied. In each iteration, the set of linearized equations can be expressed by $\mathbf{J}\Delta\mathbf{U} = -\mathbf{R}$. Figure 4.8 provides a glimpse on the Jacobian matrix $\mathbf{J}$ for the test example 2 presented below.

Algorithm 1 Fully integrated reservoir–network solution algorithm

```
Initialization: x0 = [U_res^0; U_net^0], x ← x0, u ← u0
for t ← 1, nStep do
    while not converged do
        get residuals: R(x) = R(x, u)
        solve linear problem: Δx = −R(x)/J(x)
        check if converged
        update: x ← x + Δx
    end while
end for
```

4.2.3 Test example 2

A simple one-well model is built to test the performance of the fully integrated model established above. In this example, the focus is on comparing the results of an integrated model with a stand-alone reservoir model to show the importance of the integrated approach. Since the coded network model has been verified in test example 1 (section 4.1.4), the results of this test example 2 is believed to be reliable as well. A comparison with explicitly coupled simulations, which will be presented in the next chapter (section 5.5), also supports the validity of the coded model in MATLAB environment.

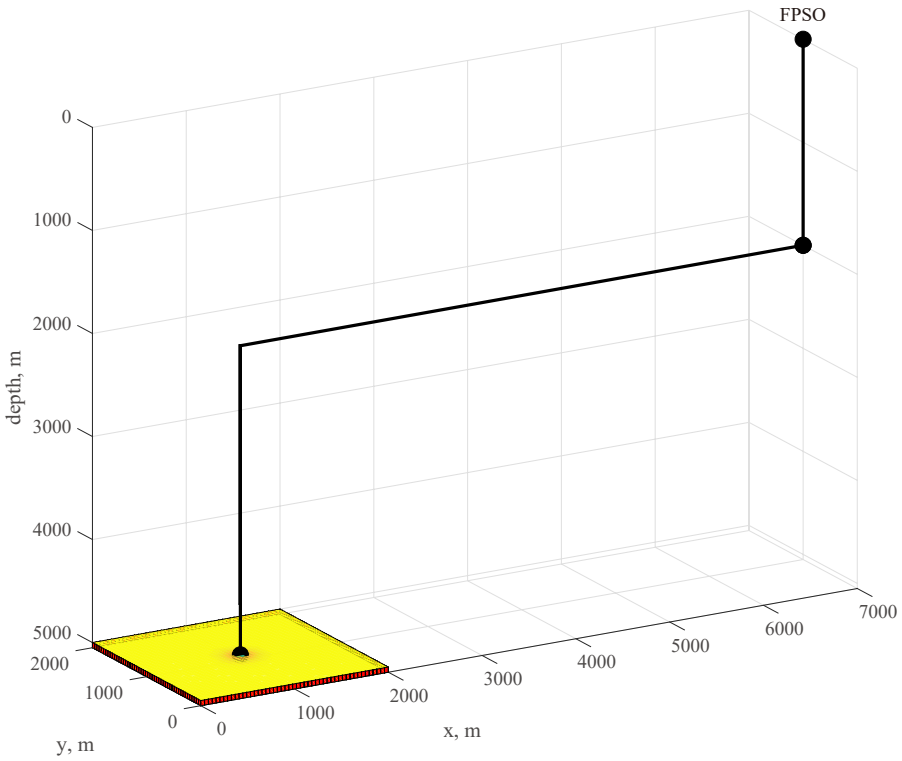

Figure 4.6: Sketch of the integrated model for test example 2.

The fluid properties used in this test example 2 is the same as those in test example 1. The reservoir consists of a homogeneous $2000\times2000\times50$ m^3 sandbox with an isotropic permeability of 500 mD, represented on a regular $49\times49\times1$ Cartesian grid. The four sides are set as constant pressure boundaries to avoid the need to place injection wells. Two simulations are performed and compared:

1. MRST stand-alone, where only the reservoir domain is simulated under constant bottomhole pressure.

2. MRST–NET fully-implicit, where the tubing, flowline, and riser for the well are considered, and the fully integrated model is applied. A sketch of the integrated model is shown in Figure 4.6.

Each simulation involves 15 years of production with an average timestep length of 1 month. Simulated production curves are shown in Figure 4.7. It is clear that the stand-alone reservoir simulation with predefined well bottomhole pressure can not reflect the impact of the production line on well production. There is a large deviation in production rates for the integrated and non-integrated models. The constant bottomhole pressure setting for the stand-alone simulation is facing a risk of underestimating production in early development years and overestimating production in late years. With the fully integrated model, more realistic variations of the bottomhole pressure are predicted since the back pressure from the production line in each simulation step is included.

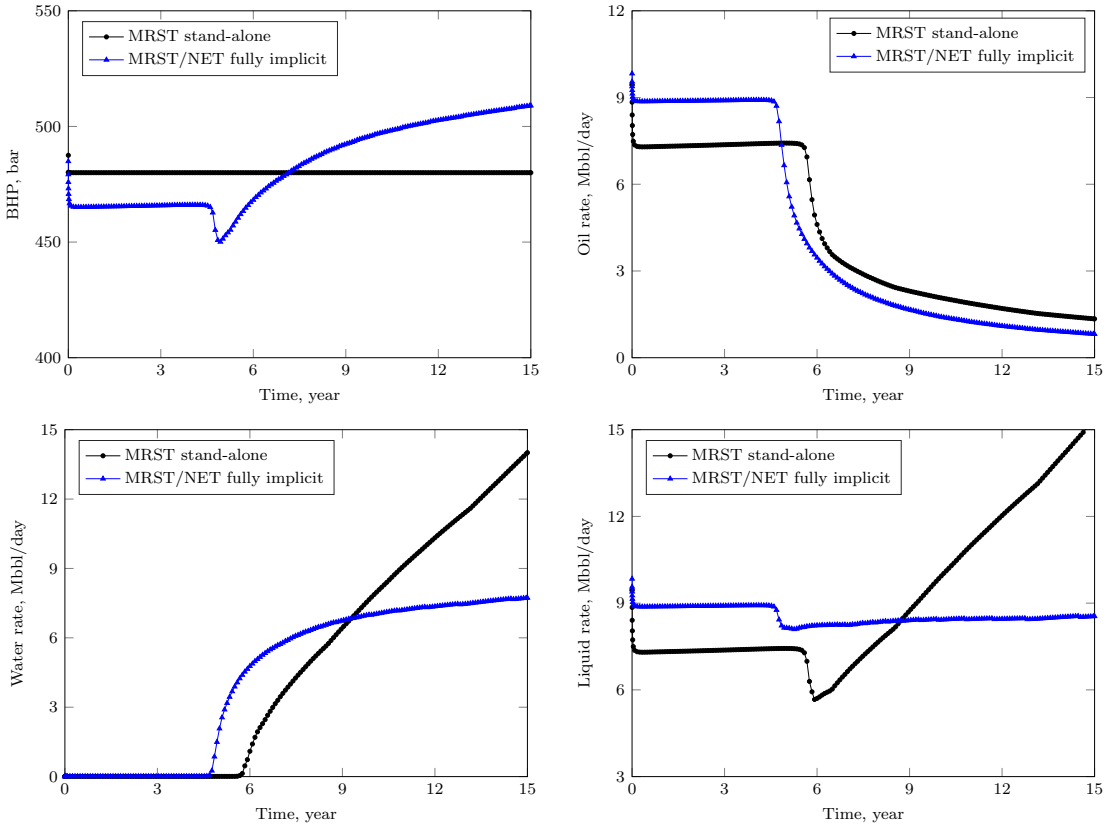

Figure 4.7: Result comparison between stand-alone and fully integrated simulations.

Figure 4.8 shows the Jacobian matrix of the fully integrated model. It takes the partitioned banded form as shown in Figure 4.8, with size 7657×7657 and 74257 non-zeros. Compared to Figure 4.3, the 3-D reservoir equations clearly make up most of the model.

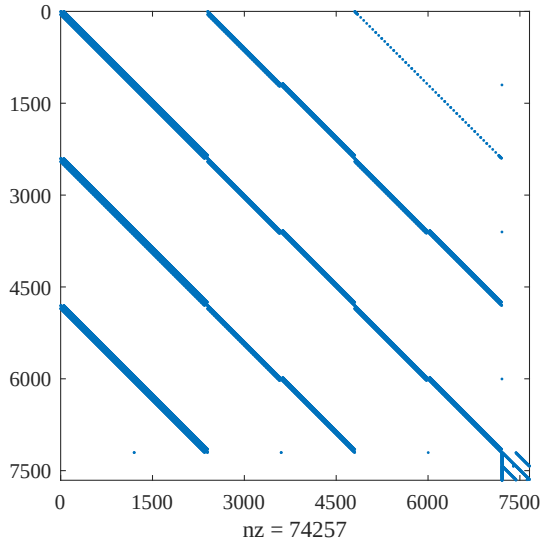

Figure 4.8: Jacobian matrix of the fully integrated model, test example 2.

4.3 Comparison and comments on the two fully integrated models

The two fully integrated models established in this chapter differ only in the method used in predicting reservoir dynamics. Naturally, the advantages and drawbacks of a tank model and a full-field 3-D model are inherited by the two integrated models, respectively. In general, a 3-D reservoir model is always preferential if reasonable computational time is approved. The simple IPM model is more helpful when a quick estimation of production profile for scenario design and screening is required at the conceptual stage where a numeric reservoir model may not be available yet. Apart from this, it is necessary to make clear the following points:

1. The modeling strategy related to water injection is different in the two models. In the simple IPM model, injection wells are not modeled in detail. That is, the number of injection wells is not concerned. Therefore, the allocation of injection rates for each injector as well as their injection pressure are not calculated. It is sufficient to simply provide a total injection rate for each reservoir in each simulation step, such as the "depletion" strategy described in example 1 (section 4.1.4). On the contrary, the full-field 3-D model includes both production and injection wells, making it possible to set controls on both injection rates and injection pressure.

2. The simple IPM model is not able to reflect the well interference induced by well locations because the positions of wells are not taken into consideration. For example, some production wells may locate closer to their injection wells,

or to a natural aquifer. For these wells, earlier water breakthrough is highly possible. The even worse consequence is that when water channels form, theses production wells tend to "attract" more water to produce, changing the pressure distribution in the reservoir and impeding displacement towards other production wells. The simple integrated model is not able to capture this phenomenon, which is one of the explanations for why in some cases the two models will provide different trends on oil recovery.

A brief comparison between the two fully integrated models is listed in Table 4.3. One may choose the more appropriate approach for specific modeling purpose.

Table 4.3: Comparison between the two fully integrated models

simple IPM (section 4.1)	full IPM (section 4.2)
• minimum information required • less variables and equations • vague injection modeling • cumulative production is positively correlated with cumulative injection	• numerical reservoir model required • solve partial differential equations • control on injection wells • production affected by factors like well interference and water channeling

Chapter 5

Coupled Reservoir–Pipeline Network Simulation

In this chapter, explicit and partially-implicit coupling between an open-source reservoir simulator MRST and a multiphase flow simulator OLGA are discussed.

Developing coupled simulations between MRST and OLGA is motivated by three reasons. First, the program for fully-integrated model presented in section 4.2 can be verified in comparing its performance with a coupled simulation using standard simulators. Second, the difference among different coupling schemes, explicit, partially-implicit and implicit, can be evaluated and recommendations on their application can be made. Third, since software OLGA has mature functionalities related to complex flow assurance issues such as corrosion and hydrate simulation, as well as equations for inline equipment such as centrifugal pump, future explorations of these functionalities with evolving reservoir conditions can be realized through the explicit coupling framework.

Short introductions of the two simulators, MRST and OLGA, are first presented, followed by explicit and partially-implicit couplings between them. At the end of this chapter, a comparison among different coupling schemes is provided.

5.1 MRST blackoil module

MRST is a free open-source software for reservoir modeling and simulation, primarily developed by the Computational Geosciences group in the Department of Mathematics and Cybernetics at SINTEF Digital, with several third-party modules developed by Heriot-Watt University, NTNU, TNO, and TU Delft. The toolbox offers a wide range of data structures and computational methods that users can easily combine to make their own custom-made modeling and simulation tools. It includes a minimal core module which offers basic data structures and functionality,

and a large set of add-on modules that offer discretization, solvers, physical models, and so on. In this work, the blackoil module called **ad-blackoil** is applied together with the core solver embedded in **ad-core**.

5.1.1 General framework of MRST

MRST applies an object-oriented (OO) programming paradigm with automatic differentiation (AD) in linearization of reservoir equations. It also provides modules for importing models in standard data format and multiple visualization functions.

The overall structure of MRST is briefly illustrated by Figure 5.1, where the main functions (green blocks), classes (red blocks) and structures (yellow blocks), as well as their interactions, are illustrated.

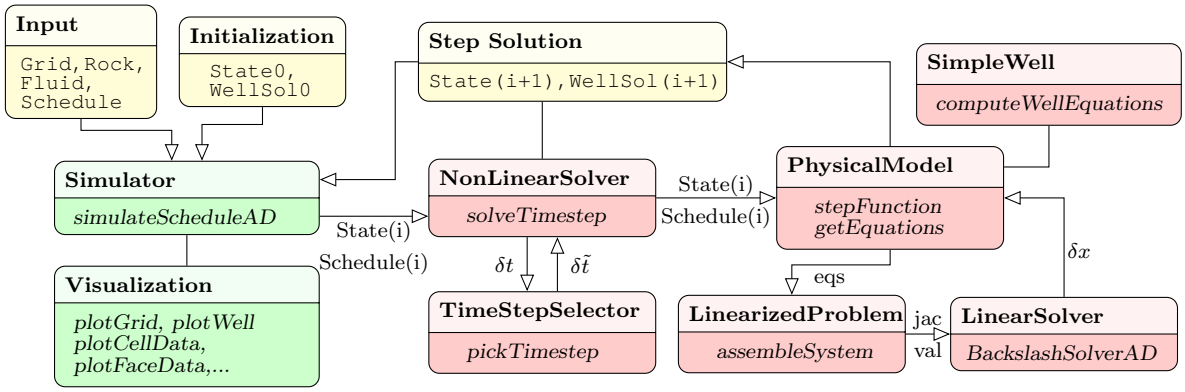

Figure 5.1: Schematics of the framework of MRST.

There are six key structures (Figure 5.2) in MRST that contains the necessary information for constructing a reservoir model. `Grid`, `Rock` and `Fluid` stores information of the reservoir. `Well` and `Schedule` contain the production strategy. `State` and its associated structure `WellSol` store primary variables. These structures can either be generated by MRST functions, or be converted from industrial standard data format using the MRST add-on module **deckformat**. As shown in Figure 5.1, the basic structures are manipulated by functions and solvers.

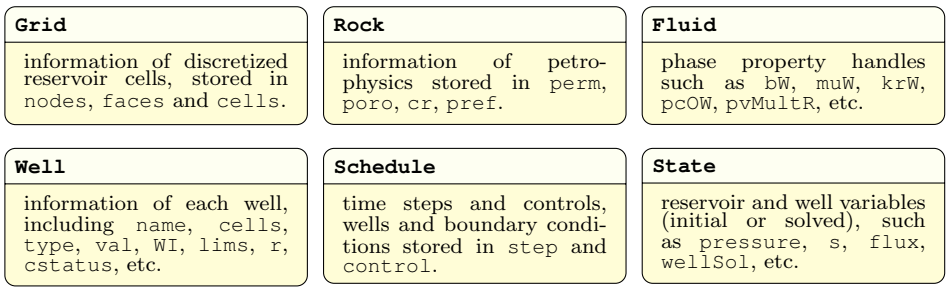

Figure 5.2: Key structures in MRST for constructing a 3-D reservoir model.

With all the reservoir and operation information provided, solution of the governing equations is achieved by a Newton-Raphson iteration method in MRST. The pseudo code in Algorithm 2 presents the main loop.

Algorithm 2 Stand-alone reservoir simulation algorithm (MRST)

Initialization: $x0 = U^0_{res}, x \leftarrow x0, u \leftarrow u0$
for $t \leftarrow 1, nStep$ **do**
    while not converged **do**
        get residuals: $R(x) = R(x, u)$
        solve linear problem: $\Delta x = -R(x)/J(x)$
        check if converged
        update: $x \leftarrow x + \Delta x$
    end while
end for

5.1.2 Object-oriented programming

Object-oriented programming paradigm encapsulates data and operations in objects that interact with each other via the object's interface. Model classes in MRST are mainly derived from the base class `PhysicalModel`. Objects of these value classes are associated with data (*attributes*) of reservoir information stored in the key structures, as well as functions (*methods*) to interact with other objects. The general value class hierarchy in MRST is shown in Figure 5.3.

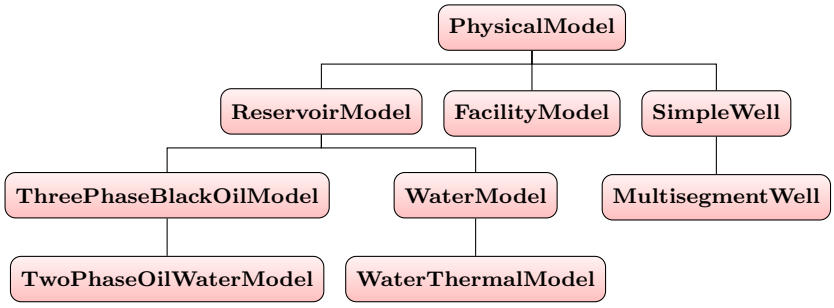

Figure 5.3: MRST value class hierarchy.

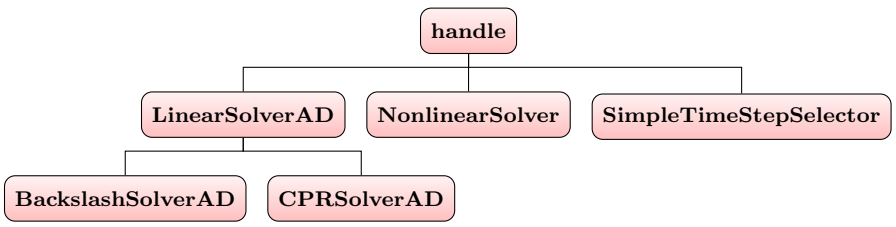

Figure 5.4: MRST handle class hierarchy.

Another important value class in MRST is the `ADI` class, which is the foundation for efficient linearization of nonlinear algebraic equations.

The solvers of MRST are handle classes which manipulate multiple components to solve each ministep (Figure 5.1). The general handle class hierarchy in MRST is shown in Figure 5.4.

5.1.3 Automatic differentiation

To solve the partial differential equations for multiphase flow, the equations shall be discretized at the reservoir grids. MRST applies an automatic differentiation technique through the embedded `ADI` class.

Automatic differentiation is a technique that exploits the fact that any computer code, regardless of complexity, can be broken down to a limited set of arithmetic operations, and the key idea is to keep track of quantities and their derivatives simultaneously. That is, every time an operation is applied to a quantity, the corresponding differential operation is applied to its derivative. There are many automatic differentiation libraries in MATLAB environment, e.g., ADiMat, ADMAT.

The `ADI` class in MRST generates AD objects with property *val* and *jac*. Once the object is manipulated, its *val* and *jac* properties is calculated accordingly. Consider a scalar primary variable x and a function $f = f(x)$. Their AD-representations would be the pairs $\langle x, 1\rangle$ and $\langle f, f_x\rangle$, where 1 is the derivative dx/dx and f_x is the numerical value of the derivative df/dx.

The main use of AD objects in MRST is to linearize and assemble systems of discrete equations. For example, to use automatic differentiation to solve a linear system $Ax = b$, the equivalent residual form is $f(x) = Ax - b = 0$. By initiating the variable x as an AD object, $f(x)$ will have two fields: $f.val$ and $f.jac$. The solution x^* for $Ax = b$ is therefore simply calculated as $x^* = x.val - f.val/f.jac$.

5.2 OLGA workflow

OLGA is the industry standard tool for transient simulation of multiphase petroleum production [112]. The oil industry started using OLGA in 1984 when Statoil had supported its development for 3 years. Data from the large scale flow loop at SINTEF, and later from the medium scale loop at IFE, were essential for the development of the multiphase flow correlations and also for the validation of OLGA. Oil companies have since then supported the development and provided field data to help manage uncertainty, predominantly within the OLGA verification and improvement project. OLGA has been commercially available since the SPT Group started marketing it in 1990. OLGA is used for networks of wells, flowlines and pipelines, and process equipment, covering the production from bottom hole into the production system. The transient capabilities of OLGA dramatically increase its applicability compared

with steady-state simulators. However, OLGA does come with a steady-state pre-processor which is intended for calculating initial values for the transient simulations and is useful for traditional steady-state flow simulations.

The simulation model in OLGA handles a network of diverging and converging flowpaths. Each flowpath consists of a sequence of pipes and each pipe is divided into sections (i.e. control volumes). These sections correspond to the spatial mesh discretization in the numerical model. The staggered spatial mesh applied in OLGA defines flow variables (e.g. velocity, mass flow, flux) at section boundaries and volume variables (e.g. pressure, temperature, mas, volume fractions) as average values in the middle of the section. Each flowpath must start and end at a node. The flowpath is the main component in the simulation network, and can also contain other simulation objects on each pipe segment, e.g. pump, valve, transmitter.

The basic workflow of OLGA is as shown in Figure 5.5. The user defines an OLGA model by providing the required information included in the yellow boxes. After verifying the validity of the input model, OLGA carries out steady-state or transient calculation accordingly and generates output files for post visualization of the simulation results.

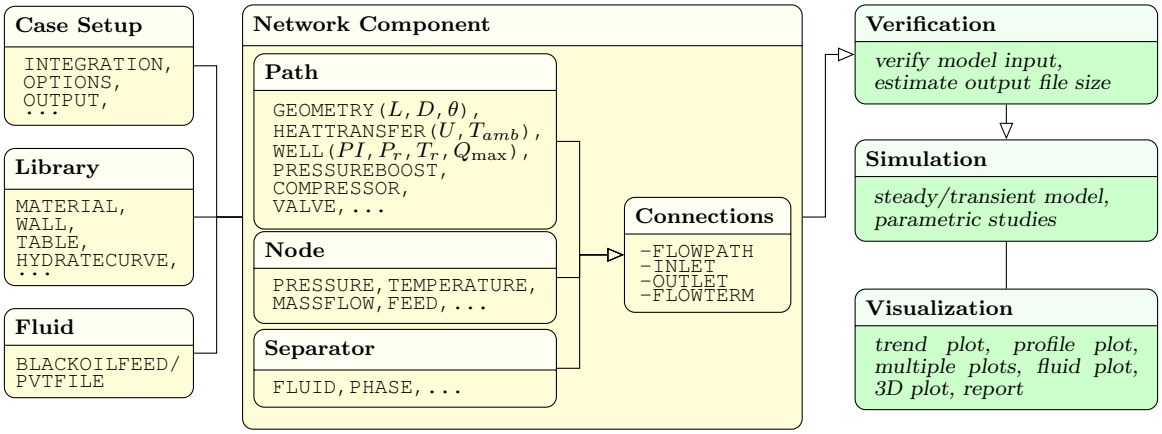

Figure 5.5: OLGA workflow diagram.

CASE level input includes the selection of model, definition of integration options and output variables, etc. Information such as pipe material, wall, and hydrate curve tables are defined in the LIBRARY section. The FLUID choice in OLGA includes input tables generated from compositional models like PVTsim [113], or the built-in black oil model in which several black oil correlations are optional, including the ones provided in Appendix A. The main body of an OLGA model is defined by NETWORKCOMPONENT including flow paths, nodes, separators, controllers, as well as their interconnections. Equipment like pump, valve, compressor, are declared in path keyword.

5.3 Explicit coupling between MRST and OLGA

When coupling MRST and OLGA explicitly, the fluid properties are kept consistent, as well as the naming conventions of wells. Fluid consistency is achieved by either applying the same black oil correlations in both simulators or making interpolations from the same PVT table. The example presented in this chapter applies the same PVT table for both simulators.

In explicit coupling between MRST and OLGA, the network is modeled in OLGA and solved at the beginning of each timestep. Strict convergence should be achieved only with a rigorous convergence algorithm, which is referred to as tightly coupled. However, a tightly coupled scheme will require an extra loop seeking convergence between the solutions from the two domains. To reduce the calculation load, researchers have proposed to omit the convergence loop and perform loose couplings. The pseudo code given in Algorithm 3 shows a loose coupling procedure, where no reservoir–network convergence loop presents. The coupling location is at the reservoir level with IPR overlapped.

Algorithm 3 Explicit coupling algorithm (MRST+OLGA)

Initialization: $x0 = U^0_{res}, x \leftarrow x0, u \leftarrow u0$
for $t \leftarrow 1, nStep$ **do**
    OLGA solve network and update well control $\boldsymbol{u \leftarrow u*}$
    while not converged **do**
        get residuals: $R(x) = R(x, \boldsymbol{u})$
        solve linear problem: $\Delta x = -R(x)/J(x)$
        check if converged
        update: $x \leftarrow x + \Delta x$
    end while
end for

The test example 2 in 4.2.3 is used again in testing the coupling between MRST and OLGA. Liquid rates from reservoir simulator MRST and network simulator OLGA are compared in Figure 5.6. Applying the loose coupling algorithm (Algorithm 3), there is a large discrepancy in the solution of different domains when production rate changes rapidly. The relative errors between reservoir solution and network solution plotted in Figure 5.7 show the shortcoming of this loose explicit coupling algorithm. That is, in early production years and around water breakthrough, large errors are observed. As a comparison, Figure 5.8 shows the tightly coupled results of the first 15 simulation steps, which is the actual coupled solution. To achieve rigorous explicit coupling between the two domain, an extra loop and a robust convergence algorithm is on demand at the expense of increased algorithm complexity and simulation time.

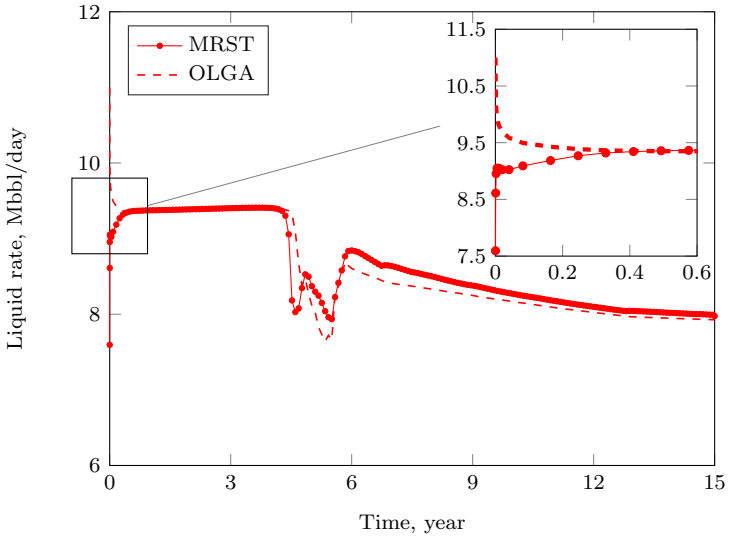

Figure 5.6: Comparison of liquid rate from reservoir domain solution and network domain solution, explicit coupling between MRST and OLGA.

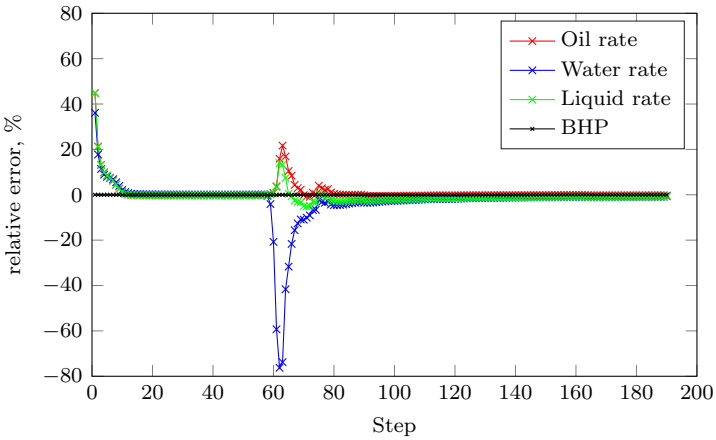

Figure 5.7: Relative error between reservoir domain solution and network domain solution, explicit coupling between MRST and OLGA.

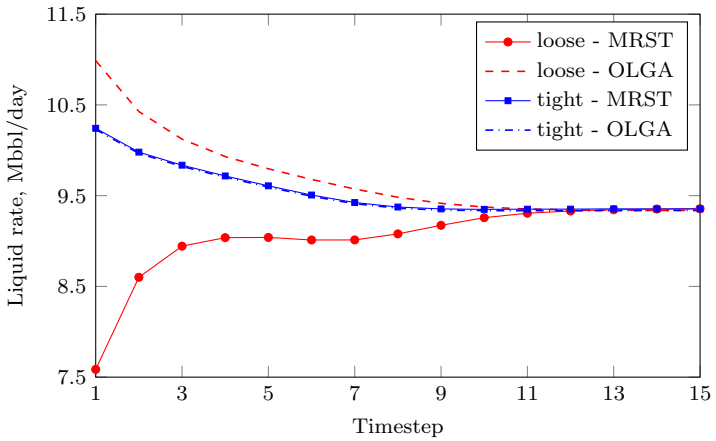

Figure 5.8: Comparison of liquid rate by loose and tight explicit coupling.

5.4 Partially-implicit coupling between MRST and OLGA

In partially-implicit coupling between MRST and OLGA, the network is modeled in OLGA and solved at the beginning of every specified Newton iteration. A pseudo code for partially-implicit coupling is given in Algorithm 4.

Algorithm 4 Partially-implicit coupling algorithm (MRST+OLGA)

Initialization: $x0 = U^0_{res}, x \leftarrow x0, u \leftarrow u0$
for $t \leftarrow 1, nStep$ **do**
  while not converged **do**
    OLGA solve network and update well control $\boldsymbol{u \leftarrow u*}$
    get residuals: $R(x) = R(x, \boldsymbol{u})$
    solve linear problem: $\Delta x = -R(x)/J(x)$
    check if converged
    update: $x \leftarrow x + \Delta x$
  end while
end for

The same reservoir and network model in test example 2 is coupled applying partially-implicit scheme. Figure 5.9 shows the liquid production rate variations from the reservoir and network solution. It is clear that since the network is solved at each specified Newton iteration, smaller gaps between the reservoir and network solution are observed. The relative errors between reservoir and network domain solutions shown in Figure 5.10 are reduced to within 5%.

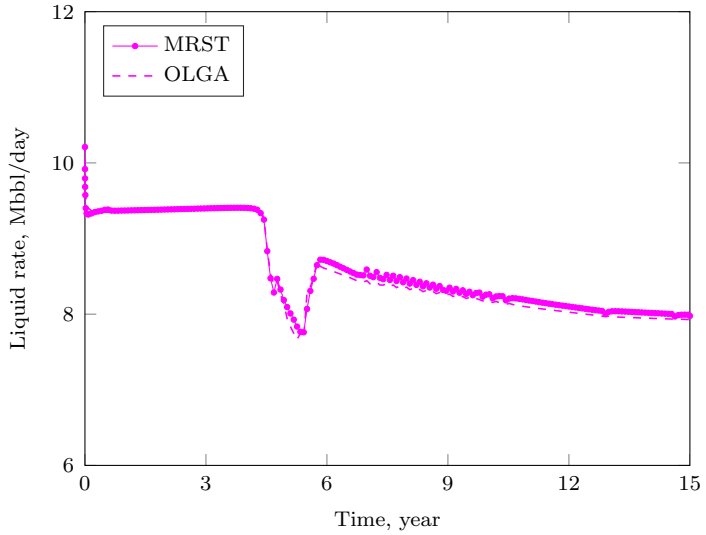

Figure 5.9: Comparison of liquid rate from reservoir domain solution and network domain solution, partially-implicit coupling between MRST and OLGA.

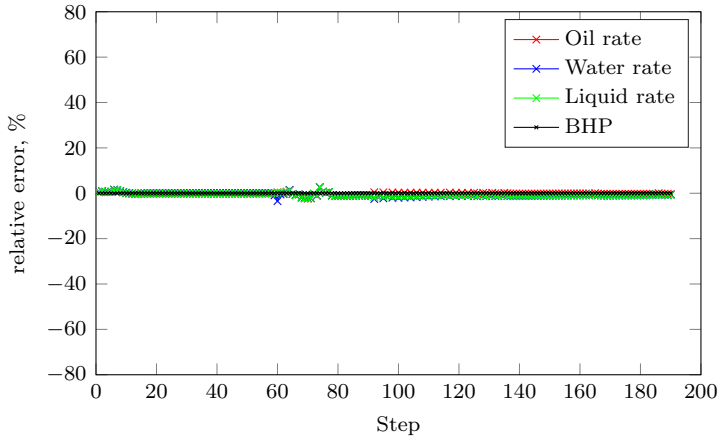

Figure 5.10: Relative error between reservoir domain solution and network domain solution, partially-implicit coupling between MRST and OLGA

5.5 Comparison and comments on different IPM techniques

So far, four types of simulations have been performed on the test example 2, namely,

- MRST stand-alone (see 4.2.3)
- MRST/NET fully-implicit integration (see 4.2.3)
- MRST/OLGA explicit coupling (see 5.3)
- MRST/OLGA partially-implicit coupling (see 5.4)

A comparison among the four simulations is presented below. Figure 5.11 shows the well bottomhole pressure from different simulations. Oil and water production rates from the four simulations are shown in Figure 5.12.

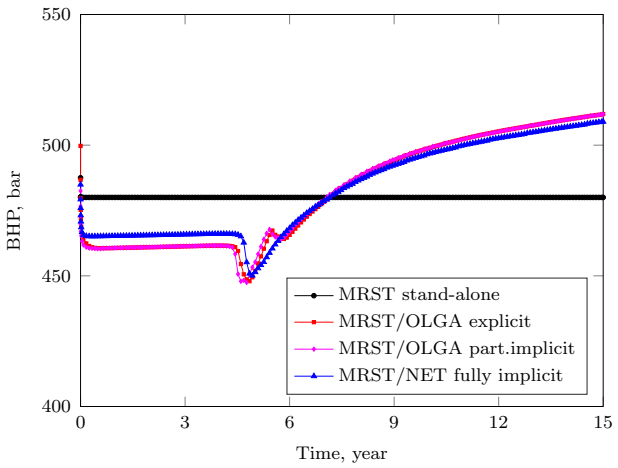

Figure 5.11: Comparison of well bottomhole pressure by different simulations.

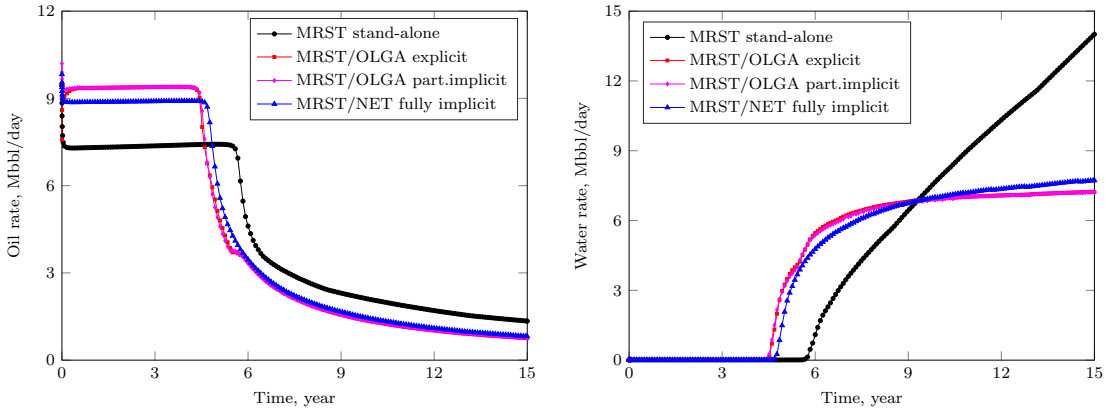

Figure 5.12: Comparison of oil and water production rate by different simulations.

Figure 5.13 shows the reaching temperature variation of the produced fluid along the entire production life. In late production years, with higher content of water, heat capacity of the fluid is higher, reducing the temperature drop along the pipeline.

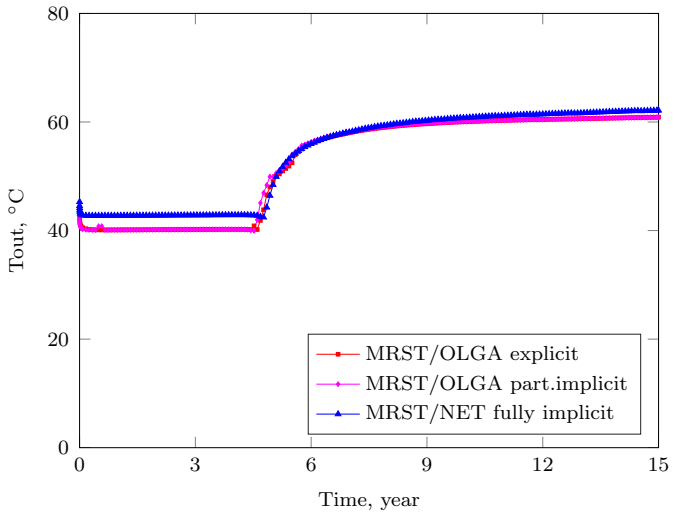

Figure 5.13: Comparison of reaching temperature by different coupling schemes.

Simulation statistics are listed in Table 5.1. As shown in Table 5.1 and Figure 5.11 to 5.13, the coupled simulations, explicit, partially-implicit, or fully-implicit, all show close results since the backpressure from the subsea production line is considered. Also, the above comparison verifies the performance of the developed code for fully-implicit modeling in section 4.2.3.

Calling for OLGA solutions takes up most of the simulation time. Both explicit and partially-implicit coupling are time-consuming. Especially for partially-implicit coupling algorithm, more Newton iterations for converging the reservoir solution in each timestep further increases the simulation time. The fully-implicit model not only ensures converged reservoir and network solution, but also performs reasonably in terms of simulation time.

Table 5.1: Statistics for different simulation schemes

	stand-alone	explicit	part.implicit	fully-implicit
$Q_{\mathrm{o\,max}}$, Mbbl/day	9.4	9.4	10.2	9.8
$Q_{\mathrm{w\,max}}$, Mbbl/day	14.0	7.2	7.2	7.7
$Q_{\mathrm{wt\,max}}$, Mbbl/day	14.0	7.2	7.2	7.7
N_p, MMbbl	22.9	22.6	22.6	22.6
W_p, MMbbl	27.3	24.5	24.4	24.2
final watercut, %	91.2	90.5	90.5	90.4
CPU time, min	1.2	31.8	54.1	15.3

In petroleum field development, at least three *operating modes* are involved: history matching, production prediction, and production optimization. A most desirable integrated production modeling technique shall be the one that is able to, or can be easily reconfigured to perform all of these tasks.

History matching is a quality control process usually carried out before any prediction or optimization task. It involves adjustment of model parameters to achieve minimum difference between model solution and the reference history, which is essentially an optimization problem with a least-square objective. In history matching mode, one knows the production history, including which wells are drilled and opened from which date, well production rates variation, dates for well intervention and workover, wellhead pressure variation, etc. Therefore, an integrated production model is no better than a traditional stand-alone reservoir or network simulator in providing more convincing model parameter estimation results since the boundary conditions for each domain are for certain. On the contrary, an integrated model may suffer with multiple solutions since reservoir and network parameters are evaluated together. However, once the history matching is terminated, more realistic predictions shall be with integrated models.

In a predictive context, a fully-implicit scheme often stands out since simultaneous solution of the reservoir and network domain is obtained regardless of the coupling location. Previous comparison among the four simulations performed on the test example 2 supports this assertion. In terms of coupled simulation between two simulators, since rates are unknowns, reservoir pressure is an appropriate boundary condition for the network simulator and a coupling location at the reservoir level is advantageous. However, the loose explicit and partially-implicit coupling algorithms between MRST and OLGA presented in this chapter are arguable because strictly converged solution between the two domains is not imposed. To acquire strict convergence, or tight coupling, between a reservoir and a network simulator, one is virtually dealing with a least-square problem with the objective of finding the minimum difference between the solutions from the two simulators in each timestep of the forecast period, where a robust optimization algorithm and two simulators

with high computational efficiency are crucial in defining the overall performance of the coupled simulation.

As for operation optimization task, a fully integrated model (fully-implicit) is advantageous because it is more convenient to generate Jacobian for the constraints and/or Hessian for the augmented objective function applying some automatic differentiation technique given that all the model equations are approachable. Gradient-based optimization methods are therefore applicable. If explicitly coupled simulations are to be applied in optimization, every evaluation of the objective requires a converged solution between the reservoir and the network simulator which implies many calls for both simulators in every single evaluation. Construction of derivatives is plaguy and time-consuming, excluding the efficient applicability of gradient-based optimization methods. Suboptimals based on a trial-and-error or heuristic process could be found.

Based on the results obtained from test example 2 and the above analysis on different operating modes, a summary of the four different simulation schemes is presented in Table 5.2.

Table 5.2: Summary of different simulation schemes

Scheme	Key notes
stand-alone	unrealistic boundary conditions without considering the impact from the pipeline network.
explicit	erroneous when reservoir condition changes rapidly within one simulation step.
partially-implicit	most time consuming, increased number of iterations to converge in each simulation step.
fully-implicit	stable but need to formulate and solve a set of nonlinear equations, has potential in optimization by gradient-based methods.

Chapter 6

Quantifying the Effect of Subsea Water Separation through IPM

In the previous chapters (4 and 5), four different IPMs have been developed. The developed fully integrated models (in-house code) have shown satisfactory performance in the test examples (section 4.1.4 and 5.5). The potential applications of the developed integrated models include scenario selection and comparison, real-time production surveillance, short-term and long-term production optimization, etc. Conforming to the general objective of this thesis, this part presents the application of IPM on evaluating the effect of subsea water separation by scenario comparisons. Considering the drawbacks of the explicit and partially-implicit approach (section 5.5), only the two implicit models are applied in this chapter.

In this work, the effect of subsea water separation is assessed from three aspects: economics, reservoir engineering, and flow assurance. Correspondingly, the following quantitative indicators are used:

• NPV	– a direct indicator of economic profitability.
• oil recovery rate	– the most important criterion of the exploitation result from a reservoir engineering point of view.
• wax-free index	– an indicator concerning the flow assurance issue under normal production. The wax-free index is defined as the percentage of wax-free (reaching temperature above wax formation temperature) time in the whole development life.

To quantify the impact of a subsea technology on an exploitation activity, specific field conditions should be provided since a conclusion drawn for one situation may not be equally suitable for another. To be as objective and comprehensive as

possible, several cases with different field layout and development conditions are studied.

In terms of the **spatial** configuration of the subsea layout, the case studies cover two typical types of subsea production systems:

- clustered well system
- satellite well system

Each type of system includes two subcategories according to whether or not subsea water separation is applied, as illustrated in Figure 6.1.

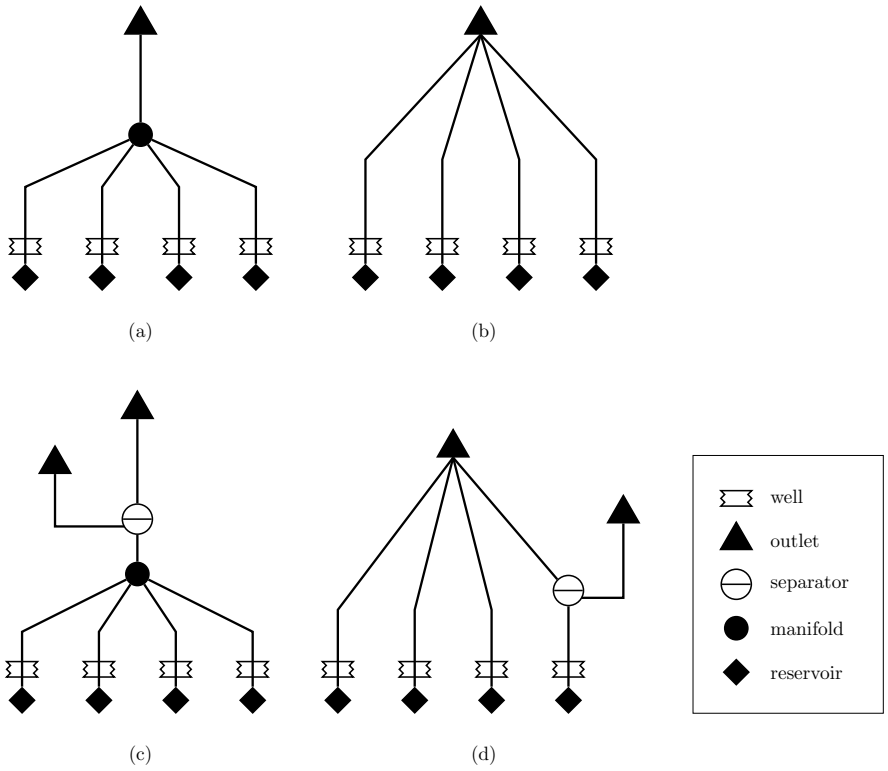

Figure 6.1: Typical subsea configurations: (a) clustered well system; (b) satellite well system; (c) clustered wells + subsea separation; (d) satellite wells + subsea separation.

On the other hand, from a **temporal** point of view, whether subsea water separation is considered for a green field development or for the revitalization of a brown field is discussed in the cases. That is:

- The field is a green field to be developed and the effect of subsea water separation on the life-time production is discussed.
- The field is a brown field where water content is reaching the processing capacity limit of current topside facilities and subsea water separation is to be

installed to handle the excessive amount of water production and prolong the production life.

Specifically, the cases are organized in the following way. Case 1 applies the simple IPM tool established in section 4.1 to a clustered well system in shallow water, with oil properties and field environment similar to a field in the North Sea. Case 2 applies the fully-implicit IPM in section 4.2 to a case with fluid and field conditions similar to a deepwater offshore Brazil. Case 3 uses the same reservoir as case 2, but with a satellite well system. The general workflow in each case is as follows:

1. perform a simulation for a system without subsea water separation as a base scenario;

2. perform a comparative simulation for a reconfigured system with subsea water separation;

3. interpret the quantitative results for the two simulations to assess the performance of subsea water separation.

6.1 Case study 1 : clustered wells + tank model

6.1.1 Field information

Case study 1 presents simulations for the development of a field including two independent reservoirs. There are in total five production wells connected to a common cluster manifold, as illustrated by Figure 6.2. Three producers are placed in reservoir TA and the other two in reservoir TB. The five producers are directional wells with 5 inch tubing and are connected to the manifold with 5 inch jumpers. The cluster is tied-in to an existing platform located approximately 11 km from the manifold with 10 inch insulated subsea pipelines.

The two reservoirs are considered with closed boundaries and water injection is used for pressure maintenance in both reservoirs from the beginning. Although injection wells are not plotted in Figure 6.2, the total injection rate in each reservoir is calculated at each timestep. The reservoir properties are listed in Table 6.1. The fluid in the two reservoirs are supposed to be the same, as listed in Table 6.2. Black oil correlations (Appendix A) are used to calculate the fluid properties.

In evaluating the effect of subsea water separation, the subsea separator is placed 800 m downstream of the manifold, as shown in Figure 6.3. From the separator, separated hydrocarbon is redirected to the 10 inch subsea pipeline to the platform while the separated water is assumed to be disposed through a fictitious disposal well nearby.

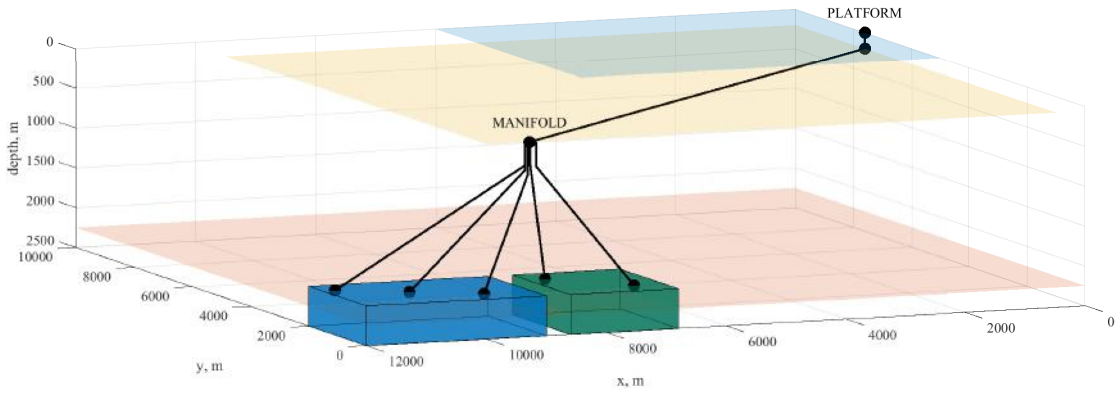

Figure 6.2: Integrated model for case 1, without subsea water separation. Reservoir TA and TB are illustrated by the blue and green box, respectively.

Table 6.1: Reservoir properties, case study 1

	TA	TB
water depth, m	200	200
OOIP, MMbbl	561.4	256.6
P_{i}, bar	335	300
T_{res}, °C	62	62
J, $\mathrm{Sm^3/day/bar}$	25	20

6.1.2 Scenario settings

The total simulated development time is 30 years, with a uniform timestep of 1 month. The tubings, jumpers, pipelines and risers are discretized into segments of around 50 meters. Three development scenarios were simulated and compared:

- **S1** – base simulation without subsea water separation.
- **S2** – subsea water separation from the beginning.
- **S3** – subsea water separation introduced from the 14th year.

The simulation results from the three scenarios provide the evaluation of subsea water separation for this field. It is worthwhile to make clear the following points about the three scenarios:

Table 6.2: Fluid property, case study 1

Oil API	34.7
GOR, $\mathrm{Sm^3/Sm^3}$	105.0
Gas specific gravity	0.79
Bubble point, bar	162.8

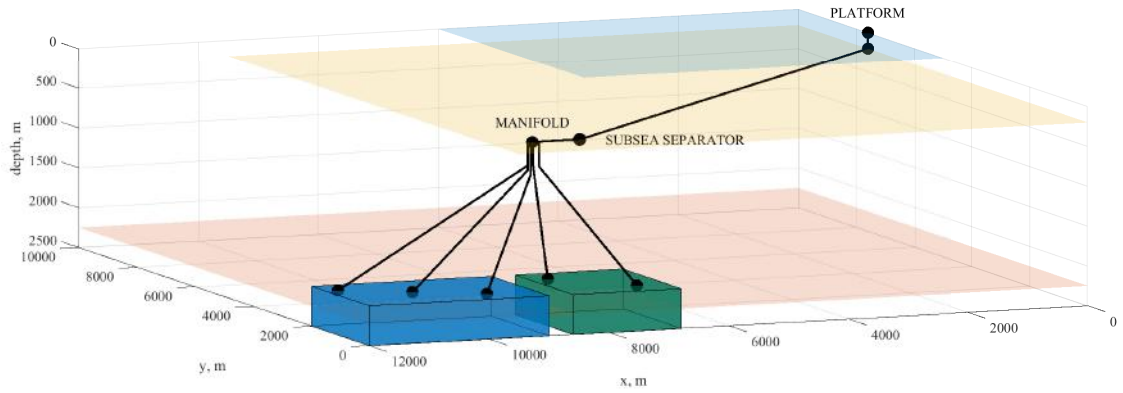

Figure 6.3: Integrated model for case 1, with subsea water separation. Reservoir TA and TB are illustrated by the blue and green box, respectively.

1. In scenario S1 and S2, the field shall be viewed as a green field to be developed. The task is to design a proper production system for it, at the appraisal or conceptual design stage. The comparison between the two scenarios helps to select the more attractive subsea layout, i.e. with or without subsea water separation.

2. For scenario S3, the field is viewed as a brown field under development with the subsea layout of scenario S1. S3 is a "restart" of S1 in the 14th year where only the subsea configuration is changed. The result indicates the added value of reconfiguring the original layout by including the new component – subsea separator.

3. It is obligated to provide an injection strategy to the model as a type of auxiliary equation. The injection strategy used in all the scenarios is "depletion", similar to that described in section 4.1.4. The injection-to-production ratio equals 0.9 in the early development years to utilize the reservoir pressure for oil recovery. Along the production life, injection rate is adjusted (increased) when the reservoir pressure drops to a point that is insufficient to deliver production to the topside. This strategy is commonly used in practice and it ensures that the model always have a solution, otherwise production will not be able to continue given that no pressure boosting methods like gas lift are considered in the system.

6.1.3 Results

As mentioned above, the simulation results of scenarios S1 to S3 will be analyzed as if the field is taken as either a green field or a brown field.

Green field design : S1 VS. S2

Simulation results of pressure and rates for scenario S1 and S2 are plotted in Figure 6.4. A summary of production statistics is provided in Table 6.3. It is shown in Figure 6.4 that with the application of subsea water separation, the required reservoir pressure to maintain production is lower. Hence, the injection rates in the two reservoirs are lower and water cut increases slower in each well. In this clustered well system, several wells in different reservoirs and with different productivities are connected to a common manifold. The back pressure on each wellhead is related to the head at the manifold. Because the producers in reservoir TA have higher productivity, the higher the manifold pressure, the higher back pressure is imposed on these producers so that their productivities are not fully explored. Therefore, after separating water from the commingled flow stream, manifold pressure decreases and the producers in reservoir TA are able to contribute more production with less water injected, making subsea water separation an effective solution to increase total production and reduce injection.

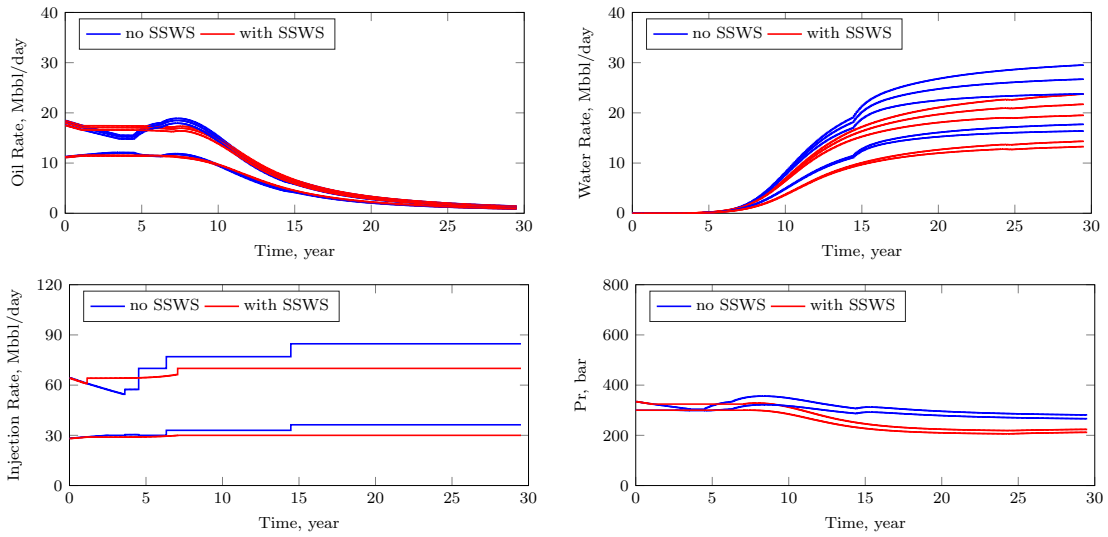

Figure 6.4: Simulated pressure and rate results, scenario S1 and S2, case study 1.

The values of the three quantitative indicators are listed in Table 6.4. With the application of subsea water separation, final recovery rate is 0.12% higher. The higher final recovery, together with less water production and injection, resulted in a positive increase of NPV (143.8 million dollars). However, in the last 6.5 years of the production life, there is an increasing risk of wax deposition in the pipeline segments close to the riser if water is separated subsea. As shown in Figure 6.6 (left), when subsea water separator presents, the reaching temperature at the platform decreases because the heat capacity of the fluid is lower without the presence of water. In late production years, inhibitors may be needed to prevent wax formation.

Table 6.3: Summary of production statistics for S1 and S2, case study 1

	S1	S2
SSWS	N	Y
$Q_{\mathrm{o\,max}}$, Mbbl/day	78.9	76.2
$Q_{\mathrm{w\,max}}$, Mbbl/day	114.1	92.6
$Q_{\mathrm{wt\,max}}$, Mbbl/day	114.1	0.0
$Q_{\mathrm{inj\,max}}$, Mbbl/day	121.0	100.0
N_p, MMbbl	409.3	410.3
W_p, MMbbl	674.2	542.6
W_i, MMbbl	1180.6	1041.1
final watercut, %	95.3	0.0
final recovery, %	50.04	50.16
NPV, $ million	7099.8	7243.6
SSWS cost, $ million	0.0	92.6

Table 6.4: Quantitative effect of subsea water separation for green field, case 1

	no SSWS	with SSWS	
NPV, $ million	7099.8	7243.6	143.8 (2.0% ↑)
recovery, MMbbl	409.3	410.3	1.0 (0.1% ↑)
wax-free index	1.00	0.78	-22% ↓

Brown field revitalization : S1 VS. S3

When examining the differences between scenario S1 and S3, we are supposed to be standing in the 14th year and all the production data before this time instance is past history. Simulation results of pressure and rates for scenario S1 and S3 are plotted in Figure 6.5.

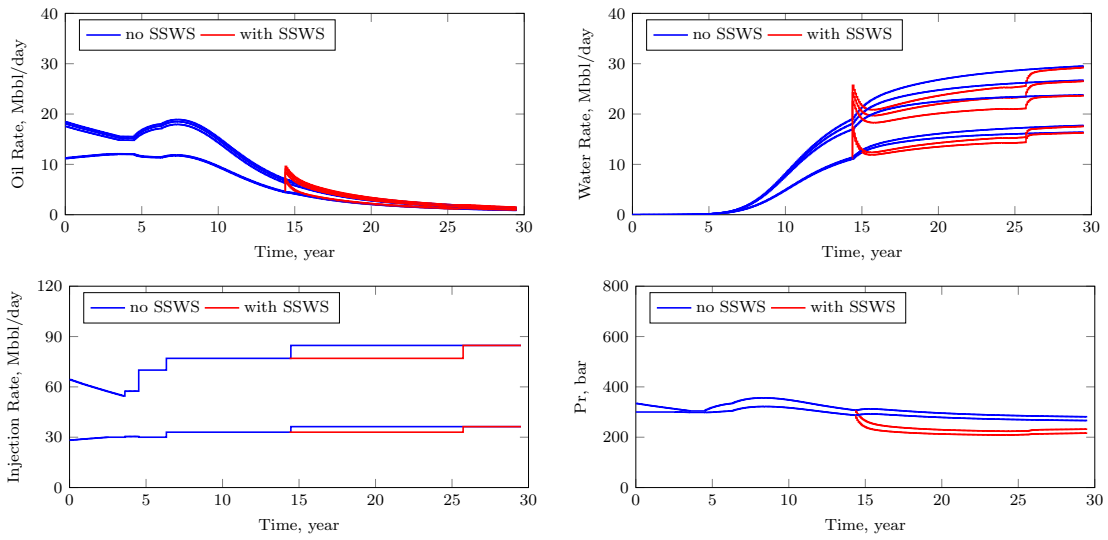

Figure 6.5: Simulated pressure and rate results, scenario S1 and S3, case study 1.

As shown in Figure 6.5, from the 14th year, if production is to be continued, an increase in reservoir pressure is required in order to lift the fluid with high content of water to the topside. The amount of water to be received on the platform is around 80 Mbbl/day. Assuming that this platform was designed with a water capacity equal to 80 Mbbl/day, the platform will not be able to handle excessive water production in the following years. The wells, at least some of them, should be closed. At this point, if water is separated out on the seafloor, the production life of the wells can be prolonged. Scenario S3 starts from the condition of S1 in the 14th year and simulates the future production with subsea separator installed. It is shown in Figure 6.5 that after separating water from the production stream, production is continued even with lower reservoir pressure because the wells are released from high wellhead back pressure.

Table 6.5 lists the values of the three quantitative indicators. With subsea water separation, the field can produce 68.2 MMbbl more oil with an increase in final recovery of 8.34% in the next 15 years, which brings about an increase of NPV of 518.4 million dollars. Again, the potential problem associated with subsea water separation is temperature reduction. Towards the end of the production life, shown in Figure 6.6 (right), there will be an increase in wax deposition risk. Inhibitors may be needed to prevent wax formation.

Table 6.5: Quantitative effect of subsea water separation for brown field, case 1

	no SSWS	with SSWS	
NPV, $ million	6732.0	7250.4	518.4 (7.7% ↑)
recovery, MMbbl	345.5	413.8	68.2 (8.3% ↑)
wax-free index	1	0.78	-22.0% ↓

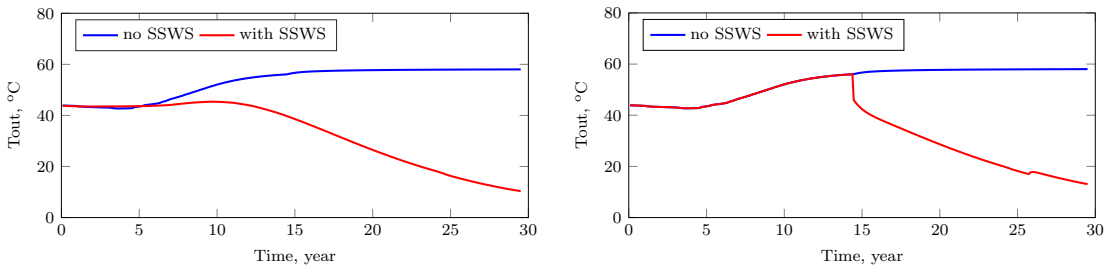

Figure 6.6: Comparison of fluid reaching temperature, case study 1. Left: S1 and S2; right: S1 and S3.

In general, this scenario setting is similar to the condition of the Tordis field where subsea water separation has been executed. Although the reservoir model is not tuned to be precisely the same as the Tordis field, the production trends are quite similar. 42 million barrels of additional oil have been extracted from the field

in the 5 years between 2007 and 2012, with the SSBI system installed in 2007. The production after 2012 is affected by other IOR activities like new drillings and are therefore not counted for.[114]

When comparing the result of scenario S2 with S3, it is shown that S3 outperforms in both NPV and final recovery while keeping the same level of wax-free index. Referring to the production curves, in early production years, where the water production is low, it is preferential to maintain higher reservoir pressure to produce more oil and get higher net return as soon (under the influence of discounting).

This case study has demonstrated the application of the simple IPM tool with a tank model. This simple tool is especially appropriate for green field design and sometimes is the only option when a numerical reservoir model is unavailable. For brown fields, better reservoir description by numerical models should have been obtained, however, the simple tool is also useful for a quick estimation, as applied in this case study.

6.2 Case study 2 : clustered wells + 3-D model

In case study 2, a three-dimensional reservoir model is applied and integrated with the pipeline network through implicit coupling. Explicit and partially-implicit coupling simulations are not performed due to their drawbacks in both computation time and convergence problem as discussed in section 5.5. The studied field is viewed as a green field focusing on the design and selection of production systems at the conceptual design stage, i.e. cluster well system or satellite well system, with or without subsea water separation.

6.2.1 Field information

The reservoir is buried at about 5000 m below sea level. It is divided into two blocks, namely, Block A and Block B (Figure 6.7). Each block is assigned homogeneous properties, as listed in Table 6.6.

Table 6.6: Reservoir properties, case study 2

	Block A	Block B
k, mD	500	450
H, m	120	80
S_{oi}	0.9	0.8
OOIP, MMbbl	1406	384

There are seven production wells in Block A, labeled A1, A2, ..., A7. Four production wells are located in Block B, labeled B1, B2, ..., B4. In total, six

water injection wells are defined, labeled I1, I2, ..., I6. The first four are located in Block A and the other two in Block B. All the production wells are placed at structural high spots and injection wells at lower edges to perform peripheral flood. The reservoir geological structure and well locations are shown in Figure 6.7 and 6.8. Table 6.7 gives coordinates information for each production well.

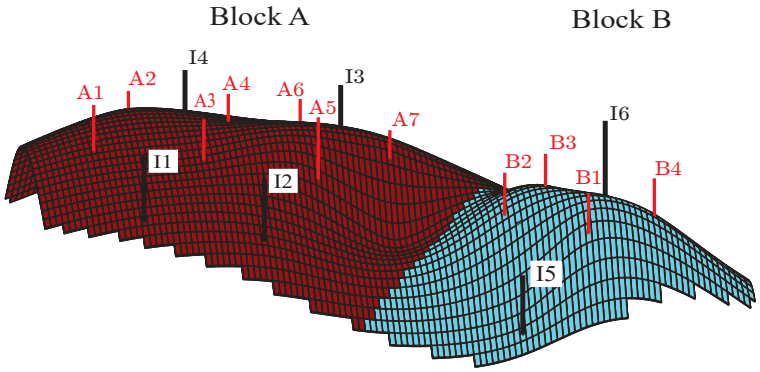

Figure 6.7: Reservoir structure and well positions (red: producers; black: injectors).

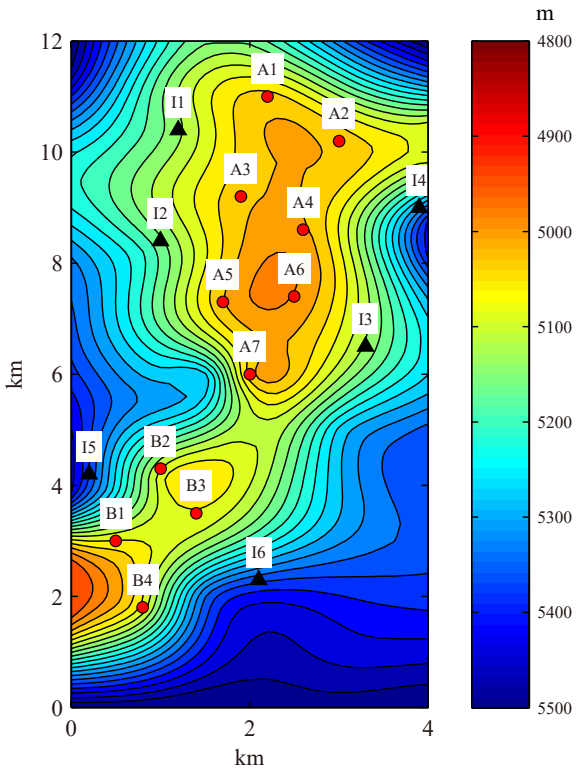

Figure 6.8: Reservoir top structure with well positions (circle: producers; triangle: injectors).

The numerical reservoir model is three-dimensional, three-phase, with no-flow boundaries. The fluid is the same as in the test example 2 in section 4.2.3. The overall layout of the scenario without subsea water separation is shown in Figure 6.9,

Table 6.7: Well information, case study 2

well name	wellhead coordinates			wellbottom coordinates			inclination angle (°)
	x (m)	y (m)	z (m)	x (m)	y (m)	z (m)	
A1	1800	8600	2000	2150	10950	5072	49
A2	1941	8541	2000	2950	10150	5067	43
A3	1659	8541	2000	1850	9150	5070	17
A4	2000	8400	2000	2550	8550	5063	15
A5	1659	8259	2000	1650	7250	5084	26
A6	1941	8259	2000	2450	7350	5060	27
A7	1800	8200	2000	1950	5950	5078	47
B1	777	2800	2000	450	2950	5083	10
B2	850	3073	2000	950	4250	5087	30
B3	1123	3000	2000	1350	3450	5076	14
B4	1050	2727	2000	750	1750	5081	26

where all the production wells are assumed deviated wells. The seven production wells in block A are connected to the 8-slot cluster manifold A and the four producers in block B are connected to the 4-slot cluster manifold B. The distance from the wellhead to the corresponding clustered manifold is 200 m. Manifold A and B are connected separately to the FPSO by flowlines of 8 inch, insulated to an overall heat transfer coefficient of 4.6 W/m^2-C.

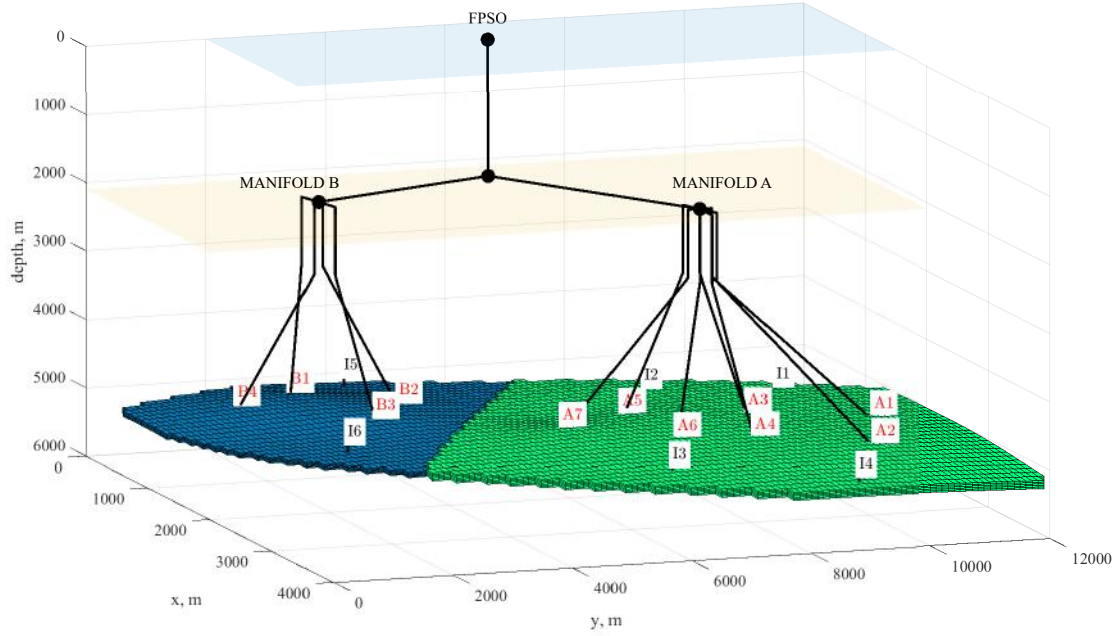

Figure 6.9: Integrated model for case study 2, without subsea water separation.

To study the effect of subsea water separation, a subsea separator is installed around 400 m downstream of manifold A, as shown in Figure 6.10. The separated

water is supposed to be disposed into a fictitious disposal well nearby while the hydrocarbon phases are transported to the FPSO. In Figure 6.9 and 6.10, the two risers for well cluster A and B are both assumed vertical and thusly the riser bases are shown as an overlapped point, but they are not connected.

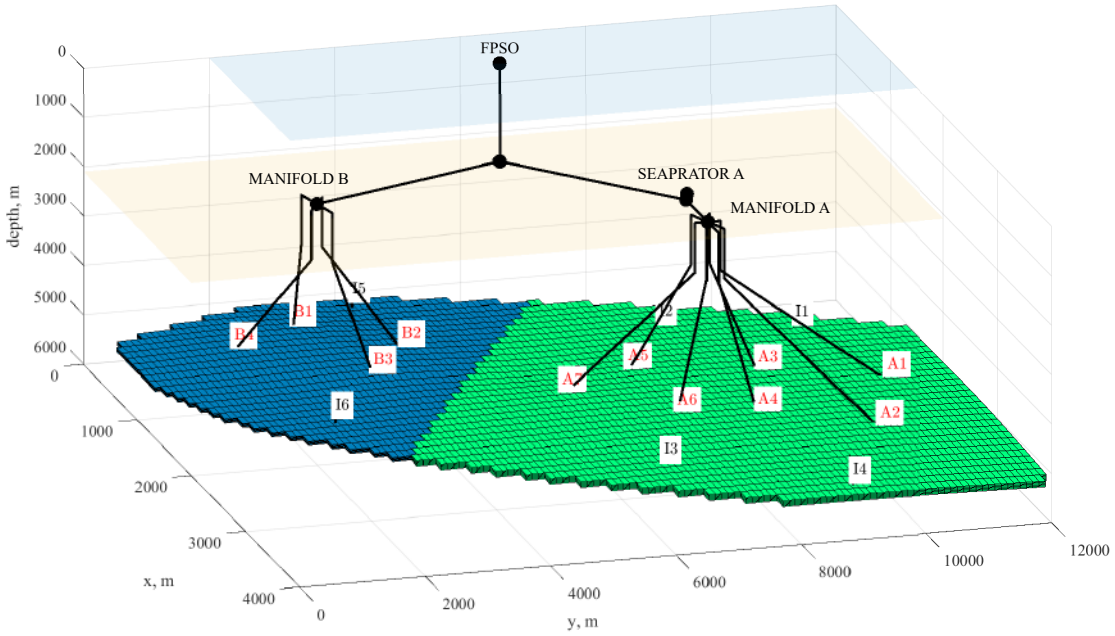

Figure 6.10: Integrated model for case study 2, with subsea water separation for cluster A.

6.2.2 Scenario settings

In this case study, three simulations are run and compared:

1. **Uncoupled**, or **stand-alone**. Traditional reservoir simulation is performed with given controls on well rates and bottomhole pressure. Simulator MRST and ECLIPSE are used and compared to verify the performance of MRST, which is key to ensure that the results of the simulations are reliable.

2. **Coupled**. Fully integrated reservoir–network model (section 4.2), without subsea water separation.

3. **Coupled + SSWS**. Fully integrated reservoir–network model, with subsea water separation introduced downstream of manifold A from the 15th year.

In each scenario, the simulated development time is 27 years. Tubings, jumpers, pipelines, and risers are discretized into segments of around 50 m.

6.2.3 Results

The results of the three simulations are compared and analyzed from three aspects: reservoir engineering, flow assurance, and economics.

Reservoir engineering

Figures 6.11 to 6.15 present the simulated production variations for each well. First of all, the comparative lines between the stand-alone simulations from MRST and ECLIPSE verified the performance of MRST, bringing in confidence on the simulation results from the open-source simulator MRST.

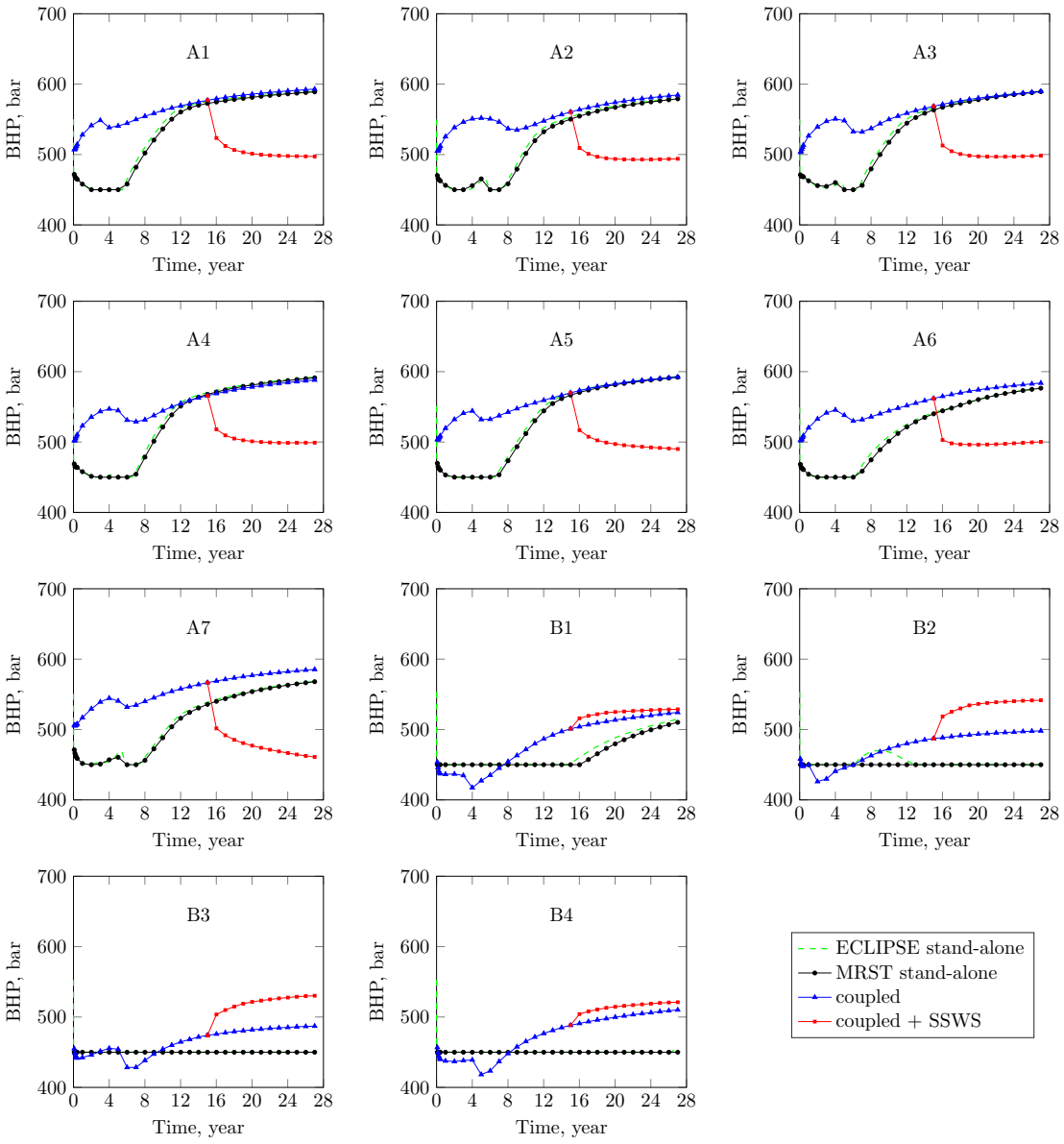

Figure 6.11: Bottomhole pressure of each production well, case study 2.

As shown in Figure 6.11, when water is separated out, the bottomhole pressure for wells in block A decreases due to lower back pressure from the production line

as one may expect. However, the bottomhole pressures for wells in block B are also influenced by the introduction of subsea water separation for well cluster A. It is observed that the bottomhole pressure of wells in block B all increases because of the change in reservoir pressure and phase distribution. The liquid production rate for well B2 and B3 increases, but unfortunately only owing to higher water production (Figure 6.13). That is because well B2 and B3 are located closer to block A, where water injection increased to support higher production resulted from subsea water separation. Oil production in well B2 and B3 are "robbed" by well A7 (Figure 6.12). However, for the whole field, the final recovery increased by 0.6 % (Table 6.8).

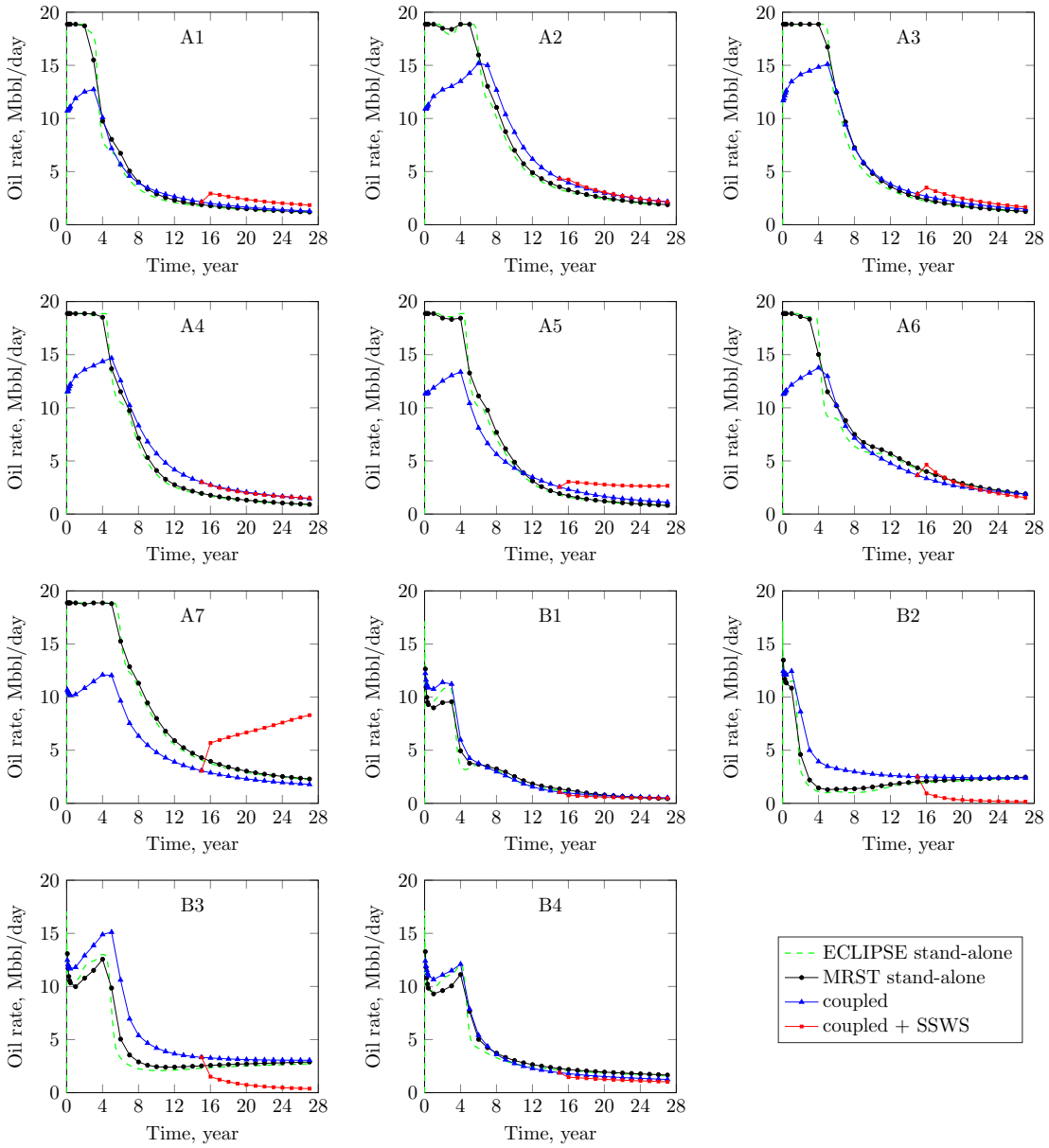

Figure 6.12: Oil production rate of each production well, case study 2.

Figure 6.16 shows the final reservoir pressure distribution for the three simulated scenarios. With subsea water separation, the reservoir pressure in block A is lower

since the back pressure on each well drops.

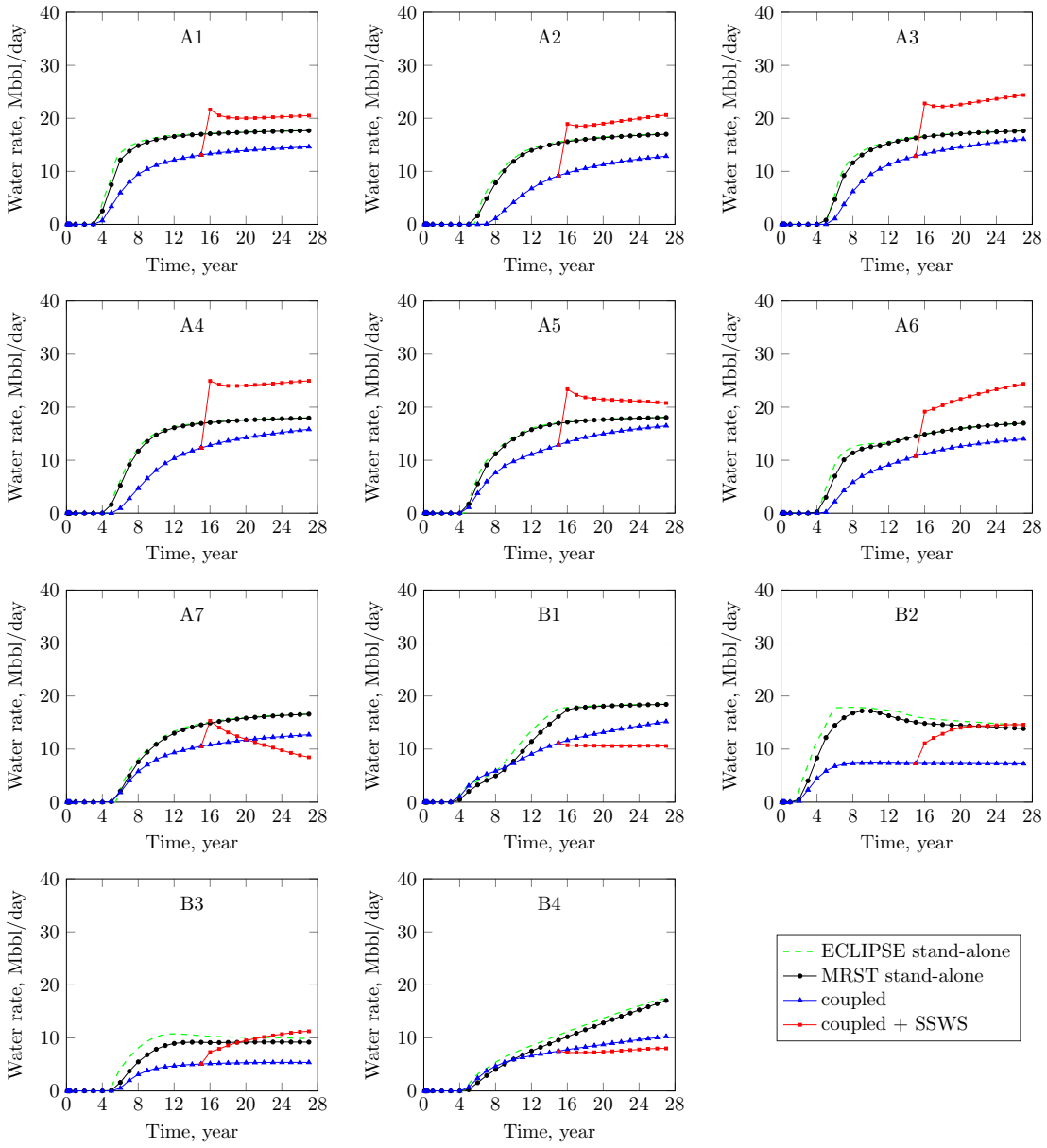

Figure 6.13: Water production rate of each production well, case study 2.

What's more, in Table 6.8, when comparing the results in the first column with those in the other two columns, the drawback of uncoupled simulation is manifested. In the uncoupled simulation, due to inappropriate estimation of well pressure and rates, an oversize FPSO is designed. Based on this production profile, the NPV is also overestimated, leading to an optimistic but improper prospect on the economical potential of the development project. On the other hand, if the uncoupled simulation had applied somehow conservative controls on well pressure and rates instead, a pessimistic NPV shall be obtained. The integrated model undoubtedly avoids such a dilemma.

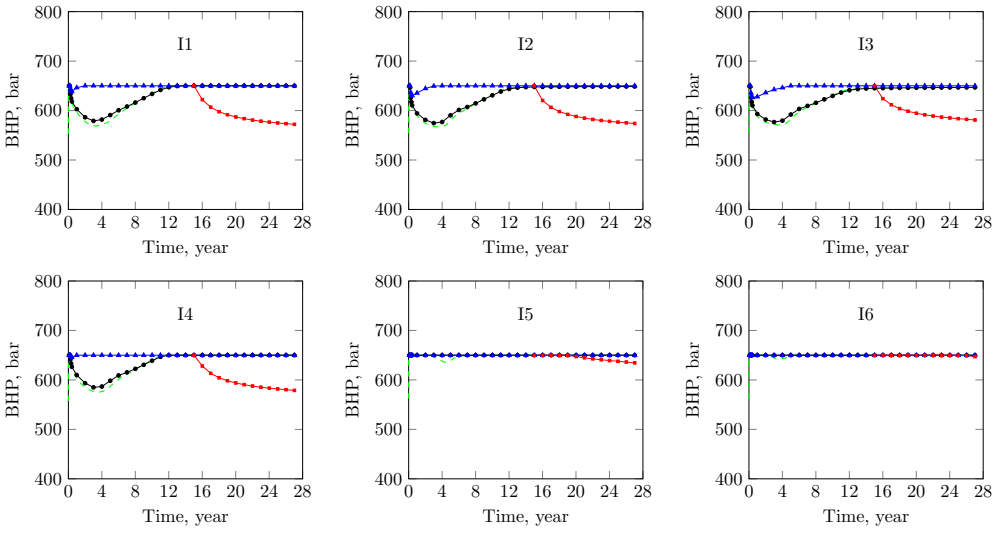

Figure 6.14: Bottomhole pressure of each injection well, case study 2.

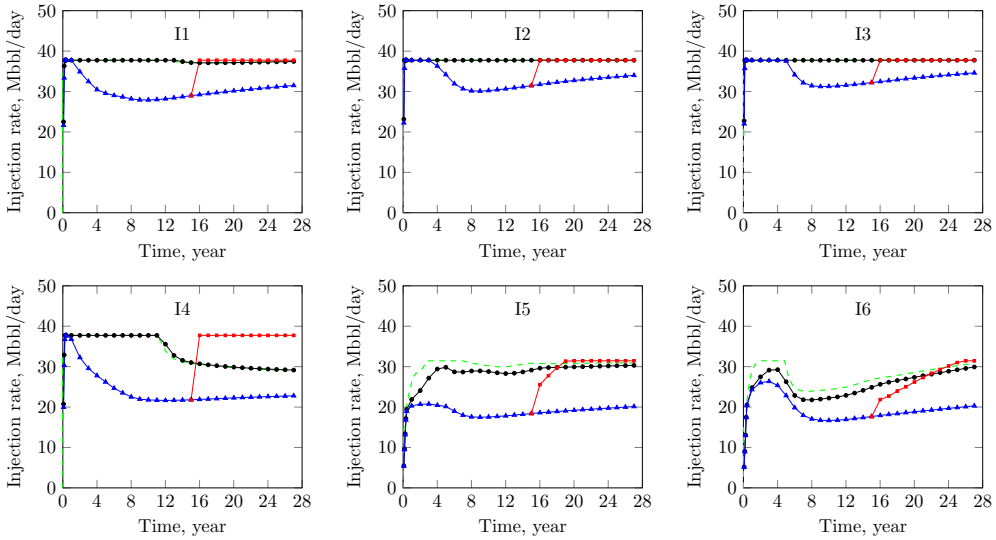

Figure 6.15: Water injection rate of each injection well, case study 2.

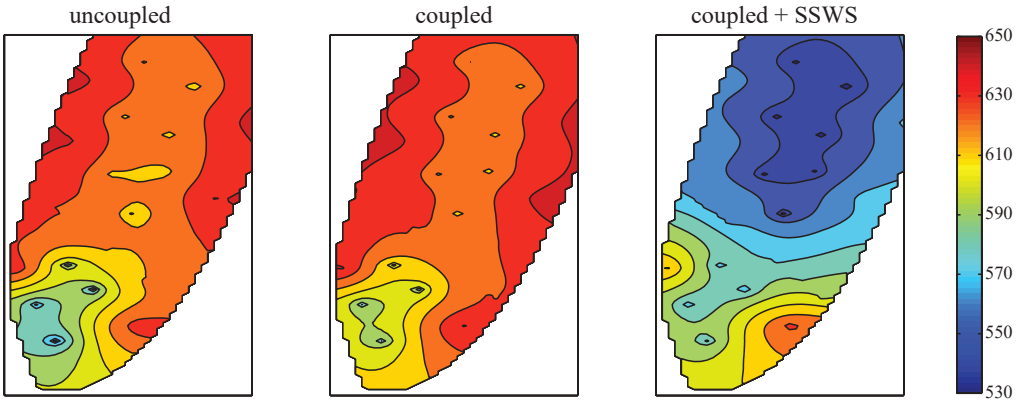

Figure 6.16: Final reservoir pressure distribution, case study 2.

Table 6.8: Summary of the production statistics, case study 2

	Uncoupled	Coupled	Coupled + SSWS
SSWS	N	N	Y
$Q_{\mathrm{o\,max}}$, Mbbl/day	184.6	133.6	133.6
$Q_{\mathrm{w\,max}}$, Mbbl/day	180.4	140.6	188.5
$Q_{wt\,\mathrm{max}}$, Mbbl/day	180.4	140.6	112.7
$Q_{\mathrm{inj\,max}}$ max, Mbbl/day	209.6	194.6	213.9
N_p, MMbbl	565.6	525.9	536.6
W_p, MMbbl	1241.2	874.1	1109.5
W_i, MMbbl	1977.7	1564.2	1787.1
final top watercut, %	91.1	88.4	67.2
final recovery, %	31.6	29.4	30.0
simulation time, min	9.7	23.0	24.2
average iterations per step	5.5	9.6	10.1

Flow assurance

The initial pressure–temperature route for each production well is shown in Figure 6.17. Under normal production, the reaching temperature of the two risers is above 45 °C. Along the production life, the reaching temperature at the FPSO gradually increases because of higher heat capacity of the water phase, as shown in Figure 6.18. When subsea water separation is performed, the reaching temperature for cluster A does not decrease too much because the oil production rate in riser A is still high enough. In the meantime, the reaching temperature in riser B reduces a little bit due to the change in pressure distribution.

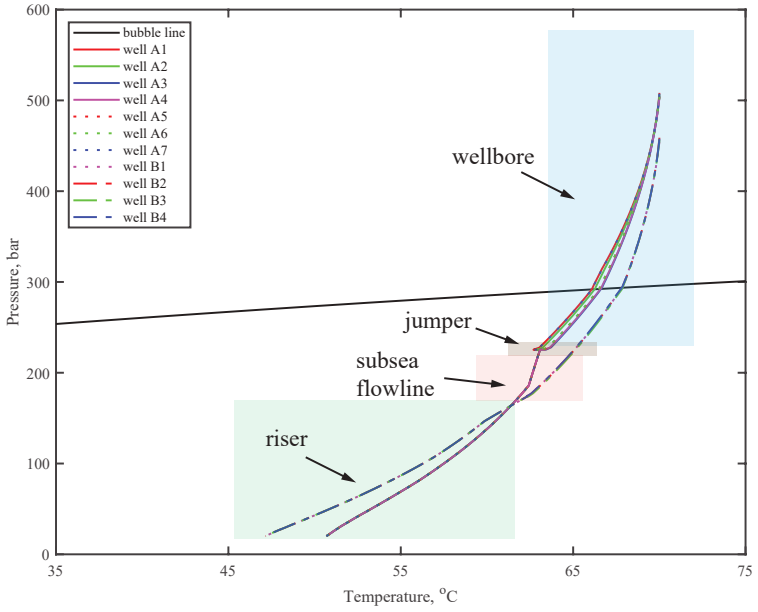

Figure 6.17: Pressure–temperature route of each production well, case study 2.

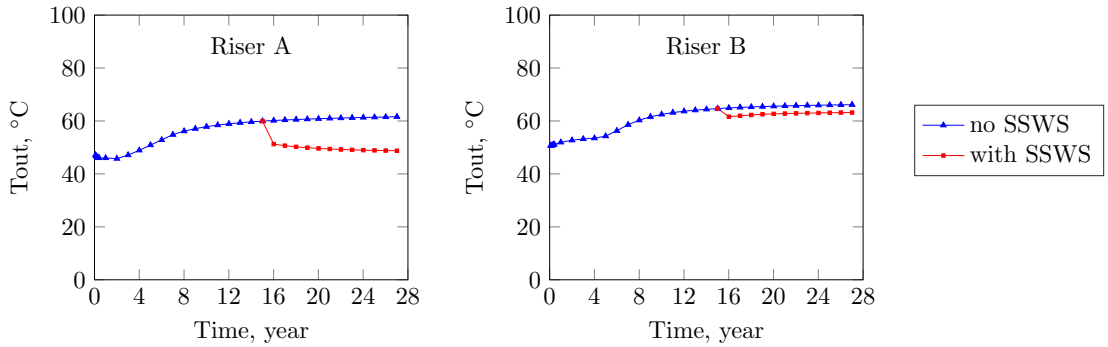

Figure 6.18: Reaching temperature of well cluster A and B, case study 2.

Economics

Figure 6.19 shows the estimated capex and opex of case study 2 based on the economics model in Appendix B.

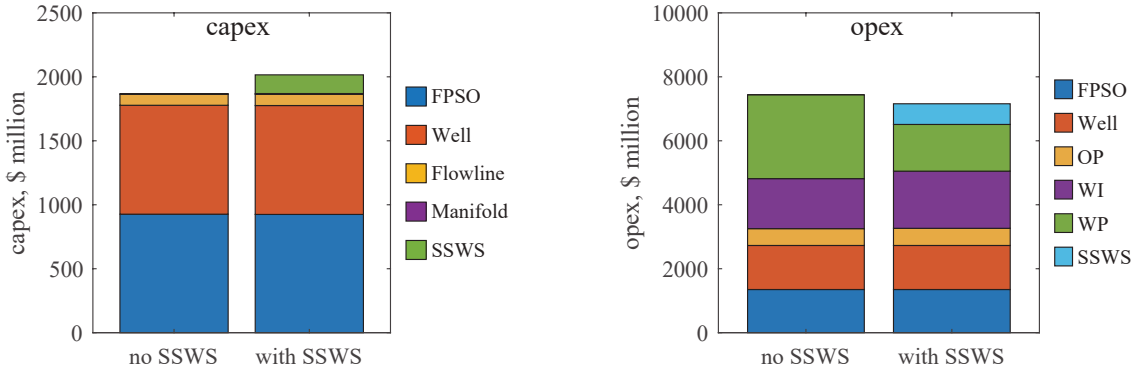

Figure 6.19: Comparison of the capex and opex components for scenarios with or without subsea water separation, case study 2.

Table 6.9 lists the values of the three quantitative indicators for case 2. With the economic parameters provided in Appendix B, the price of subsea water separator is estimated to be $146.2 million, and the NPV for the scenario with subsea water separation is 1.2% higher because of higher oil production.

Table 6.9: Quantitative indicators, case study 2

	no SSWS	with SSWS	
NPV, $ million	8268.5	8365.9	97.4 (1.2% ↑)
recovery, MMbbl	525.9	536.6	10.7 (0.6% ↑)
wax-free index	1.0	1.0	0.0%

Figure 6.20 shows the sensitivity of subsea water separator price on NPV. For this case study, the break-even capex of subsea water separator is $687 million, meaning that with an investment on the subsea separator higher than this value,

there will be no additional benefit compared to a scenario without subsea separator. Or, it will pay off the efforts in developing this subsea technology if the investment on it is less than $687 million.

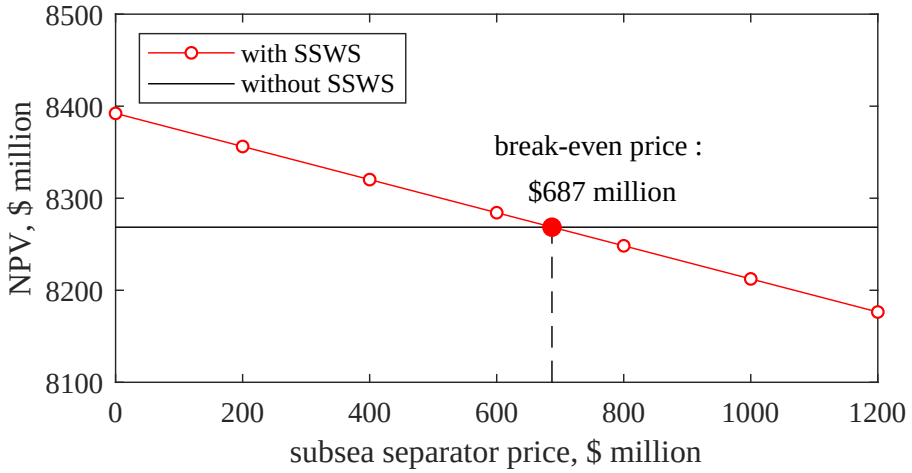

Figure 6.20: Relationship between subsea separator price and project NPV, case study 2.

6.3 Case study 3 : satellite wells + 3-D model

In this case study, the same reservoir of case study 2 is used, but with satellite wells. The purpose of this case study is to evaluate the effect of subsea water separation applied to individual wells. Also, a comparison with case study 2 provides a more comprehensive understanding of the effect of subsea water separation on different subsea configurations for the same field.

Table 6.10: Well information, case study 3

well name	wellbottom coordinates			wellhead to FPSO (m)	riser length (m)
	x (m)	y (m)	z (m)		
A1	2150	10950	5072	5028	2000
A2	2950	10150	5067	4648	2000
A3	1850	9150	5070	3244	2000
A4	2550	8550	5063	3118	2000
A5	1650	7250	5084	1557	2000
A6	2450	7350	5060	2264	2000
A7	1950	5950	5078	1471	2000
B1	450	2950	5083	3250	2000
B2	950	4250	5087	2001	2000
B3	1350	3450	5076	2878	2000
B4	750	1750	5081	4457	2000

The coordinates and the distances of the subsea flowlines of each production well are given in Table 6.10. The integrated model for a base scenario without subsea water separation is shown in Figure 6.21, where all the production wells are directly connected to the FPSO as satellite wells.

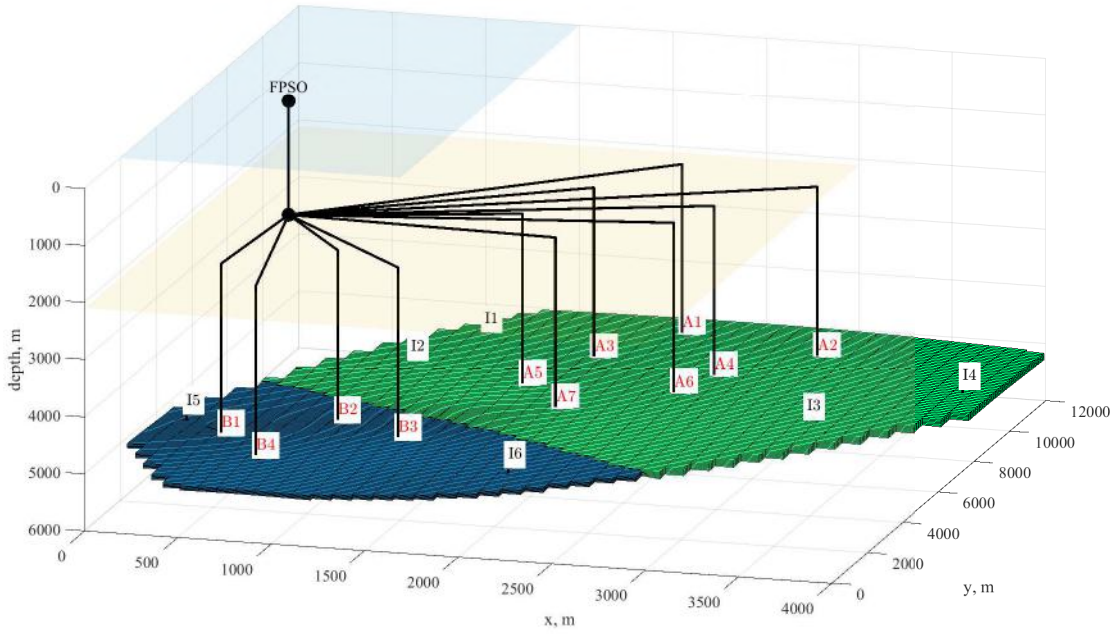

Figure 6.21: Integrated model for case study 3, without subsea water separation.

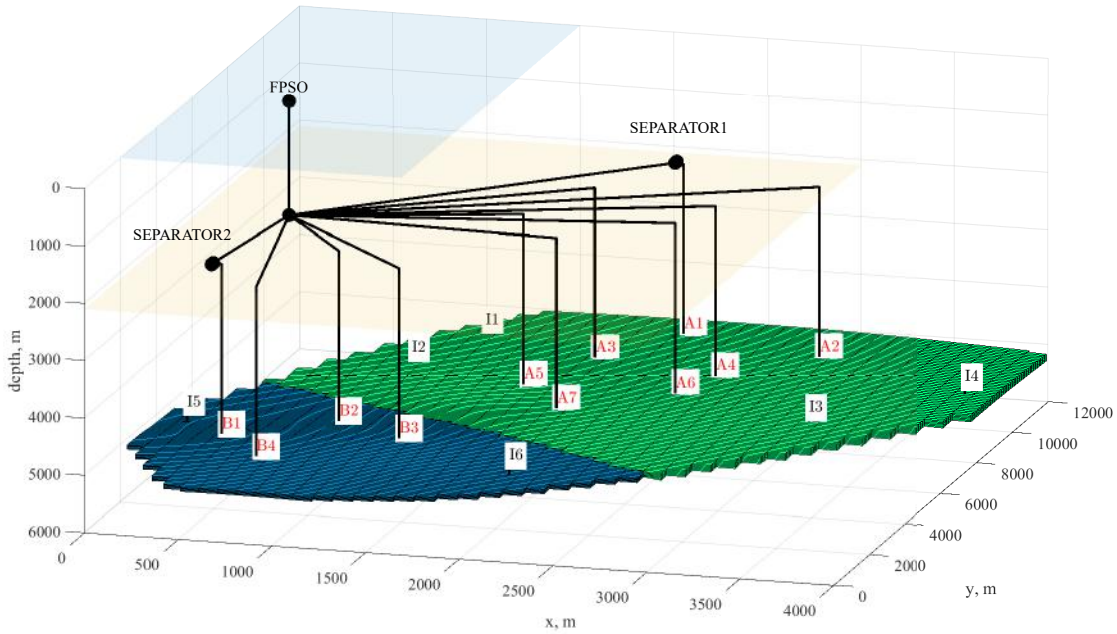

Figure 6.22: Integrated model for case study 3, with subsea water separation introduced on producer A1 and B1 from the 15th year.

In a comparative scenario, two subsea separators are introduced to the system in the 15th year. One for production well A1 and the other for B1, as shown in Figure 6.22. Well A1 and B1 are chosen because they exhibit highest watercut level in the 15th year. Water separation on these two wells are supposed to help lowering down their wellhead pressures and boosting higher oil productions. The two subsea separators are installed 50 m away from the corresponding wellheads. The separated water is supposed to be disposed into a fictitious disposal well nearby, and the hydrocarbon phases are transported to the FPSO. Detailed configurations of risers are avoided and all the 11 risers are assumed strictly vertical. Therefore, in Figure 6.21 and 6.22, there are actually 11 individual risers being connected to the FPSO, even though all the riser bases are shown overlapped as one point in the figures. The flowpaths are discretized into segments of similar size as in case study 2, and controls on injection wells are also the same.

6.3.1 Scenario settings

Two simulations are performed and compared:

1. **Coupled**. Fully integrated reservoir–network model without subsea water separation.

2. **Coupled + SSWS**. Fully integrated reservoir–network model with subsea water separation introduced to well A1 and B1 from the 15th year. The simulation is a "restart" of the first scenario on the 15th year where only the subsea network is reconfigured.

6.3.2 Results

The results of the two simulations in case study 3 are compared and analyzed from three aspects: reservoir engineering, flow assurance, and economics. Compared to case study 2, applying subsea water separation on satellite wells has a quite different impact on both production and temperature variation.

Reservoir engineering

Figures 6.23 to 6.27 present the simulated production variations for each well, and Figure 6.28 shows the final reservoir pressure distribution. Table 6.11 presents the simulated production statistics.

Results show that the introduction of subsea water separation on the two producers has an impact on all the wells in the field, not only on the two selected ones. While an increase of oil production from A1 and B1 is achieved as expected,

reduction of oil in other producers is also observed (Figure 6.24). This is because the different pressure distribution in the field requires an increase in water injection rate, and well interference plays an important role in characterizing the overall production of the field. As shown in Figure 6.25, when injection increases, the other offset producers of each injection well also receive more water, leading to a decrease of oil production in these producers. The simulation shows that the competing oil production of well A1 and B1 with other producers results in a negative effect on the overall oil production. Also, the final watercut on the FPSO is close (>88%) whether or not subsea water separation is applied, since only a small amount of water is handled by the subsea separators.

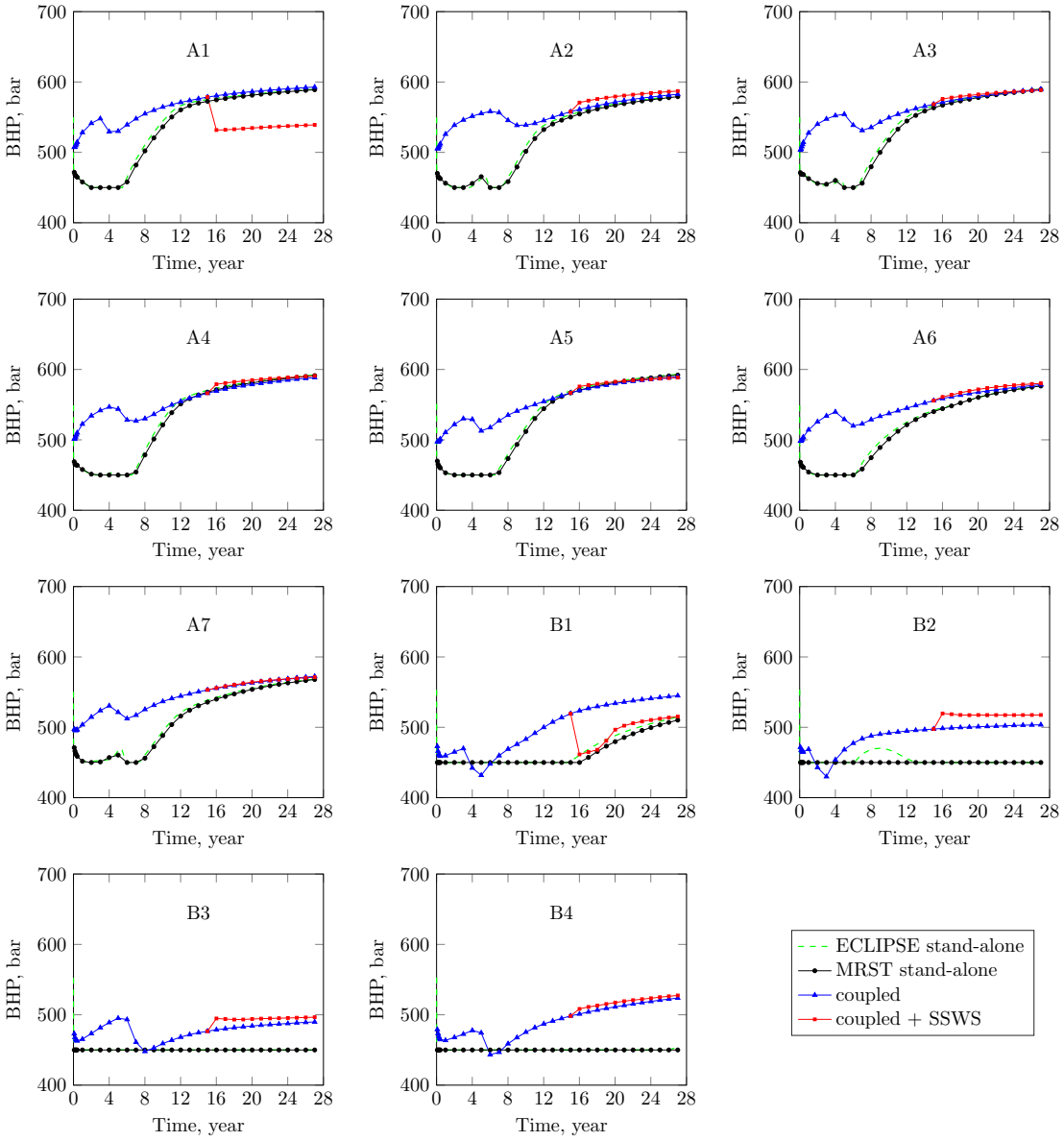

Figure 6.23: Bottomhole pressure of each production well, case study 3.

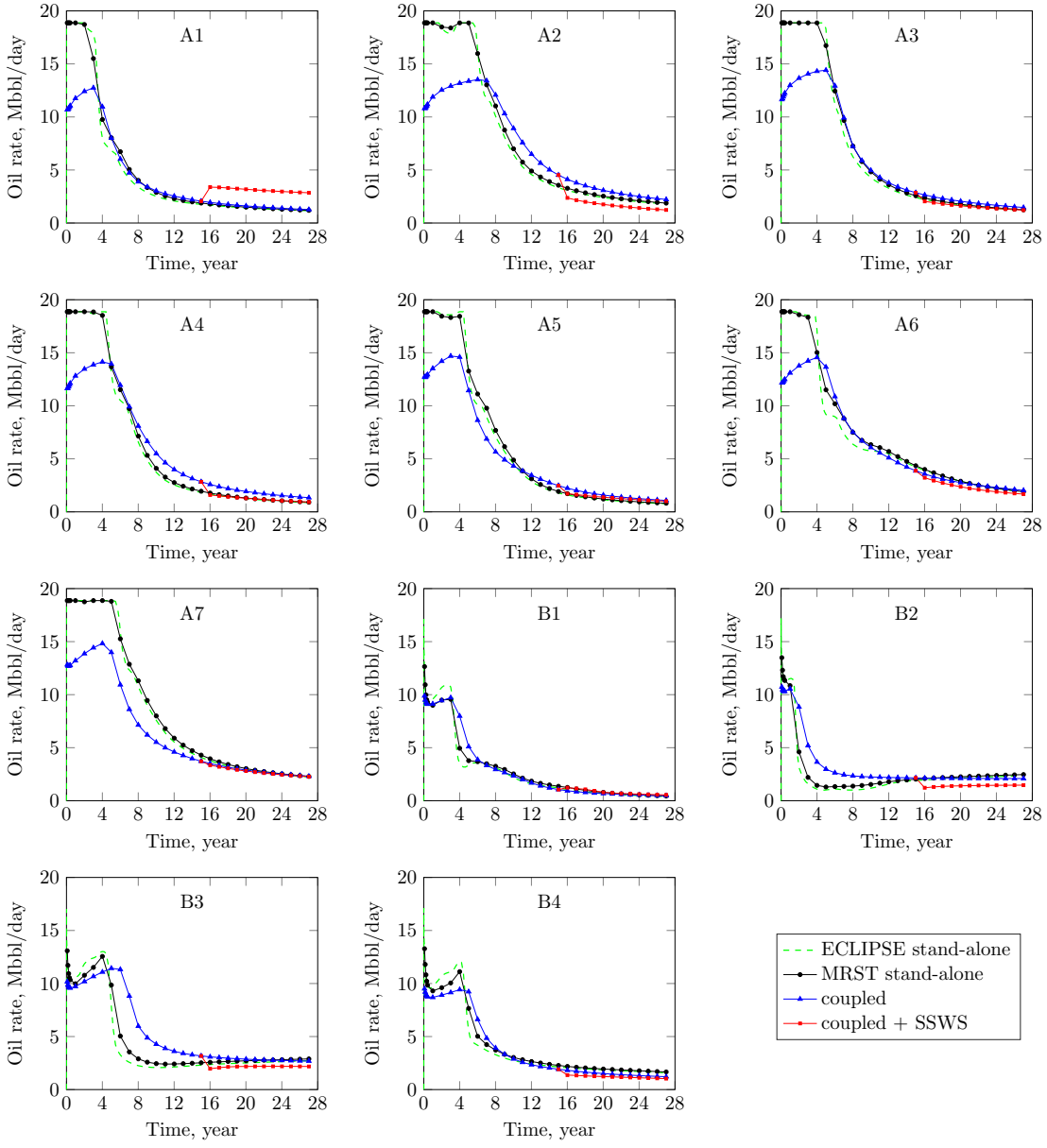

Figure 6.24: Oil production rate of each production well, case study 3.

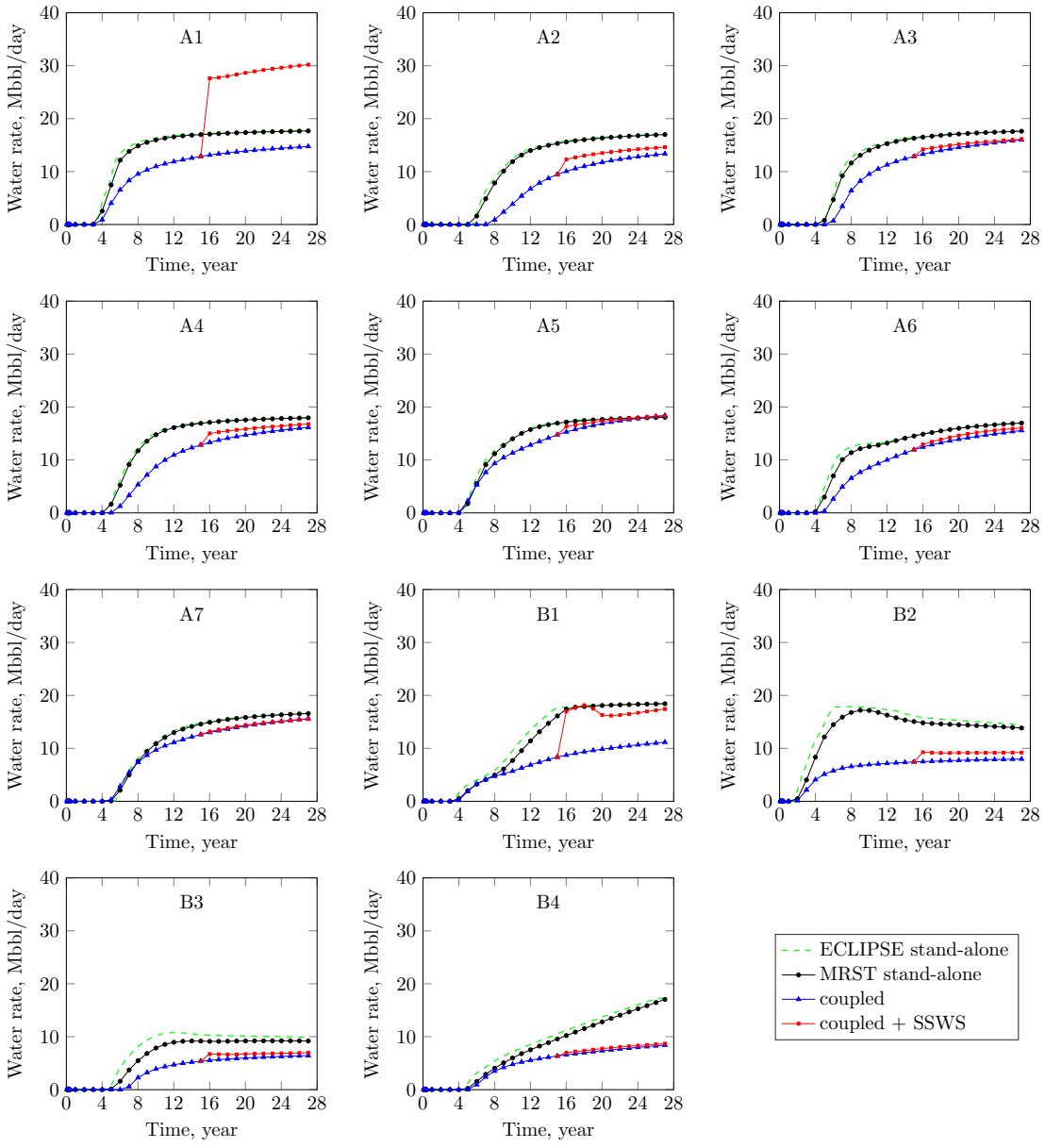

Figure 6.25: Water production rate of each production well, case study 3.

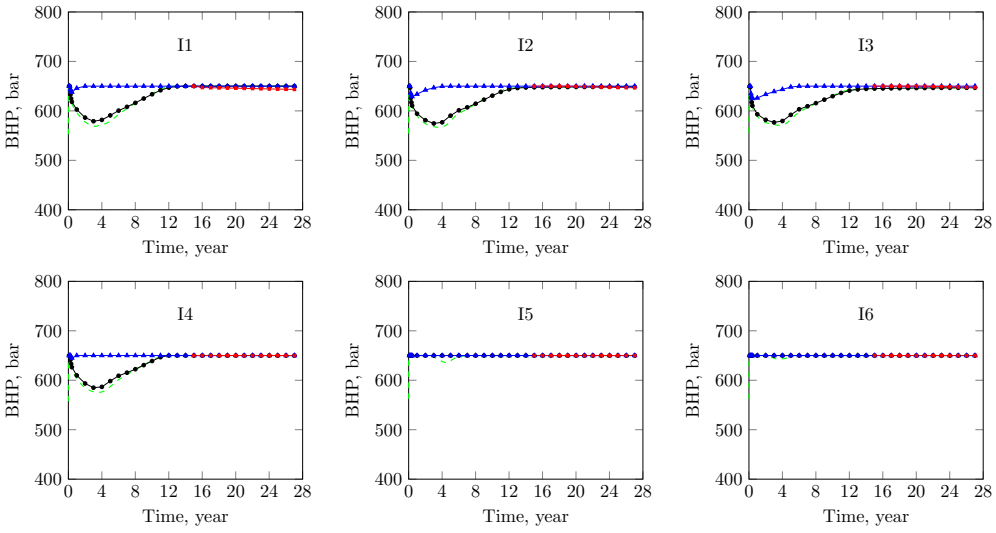

Figure 6.26: Bottomhole pressure of each injection well, case study 3.

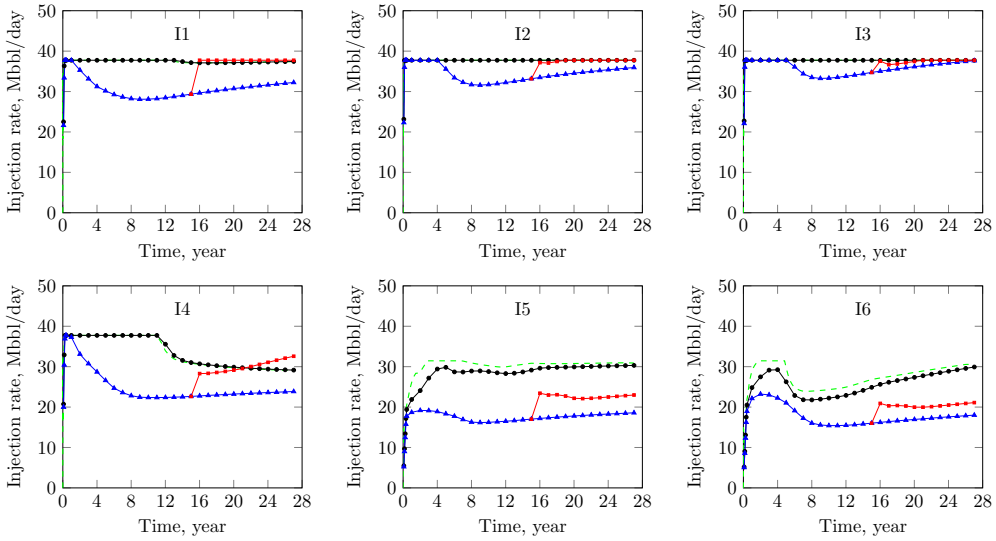

Figure 6.27: Water injection rate of each injection well, case study 3

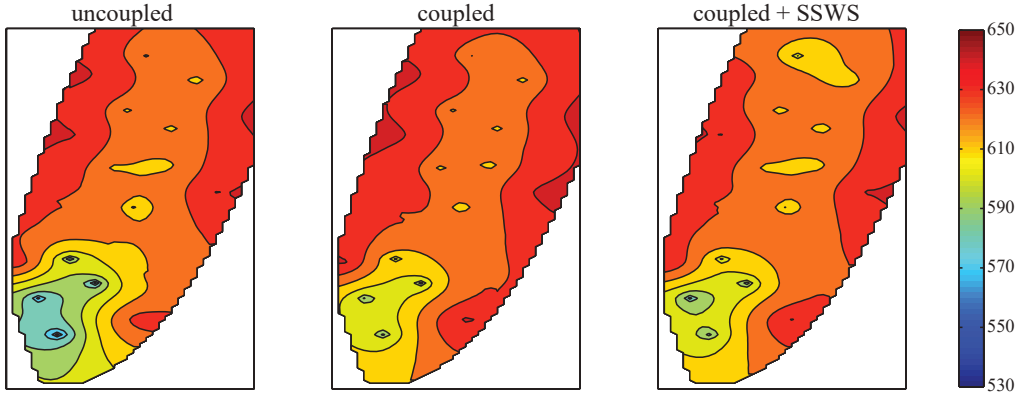

Figure 6.28: Final reservoir pressure distribution, case study 3.

Table 6.11: Summary of the production statistics, case study 3

	Coupled	Coupled + SSWS
SSWS	N	Y
$Q_{\mathrm{o\,max}}$, Mbbl/day	131.7	131.7
$Q_{\mathrm{w\,max}}$, Mbbl/day	143.8	169.9
$Q_{\mathrm{wt\,max}}$, Mbbl/day	143.8	122.3
$Q_{\mathrm{inj\,max}}$, Mbbl/day	191.4	191.4
N_p, MMbbl	526.4	513.5
W_p, MMbbl	889.3	1014.3
W_i, MMbbl	1579.7	1690.2
final top watercut, %	88.8	88.2
final recovery, %	29.4	28.7
simulation time, min	27.6	26.9
average iterations per step	11.5	11.8

Flow assurance

The pressure–temperature route of each satellite well at the beginning of production is shown in Figure 6.29. Under normal production, the reaching temperatures for each well are all above 35 °C. However, after adding subsea water separation on well A1 and B1, the reaching temperature of these two wells drops dramatically, as shown in Figure 6.30, which may induce wax deposition and consequently an injection of inhibitor would be required.

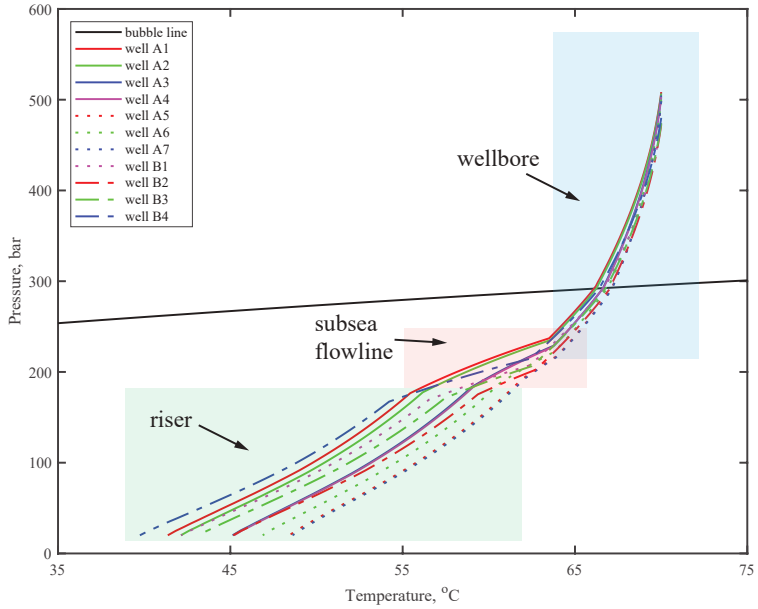

Figure 6.29: Pressure–temperature route of each production well, case study 3.

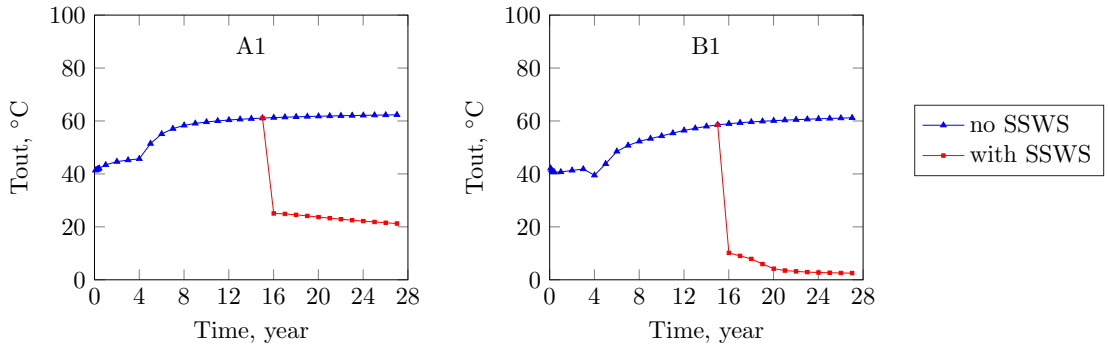

Figure 6.30: Reaching temperature of producer A1 and B1, case study 3.

Economics

Figure 6.31 shows the estimated capex and opex of case study 3. The estimated capex for the subsea water separators is $48.3 million.

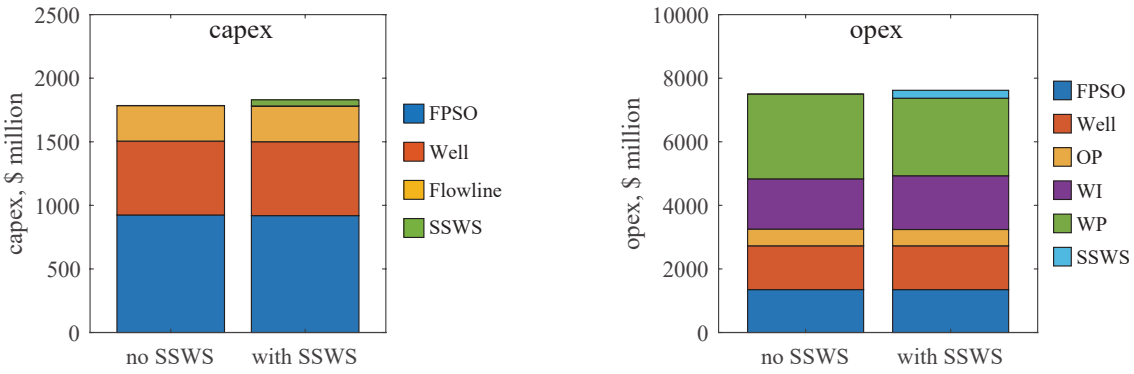

Figure 6.31: Comparison of the capex and opex components for scenarios with or without subsea water separation, case study 3.

Table 6.12 lists the values of the three quantitative indicators for case study 3. All the three indicators exhibit the negative effect of subsea water separation on field development. Specifically, the interference among wells leads to a decrease of oil recovery by 0.7% and a resulting decrease of NPV by 1.8%. There is also a high risk of wax deposition near the riser of well B1, making it not advantageous to apply subsea water separation on individual satellite wells.

Table 6.12: Quantitative indicators, case study 3

	no SSWS	with SSWS	
NPV, $ million	8314.1	8168.8	-145.3 (1.8% ↓)
recovery, MMbbl	526.4	513.5	-12.9 (0.7% ↓)
wax-free index	1.00	0.56	-44.0% ↓

6.4 Summary and discussion

In this chapter, three case studies are presented to study the effect of subsea water separation on three quantitative indicators: NPV, final recovery, and wax-free index, applying either the simple or fully integrated model.

It is learned from case 1 and 2 that subsea water separation on clustered well system has positive impacts on both NPV and final oil recovery because the effective reduction on wellhead back pressure stimulates higher oil production as well as less injection requirement. However, case 3 shows that subsea water separation on selected satellite wells is not as advantageous. When multiple satellite wells present, the change on one particular well will bring about changes for all the other wells through intricate injection–production relationships, not only for the ones on which subsea water separation is applied. The combined effect could be a reduction in final recovery and needs close analysis for each specific field condition.

Compared to a satellite well system, a clustered well system also manifests less risk related to temperature drop. Two factors contribute to the large temperature drop when applying subsea water separation on satellite wells. On one hand, the total subsea flowline length is larger for a satellite well compared to a clustered scenario. Longer exposure to the low seabed temperature makes higher cool down along the flowline. On the other hand, in late production life, the oil production rate is much lower in every single satellite well, while the commingled production from several wells in a clustered scenario is helpful in maintaining appropriate flow velocities.

For a clustered well system, even though subsea water separation has the potential to improve NPV, it is not a technology to enhance oil recovery since neither the sweep efficiency nor the displacement efficiency is improved. Based on case study 2 and the economic model used in this study, an estimated break-even price for a subsea separator with capacity of around 150 Mbbl/day is $687 million. The wide industrial application of this subsea technology for deepwater still requires results on issues including structural design, material qualification, manufacturing and installation, and so on.

Chapter 7

Conclusion

In this work, four integrated production modeling approaches applying two types of reservoir models and three types of coupling schemes were established and coded in MATLAB environment:

1. Tank reservoir model + network model NET (implicit scheme)
2. 3-D reservoir model + network model NET (implicit scheme)
3. 3-D reservoir simulator MRST + network simulator OLGA (explicit scheme)
4. 3-D reservoir simulator MRST + network simulator OLGA (partially-implicit)

The established models were applied to three case studies with different subsea configurations to evaluate the effect of subsea water separation. The case studies cover both clustered well system and satellite well system. Also, the effect of subsea water separation both for green field layout design and brown field revitalization is discussed.

The main conclusions related to the performance of different integrated models established in the this work include:

1. **Explicit coupling scheme** is flexible in terms of software choice, but a rigorous convergence algorithm should be applied to obtain real coupled solutions from the two software. Loose coupling between the two domains can lead to large errors when reservoir condition and flow rates change significantly during one simulation timestep since the two domains are never solved at the same time. The example in the thesis reported the largest relative error about 80% in water production rate around water breakthrough.
2. **Partially-implicit scheme** provides less relative errors between the two domains but more Newton iterations are required for convergence which results in longer simulation time. The example in the thesis reported 1.7 times the

simulation time compared to a loose explicit coupling scheme. To perform partially-implicit scheme, the reservoir simulator should be open-source at least to Newton iteration level.

3. **Fully integrated**, or **implicit scheme**, is preferential to explicit and partially-implicit schemes in both reliability and simulation time since the reservoir and network equations are solved simultaneously. To establish a fully integrated model, both the reservoir and network equations should be approachable.

4. **Simple implicit IPM with tank model** can perform fast forecasts when a numerical reservoir model is unavailable, but is not able to reflect the impact of water channeling on recovery.

Conclusions considering subsea water separation include:

1. **Subsea water separation for clustered well system** can stimulate higher production from wells suppressed by the header at the manifold, and reduce the injection requirement or equivalently, lower down injection pressure.

2. **Subsea water separation on selected satellite wells** impacts not only the working conditions for the selected wells but also all the other producers and injectors in the field, which may lead to a decrease in overall oil production.

3. **Subsea water separation leads to lower reaching temperature** due to decreased fluid flow rate and lower fluid heat capacity. Special care should be taken to prevent wax deposition risk in late production years. Clustered well system is less vulnerable in this sense.

4. **Subsea water separation has the potential to improve project NPV** but not to enhance oil recovery since neither the sweep efficiency nor the displacement efficiency changes.

As extensions of this study, several future topics are listed below:

1. **Injection system** can be incorporated into the integrated model to further discuss the possibility of re-injecting the separated water on the seafloor, reducing the amount of water injected from the topside host.

2. **Separation efficiency** of the subsea separator can be included for a better representation of the separator model.

3. **Production optimization** based on the integrated production models can further reflect all types of constraints in the system.

Bibliography

[1] SIFUENTES, W., MORENO, J., KUMARAN, P., et al. "Samarang Integrated Operations (IO): Integrated Asset Modeling – An Innovative Approach For Long Term Production Planning Focused On Enhance Oil Recovery". In: *SPE/IATMI Asia Pacific Oil & Gas Conference and Exhibition*. Society of Petroleum Engineers, 2015.

[2] OKAFOR, C. C. "Breaking the Frontiers for Effective Flow Assurance Using Integrated Asset Models (IAM)". In: *SPE Arctic and Extreme Environments Conference and Exhibition*. Society of Petroleum Engineers, 2011.

[3] DEKKER, M., THAKKAR, A., OTHERS. "Digitalisation – The Next Frontier for the Offshore Industry". In: *Offshore Technology Conference*. Offshore Technology Conference, 2018.

[4] UDOFIA, E., OBONG, B. "Digital Oilfield Implementation Challenges Management in Offshore Environment". In: *Offshore Technology Conference*. Offshore Technology Conference, 2018.

[5] TALABI, O., NITURA, J., BINIWALE, S., et al. "Integrated Asset Modeling: Modernizing the Perspective for Short-Term Forecasting and Production Enhancements". In: *SPE Asia Pacific Oil & Gas Conference and Exhibition*. Society of Petroleum Engineers, 2016.

[6] BINIWALE, S., NITURA, J., SIFUENTES, W., et al. "Integrated Live Asset Modeling – A Necessity to Unlock Oil in Mature Fields Achieving True Integrated Operations IO". In: *International Petroleum Technology Conference*. International Petroleum Technology Conference, 2016.

[7] SAPUTELLI, L. A., RUDOLPH, S. R., EMBSER, J. T. "Integrated Production Model Calibration Applied to a Gulf of Mexico Sub-sea Field". In: *SPE Intelligent Energy Conference and Exhibition*. Society of Petroleum Engineers, 2010.

[8] ROTONDI, M., COMINELLI, A., DI GIORGIO, C., et al. "The Benefits of Integrated Asset Modeling: Lesson Learned from Field Cases". In: *SPE*

Europec/EAGE Annual Conference and Exhibition. Society of Petroleum Engineers, 2008.

[9] DEMPSEY, J., PATTERSON, J., COATS, K., et al. "An Efficient Model for Evaluating Gas Field Gathering System Design", *Journal of Petroleum Technology*, v. 23, n. 09, pp. 1067–1073, 1971.

[10] STARTZMAN, R. A., BRUMMETT, W., RANNEY, J., et al. "Computer Combines Offshore Facilities and Reservoir Forecasts", *Petroleum Engineer*, v. 65, 1977.

[11] EMANUEL, A. S., RANNEY, J. C. "Studies of Offshore Reservoir with an Interfaced Reservoir/Piping Network Simulator", *Journal of Petroleum Technology*, v. 33, n. 03, pp. 399–406, 1981.

[12] BREAUX, E., MONROE, S., BLANK, L., et al. "Application of a Reservoir Simulator Interfaced with a Surface Facility Network: A Case History", *Society of Petroleum Engineers Journal*, v. 25, n. 03, pp. 397–404, 1985.

[13] HOOI, H., GOOBIE, L., COOK, R., et al. "The Integrated Team Approach to the Optimization of a Mature Gas Field". In: *SPE Gas Technology Symposium*. Society of Petroleum Engineers, 1993.

[14] DEUTMAN, R., VAN RIJEN, M. "A Case Study of Integrated Gas Field System Modelling in the North Sea Environment". In: *Offshore Europe*. Society of Petroleum Engineers, 1997.

[15] LITVAK, M., DARLOW, B. "Surface Network and Well Tubinghead Pressure Constraints in Compositional Simulation". In: *SPE Symposium on Reservoir Simultion*. Society of Petroleum Engineers, 1995.

[16] LITVAK, M. L., WANG, C. H. "Integrated Reservoir and Surface Pipeline Network Compositional Simulations". In: *SPE International Conference and Exhibition in China*. Society of Petroleum Engineers, 1998.

[17] SCHIOZER, D. J. *Simultaneous Simulation of Reservoir and Surface Facilities*. Tese de Doutorado, Stanford University, 1994.

[18] BYER, T. J., EDWARDS, M. G., AZIZ, K. "Preconditioned Newton Methods for Fully Coupled Reservoir and Surface Facility Models". In: *SPE Annual Technical Conference and Exhibition*. Society of Petroleum Engineers, 1998.

[19] BYER, T. J. *Preconditioned Newton Methods for Simulation of Reservoirs with Surface Facilities*. Tese de Doutorado, Stanford University, 2000.

[20] HEPGULER, G., BARUA, S., BARD, W. "Integration of a Field Surface & Production Network With a Reservoir Simulator", *SPE Computer Applications*, v. 9, n. 03, pp. 88–92, 1997.

[21] TRICK, M. "A Different Approach to Coupling a Reservoir Simulator with a Surface Facilities Model". In: *SPE Gas Technology Symposium*. Society of Petroleum Engineers, 1998.

[22] ARIAS, B., CHITALE, A., BISHOP, S., et al. "Role of Integrated Asset Modeling in Optimizing Na Kika Production". In: *International Petroleum Technology Conference*. International Petroleum Technology Conference, 2007.

[23] AGEH, E. A., ADEGOKE, A., UZOH, O. J. "Using Integrated Production Modeling (IPM) as an Optimization Tool for Field Development Planning and Management". In: *Annual SPE International Conference and Exhibition*. Society of Petroleum Engineers, 2010.

[24] COUËT, B., DJIKPESSE, H., TONKIN, T., et al. "Production Enhancement Through Integrated Asset Modeling Optimization". In: *SPE Production and Operations Conference and Exhibition*. Society of Petroleum Engineers, 2010.

[25] BYBEE, K. "Integrated Production and Reservoir Modeling To Optimize Deepwater Development", *Journal of Petroleum Technology*, v. 63, n. 05, pp. 70–73, 2011.

[26] STEVENSON, A. E., WANORUE, E. P., OKORO, E. C., et al. "Lessons Learned from Building a Large Integrated Production Model for Offshore Assets in Nigeria". In: *SPE Annual Technical Conference and Exhibition*. Society of Petroleum Engineers, 2012.

[27] ORIOHA, H. I., GRUBA, C. J., MUONEKE, G., et al. "Application of IPM Modeling for Production Surveillance, Allocation and Optimization". In: *SPE International Production and Operations Conference & Exhibition*. Society of Petroleum Engineers, 2012.

[28] NAZAROV, R., ZALAMA, P., HERNANDEZ, M., et al. "Integrated Asset Modeling in Mature Offshore Fields: Challenges and Successes". In: *SPE Biennial Energy Resources Conference*. Society of Petroleum Engineers, 2014.

[29] KABDENOV, S., AITKAZIN, M., MACARY, S., et al. "IPM Tool for Strategic Decisions: Diverse Applications of IPM in the Supergiant Tengiz Field". In: *International Petroleum Technology Conference*. International Petroleum Technology Conference, 2014.

[30] ALAIGBA, D., ORODU, O. D., AGUILERA, M. "Production Optimization in the Duke Field Using the IPM Suite". In: *SPE Nigeria Annual International Conference and Exhibition*. Society of Petroleum Engineers, 2016.

[31] ONBERGENOV, U., AITKAZIN, M., TANG, Y., et al. "Best Practices in Calibration of Integrated Production Modeling for Tengiz Field". In: *SPE Annual Caspian Technical Conference and Exhibition*. Society of Petroleum Engineers, 2017.

[32] GONG, X., SIMMS, G., FOWLER, R., et al. "Integrated Reservoir Study of the Who Dat Field". In: *Offshore Technology Conference*. Offshore Technology Conference, 2018.

[33] WATSON, M. J., HAWKES, N., PICKERING, P. F., et al. "Integrated Flow-Assurance Modeling of the BP Angola Block 18 Western Area Development", *SPE Projects, Facilities & Construction*, v. 2, n. 02, pp. 1–12, 2007.

[34] HALLIBURTON. *Nexus Technical Reference Guide*. 2016.

[35] CLARA, C. P. R., SHERIEF, M., CHONG, T. S., et al. "Stacked Reservoirs Development Optimization Based on a Fully Implicit Surface-Subsurface Nexus Modeling – A Case Study from the UAE". In: *SPE Reservoir Characterization and Simulation Conference and Exhibition*. Society of Petroleum Engineers, 2013.

[36] HATVIK, M., NØRGÅRD, J. P., BERG, K., et al. "Optimized Field Development through Integrating Field Network with Dynamic Reservoir Model Methods". In: *Offshore Technology Conference*. Offshore Technology Conference, 2018.

[37] MARMIER, R., DECROUX, B., PARAN, M., et al. "Unlocking the Development of Absheron Gas Condensate Field through an Integrated Asset Work and Modeling". In: *SPE Annual Caspian Technical Conference and Exhibition*. Society of Petroleum Engineers, 2017.

[38] MARIR, B., ALLOUTI, A., COBB, D. O., et al. "Fully-Coupled Surface Network Model with Stacked Multi-Reservoir Model of a New Abu Dhabi Offshore Field". In: *Abu Dhabi International Petroleum Exhibition and Conference*. Society of Petroleum Engineers, 2014.

[39] PATACCHINI, L., BEDEWI, M., FAROUK, M. "Fully Implicit Coupling of Multiple Reservoir Models with Common Water Injection Facilities". In: *Abu Dhabi International Petroleum Exhibition and Conference*. Society of Petroleum Engineers, 2016.

[40] SU, S. J., PATACCHINI, L., MOHMED, F., et al. "Coupling Production and Injection Systems with Multiple Reservoir Models: A Novel Method of Optimizing Development Strategies in a Mature Giant Oilfield". In: *Abu Dhabi International Petroleum Exhibition and Conference*. Society of Petroleum Engineers, 2016.

[41] MARMIER, R., AJIBOYE, A., BERSON, F., et al. "Unlocking Marginal Deep Water Fields Development through Reservoir to Surface Integrated Asset Modelling". In: *International Petroleum Technology Conference*. International Petroleum Technology Conference, 2019.

[42] EDIH, M., NNANNA, E., NWANKWO, C. "A Systematic Approach to Intelligent Well Performance Modelling Using IPM Suite". In: *SPE Nigeria Annual International Conference and Exhibition*. Society of Petroleum Engineers, 2016.

[43] COSTA, D., VU, V. K., BARNAY, G. C., et al. "Investigation of a Subsea Separation Station Operating Envelope Using Subsurface-to-Topsides Integrated Dynamic Simulations". In: *Offshore Technology Conference*. Offshore Technology Conference, 2007.

[44] TEIXEIRA, G. N. R., SCHIOZER, D. J. "Integration of Production Facilities and Reservoir Simulation for Comparison of Subsea and Conventional Lift Technologies". In: *EAGE Annual Conference & Exihibition*. Society of Petroleum Engineers, 2013.

[45] GALVAN, D., MCVINNIE, G., DINDORUK, B. "Perdido Development: Unified Fluid Model for Integrated-Production-System Modeling", *SPE Reservoir Evaluation & Engineering*, v. 18, n. 03, pp. 303–317, 2015.

[46] AL-SHAMMARI, H., BORA, A. "Integrated Water Management Challenges". In: *International Petroleum Technology Conference*. International Petroleum Technology Conference.

[47] ALARY, V., MARCHAIS, F., PALERMO, T. "Subsea Water Separation and Injection: A Solution for Hydrates". In: *Offshore Technology Conference*. Offshore Technology Conference, 2000.

[48] ALARY, V., FALCIMAIGNE, J. "Subsea Water Separation: A Cost-Effective Solution for Ultra Deep Water Production". In: *17th World Petroleum Congress*. World Petroleum Congress, 2002.

[49] HENDRICKS, R., MCKENZIE, L. J., JAHNSEN, O. F., et al. "Subsea Separation – An Undervalued Tool for Increased Oil Recovery IOR". In: *SPE Asia Pacific Oil & Gas Conference and Exhibition*. Society of Petroleum Engineers, 2016.

[50] MORAES, C., DA SILVA, F., MONTEIRO, A., et al. "Subsea versus Topside Processing – Conventional and New Technologies". In: *Offshore Technology Conference Brasil*. Offshore Technology Conference, 2013.

[51] WU, X., BABATOLA, F., JIANG, L., et al. "Applying Subsea Fluid-Processing Technologies for Deepwater Operations", *Oil and Gas Facilities*, v. 5, n. 04, pp. 1–10, 2016.

[52] RASMUSSEN, A. W. "Troll Pilot Technology – The Next Step". In: *Offshore Technology Conference*. Offshore Technology Conference, 2002.

[53] DO VALE, O., GARCIA, J., VILLA, M. "VASPS Installation and Operation at Campos Basin". In: *Offshore Technology Conference*. Offshore Technology Conference, 2002.

[54] PEIXOTO, G. D. A., RIBEIRO, G., BARROS, P. A., et al. "VASPS Prototype in Marimba Field – Workover and Re-Start". In: *SPE Latin American and Caribbean Petroleum Engineering Conference*. Society of Petroleum Engineers, 2005.

[55] GJERDSETH, A. C., FAANES, A., RAMBERG, R. "The Tordis IOR Project". In: *Offshore Technology Conference*. Offshore Technology Conference, 2007.

[56] ERIKSEN, S., MCLERNON, H., MOHR, C. "Pazflor SSPS Project; Testing and Qualification of Novel Technology: A Key to Success". In: *Offshore Technology Conference*. Offshore Technology Conference, 2012.

[57] GILYARD, D. T., BROOKBANK, E. B., OTHERS. "The Development of Subsea Boosting Capabilities for Deepwater Perdido and BC 10 Assets". In:

SPE Annual Technical Conference and Exhibition. Society of Petroleum Engineers, 2010.

[58] PARSHALL, J. "Brazil Parque das Conchas Project Sets Subsea Separation, Pumping Milestone", *Journal of Petroleum Technology*, v. 61, n. 09, pp. 38–42, 2009.

[59] DEVEGOWDA, D., SCOTT, S. "An Assessment of Subsea Production Systems". In: *SPE Annual Technical Conference and Exhibition*. Society of Petroleum Engineers, 2003.

[60] MUKTADIR, G., AMRO, M. M., SCHRAMM, A. "Review and Applicability of Downhole Separation Technology". In: *SPE Middle East Artificial Lift Conference and Exhibition*. Society of Petroleum Engineers, 2016.

[61] SHERIDAN, E., AYLING, I., HIXSON, J. "Downhole Oil and Water Seperation: a New Start". In: *International Petroleum Technology Conference*. International Petroleum Technology Conference, 2013.

[62] BRINGEDAL, B., INGEBRETSEN, T., HAUGEN, K. "Subsea Separation and Reinjection of Produced Water". In: *Offshore Technology Conference*. Offshore Technology Conference, 1999.

[63] MIKKELSEN, J. K., NORHEIM, T., SAGATUN, S. I. "The Troll Story". In: *Offshore Technology Conference*. Offshore Technology Conference, 2005.

[64] KLOEVE, B., HESTAD, E. "Tordis Field Development: Single Satellite Wells With Subsea Manifold Centre". In: *Offshore Europe*. Society of Petroleum Engineers, 1991.

[65] FANTOFT, R., HENDRIKS, T., CHIN, R. "Compact Subsea Separation System with Integrated Sand Handling". In: *Offshore Technology Conference*. Offshore Technology Conference, 2004.

[66] MOGSETH, G. "Functional Verification of the Worlds First Full Field Subsea Separation System – TIORA". In: *Offshore Technology Conference*. Offshore Technology Conference, 2008.

[67] FANTOFT, R., HENDRIKS, T., ELDE, J. "Technology Qualification for the Tordis Subsea Separation, Boosting, and Injection System". In: *Offshore Technology Conference*. Offshore Technology Conference, 2006.

[68] NEUENKIRCHEN, J. H. "Tordis Subsea Separation Boosting and Injection (SSBI) Project : Project Presentation and Description of the Production Control System". In: *Subsea Controls and Data Acquisition 2006: Controlling the Future Subsea*. Society of Underwater Technology, 2006.

[69] LORENZATTO, R. A., JUINITI, R., GOMES, J. A. T., et al. "The Marlim Field Development: Strategies and Challenges". In: *Offshore Technology Conference*. Offshore Technology Conference, 2004.

[70] EUPHEMIO, M., OLIVEIRA, R., NUNES, G., et al. "Subsea Oil/Water Separation of Heavy Oil: Overview of the Main Challenges for the Marlim Field-Campos Basin". In: *Offshore Technology Conference*. Offshore Technology Conference, 2007.

[71] SAGATUN, S. I., GRAMME, P., LIE, G. H., et al. "The Pipe Separator – Simulations and Experimental Results". In: *Offshore Technology Conference*. Offshore Technology Conference, 2008.

[72] ORLOWSKI, R. T. C., EUPHEMIO, M. L. L., CASTRO, F. G., et al. "Marlim 3 Phase Subsea Separation System – Challenges and Solutions for the Subsea Separation Station to Cope with Process Requirements". In: *Offshore Technology Conference*. Offshore Technology Conference, 2012.

[73] PEREIRA, R. M., CAMPOS, M. C. M. M. D., DE OLIVEIRA, D. A., et al. "SS: Marlim 3 Phase Subsea Separation System: Controls Design Incorporating Dynamic Simulation Work". In: *Offshore Technology Conference*. Offshore Technology Conference, 2012.

[74] CAPELA MORAES, C. A., DA SILVA, F. S., MARINS, L. P. M., et al. "Marlim 3 Phase Subsea Separation System: Subsea Process Design and Technology Qualification Program". In: *Offshore Technology Conference*. Offshore Technology Conference, 2012.

[75] DUARTE, D. G., DE MELO, A. V., CARDOSO, C. B., et al. "Marlim 3 Phase Subsea Separation System – Challenges and Innovative Solutions for Flow Assurance and Hydrate Prevention Strategy". In: *Offshore Technology Conference*. Offshore Technology Conference, 2012.

[76] MORAES, C. A., MONTEIRO, A. S., SILVA, F. S., et al. "Commissioning and Start-up of Subsea Marlim Oil and Water Separation System". In: *Offshore Technology Conference Brasil*. Offshore Technology Conference, 2013.

[77] LORENZATTO, R., JUINITI, R., GOMES, J., et al. "The Marlim Field Development: Strategies and Challenges". In: *Offshore Technology Conference*. Offshore Technology Conference, 2004.

[78] ORLOWSKI, R., EUPHEMIO, M. L. L., EUPHEMIO, M. L., et al. "Marlim 3 Phase Subsea Separation System – Challenges and Solutions for the Subsea Separation Station to Cope with Process Requirements". In: *Offshore Technology Conference*. Offshore Technology Conference, 2012.

[79] TAITEL, Y. "Advances in Two-Phase Flow Mechanistic Modeling". In: *University of Tulsa Centennial Petroleum Engineering Symposium*. Society of Petroleum Engineers, 1994.

[80] LIGNY, F., ROBERTS, I., JAMES, D., et al. "Integrated Subsea Supplier-Led Solution: A Case Study". In: *Offshore Technology Conference*. Offshore Technology Conference, 2018.

[81] PETEX. *Manual of MBAL, Reservoir Engineering Toolkit*. 2005.

[82] MARMIER, R., BRANCHFLOWER, M., FOUCAULT, H. "Integrated Asset Modeling – Coupling to a Dynamic Well and Network Flow Simulator for Improved Flow Assurance in Field Development Planning and Production Forecasting". In: *International Petroleum Technology Conference*. International Petroleum Technology Conference, 2016.

[83] DI LULLO, A., MANTEGAZZA, T., OMARINI, P., et al. "From Integrated Asset Model To Integrated Flow Assurance Model : A Step Forward in the Design of Complex O & G Fields". In: *Offshore Mediterranean Conference and Exhibition*. Society of Petroleum Engineers, 2011.

[84] BARROUX, C., DUCHET-SUCHAUX, P., SAMIER, P., et al. "Linking Reservoir and Surface Simulators: How to Improve the Coupled Solutions". In: *SPE European Petroleum Conference*. Society of Petroleum Engineers, 2000.

[85] COATS, B., FLEMING, G., WATTS, J., et al. "A Generalized Wellbore and Surface Facility Model, Fully Coupled to a Reservoir Simulator", *SPE Reservoir Evaluation & Engineering*, v. 7, n. 02, pp. 132–142, 2004.

[86] GHORAYEB, K., HOLMES, J., TORRENS, R., et al. "A General Purpose Controller for Coupling Multiple Reservoir Simulations and Surface Facility Networks". In: *SPE Reservoir Simulation Symposium*. Society of Petroleum Engineers, 2013.

[87] MCCAIN JR, W. D. *Properties of Petroleum Fluids*. PennWell Corporation, 2017.

[88] VERSTEEG, H. K., MALALASEKERA, W. *An Introduction to Computational Fluid Dynamics: the Finite Volume Method*. Pearson Education, 2007.

[89] BRENNEN, C. E., BRENNEN, C. E. *Fundamentals of Multiphase Flow*. Cambridge University Press, 2005.

[90] ANSYS. *ANSYS Fluent Theory Guide*. 2017.

[91] BENDIKSEN, K. H., MAINES, D., MOE, R., et al. "The Dynamic Two-Fluid Model OLGA: Theory and Application", *SPE Production engineering*, v. 6, n. 02, pp. 171–180, 1991.

[92] WATSON, M., HAWKES, N., LUNA-ORTIZ, E., et al. "Application of Advanced Chemical Process Design Methods to Integrated Production Modeling". In: *15th International Conference on Multiphase Production Technology*. BHR Group, 2011.

[93] LIE, K.-A. *An Introduction to Reservoir Simulation Using MATLAB/GNU Octave : User Guide to the Matlab Reservoir Simulation Toolbox (MRST)*. Cambridage University Press, 2019.

[94] COREY, A. T. "The Interrelation Between Gas and Oil Relative Permeabilities", *Producers Monthly*, v. 19, n. 1, pp. 38–41, 1954.

[95] EATON, B. A., KNOWLES, C. R., SILBERBRG, I. "The Prediction of Flow Patterns, Liquid Holdup and Pressure Losses Occurring during Continuous Two-Phase Flow in Horizontal Pipelines", *Journal of Petroleum Technology*, v. 19, n. 06, pp. 815–828, 1967.

[96] HAGEDORN, A. R., BROWN, K. E. "Experimental Study of Pressure Gradients Occurring during Continuous Two-Phase Flow in Small-Diameter Vertical Conduits", *Journal of Petroleum Technology*, v. 17, n. 04, pp. 475–484, 1965.

[97] ARYA, A., GOULD, T. L. "Comparison of Two Phase Liquid Holdup and Pressure Drop Correlations Across Flow Regime Boundaries for Horizontal and Inclined Pipes". In: *SPE Annual Technical Conference and Exhibition*. Society of Petroleum Engineers, 1981.

[98] MEKISSO, H. M. *Comparison of Frictional Pressure Drop Correlations for Isothermal Two-Phase Horizontal Flow*. Tese de Mestrado, Oklahoma State University, Stillwater, OK, USA, 2013.

[99] AHMED, M. M., AYOUB, M. A. "A Comprehensive Study on the Current Pressure Drop Calculation in Multiphase Vertical Wells: Current Trends and Future Prospective", *Journal of Applied Sciences*, v. 23, n. 14, pp. 3162–3171, 2014.

[100] YAHAYA, A. U., AL GAHTANI, A., OTHERS. "A Comparative Study Between Empirical Correlations and Mechanistic Models of Vertical Multiphase Flow". In: *SPE/DGS Saudi Arabia Section Technical Symposium and Exhibition*. Society of Petroleum Engineers, 2010.

[101] DUNS JR, H., ROS, N. "Vertical Flow of Gas and Liquid Mixtures in Wells". In: *6th World Petroleum Congress*. World Petroleum Congress, 1963.

[102] ORKISZEWSKI, J., OTHERS. "Predicting Two-Phase Pressure Drops in Vertical Pipe", *Journal of Petroleum Technology*, v. 19, n. 06, pp. 829–838, 1967.

[103] AZIZ, K., GOVIER, G. W. "Pressure Drop in Wells Producing Oil and Gas", *Journal of Canadian Petroleum Technology*, v. 11, n. 03, pp. 38–48, 1972.

[104] BEGGS, D. H., BRILL, J. P. "A Study of Two-Phase Flow in Inclined Pipes", *Journal of Petroleum Technology*, v. 25, n. 05, pp. 607–617, 1973.

[105] HASAN, A. R., KABIR, C. S. "A Study of Multiphase Flow Behavior in Vertical Wells", *SPE Production Engineering*, v. 3, n. 02, pp. 263–272, 1988.

[106] ANSARI, A., SYLVESTER, N., SHOHAM, O., et al. "A Comprehensive Mechanistic Model for Upward Two-Phase Flow in Wellbores". In: *SPE Annual Technical Conference and Exhibition*. Society of Petroleum Engineers, 1990.

[107] GOMEZ, L., SHOHAM, O., SCHMIDT, Z., et al. "Unified Mechanistic Model for Steady-State Two-Phase Flow: Horizontal to Vertical Upward Flow", *SPE Journal*, v. 5, n. 03, pp. 339–350, 2000.

[108] ALVES, I., ALHANATI, F., SHOHAM, O. "A Unified Model for Predicting Flowing Temperature Distribution in Wellbores and Pipelines", *SPE Production Engineering*, v. 7, n. 04, pp. 363–367, 1992.

[109] VOGEL, J. "Inflow Performance Relationships for Solution-Gas Drive Wells", *Journal of Petroleum Technology*, v. 20, n. 01, pp. 83–92, 1968.

[110] BROWN, K. E. "Technology of Artificial Lift Methods. Volume 1. Inflow Performance, Multiphase Flow in Pipes, the Flowing Well", 1977.

[111] PEACEMAN, D. W. "Interpretation of Well-Block Pressures in Numerical Reservoir Simulation", *Society of Petroleum Engineers Journal*, v. 18, n. 03, pp. 183–194, 1978.

[112] SCHLUMBERGER. *The OLGA User Manual*. 2015.

[113] CALSEP. *Method Documentation, PVTsim 20*.

[114] EQUINOR. *Tordis Field*. https://www.norskpetroleum.no/en/facts/field/tordis, 2019.

[115] VAZQUEZ, M., BEGGS, H. D. "Correlations for Fluid Physical Property Prediction". In: *SPE Annual Fall Technical Conference and Exhibition*. Society of Petroleum Engineers, 1977.

[116] BEGGS, H. D., ROBINSON, J. R. "Estimating the Viscosity of Crude Oil Systems", *Journal of Petroleum Technology*, v. 27, n. 09, pp. 1140–1141, 1975.

[117] CAMPBELL, J. M. *Gas Conditioning and Processing, Volume 1: The Basic Principles*, v. 1. Campbell Petroleum Series, 1992.

[118] LEE, A. L., GONZALEZ, M. H., EAKIN, B. E. "The Viscosity of Natural Gases", *Journal of Petroleum Technology*, v. 18, n. 08, pp. 997–1000, 1966.

[119] BRILL, J. P., MUKHERJEE, H. K. *Multiphase Flow in Wells*, v. 17. Society of Petroleum Engineers, 1999.

[120] IHS MARKIT. *Que$tor*. https://ihsmarkit.com/products/questor-oil-gas-project-cost-estimation-software.html, 2018.

Appendix A

Black Oil Correlations

A.1 Bubble point pressure

The bubble point pressure calculation used in the thesis adopted the correlation proposed in [115].

$$P_b = \left[\frac{1}{a_1}\frac{RGOR}{\gamma_{gs}}\exp\left(\frac{-a_3 \cdot \gamma_{API}}{T+460}\right)\right]^{1/a_2} \tag{A.1}$$

where, $RGOR$ is the maximum solution gas oil ratio and γ_{API} is oil API gravity. γ_{gs} represents gas gravity (air = 1) that would result from a separator condition of 100 psig, which can be calculated as:

$$\gamma_{gs} = \gamma_g|_{P_{\text{sep}},T_{\text{sep}}}\left[1 + 5.912 \times 10^{-5} \cdot \gamma_{API} \cdot T_{\text{sep}} \cdot \log\frac{P_{\text{sep}}}{114.7}\right] \tag{A.2}$$

$\gamma_g|_{P_{\text{sep}},T_{\text{sep}}}$ represents gas gravity obtained at a separator condition of pressure P_{sep} and temperature T_{sep}. Values for the coefficients in Eq. A.1 are listed in Table A.1.

Table A.1: Coefficients in Eq. A.1

Coefficient	$\gamma_{API} \leq 30$	$\gamma_{API} > 30$
a_1	0.0362	0.0178
a_2	1.0937	1.187
a_3	25.724	23.931

A.2 Solution gas oil ratio

Solution gas oil ratio under $P < P_b$ is calculated by rearranging Eq. A.1:

$$R_s = a_1\gamma_{gs}P^{a_2}\exp\left(\frac{a_3\gamma_{API}}{T+460}\right) \tag{A.3}$$

And for $P \geq P_b$,

$$R_s = RGOR \tag{A.4}$$

A.3 Oil formation volume factor

For $P < P_b$, oil formation volume factor B_o is calculated by

$$B_\mathrm{o} = 1 + b_1 R_s + b_2(T-60)\gamma_{API} + b_3 R_s(T-60)\gamma_{API}/\gamma_{gs} \tag{A.5}$$

Values for the coefficients in Eq. A.5 are listed in Table A.2.

Table A.2: Coefficients in Eq. A.5

Coefficient	$\gamma_{API} \leq 30$	$\gamma_{API} > 30$
b_1	4.677×10^{-4}	4.67×10^{-4}
b_2	1.751×10^{-5}	1.1×10^{-5}
b_3	-1.811×10^{-8}	1.337×10^{-9}

For $P \geq P_b$, oil formation volume factor is calculated based on oil compressibility. The oil compressibility is defined as:

$$c_\mathrm{o} = -\frac{1}{V}\frac{\partial V}{\partial P} = -\frac{1}{B_\mathrm{o}}\frac{\partial B_\mathrm{o}}{\partial P} \tag{A.6}$$

The correlation for c_o is

$$c_\mathrm{o} = 10^{-5} \times (-1433 + 5R_s + 17.2T - 1180\gamma_{gs} + 12.61\gamma_{API})/P \tag{A.7}$$

Therefore, B_o of undersaturated crude oil is calculated by:

$$B_\mathrm{o} = B_{ob} \exp\left[c_\mathrm{o}(P_b - P)\right] \tag{A.8}$$

where, B_{ob} is the oil formation volume factor at bubble point pressure.

A.4 Oil density

Oil density is calculated based on material balance, which follows:

$$\rho_\mathrm{o} = (\rho_{ost} + R_s\rho_{\mathrm{g}st})/B_\mathrm{o} \tag{A.9}$$

where, ρ_{ost} and $\rho_{\mathrm{g}st}$ are oil and gas density at standard condition (1.01bar, 15°C), respectively.

A.5 Oil viscosity

For $P < P_b$, live oil viscosity is calculated by Beggs-Robinson correlation [116]:

$$\mu_{\mathrm{o}} = A\mu_{oD}^{B} \tag{A.10}$$

$$A = 10.715(R_s + 100)^{-0.515} \tag{A.11}$$

$$B = 5.44(R_s + 150)^{-0.338} \tag{A.12}$$

μ_{oD}, the dead oil viscosity, is calculated by

$$\log\log(\mu_{oD} + 1) = 3.0324 - 0.02023\gamma_{API} - 1.163\log T \tag{A.13}$$

For $P \geq P_b$, Vazquez et al. [115] developed the following correlation,

$$\mu_{\mathrm{o}} = \mu_{ob}(P/P_b)^{C} \tag{A.14}$$

where, μ_{ob} is oil viscosity under bubble point pressure and C is calculated by

$$C = 2.6P^{1.187}\exp(-11.513 - 8.98 \times 10^{-5}P) \tag{A.15}$$

A.6 Oil specific heat

Oil specific heat is calculated by [117]:

$$c_{p\mathrm{o}} = 2.96 - 1.34\gamma_{\mathrm{o}} + (0.0062 - 0.00234\gamma_{\mathrm{o}})T \tag{A.16}$$

where γ_{o} is the specific gravity of oil (water = 1).

A.7 Gas density

Gas density is calculated by equation of state

$$\rho_{\mathrm{g}} = \frac{M_{\mathrm{g}}P}{ZRT} \tag{A.17}$$

where, $M_{\mathrm{g}} = 28.97\gamma_{\mathrm{g}}$, is gas molecular weight, γ_{g} is gas specific gravity, R is gas constant, and Z is gas compressibility factor, which can be calculated as follows based on the theorem of corresponding states.

$$Z = \frac{0.06125P_{pr} \cdot t \cdot \exp[-1.2(1-t)^2]}{y} \tag{A.18}$$

where, y is the solution of the following equation:

$$0 = -0.06125 P_{pr} \cdot t \cdot \exp[-1.2(1-t)^2] + \frac{y + y^2 + y^3 - y^4}{(1-y)^3} - (14.76t - 9.76t^2 + 4.58t^3)y^2 + (90.7t - 242.2t^2 + 42.4t^3)y^{2.18+2.82t} \tag{A.19}$$

Relative pressure and temperature are defined as

$$P_{pr} = \frac{P}{P_{pc}} \qquad T_{pr} = \frac{T}{T_{pc}} = \frac{1}{t} \tag{A.20}$$

where, critical pressure and temperature are calculated as:

$$P_{pc} = 756.8 - 131\gamma_{\mathrm{g}} - 3.6\gamma_{\mathrm{g}}^2 \tag{A.21}$$

$$T_{pc} = 169.2 + 349.5\gamma_{\mathrm{g}} - 74\gamma_{\mathrm{g}}^2 \tag{A.22}$$

A.8 Gas viscosity

Gas viscosity is calculated by the correlation developed by LEE *et al.* [118].

$$\mu_g = D \exp(E\rho_{\mathrm{g}}^F) \tag{A.23}$$

$$D = \frac{(9.379 + 0.01607 M_{\mathrm{g}})T^{1.5}}{209.2 + 19.26 M_{\mathrm{g}} + T} \times 10^{-4} \tag{A.24}$$

$$E = 3.448 + 986.6/T + 0.01009 M_{\mathrm{g}} \tag{A.25}$$

$$F = 2.447 - 0.2224E \tag{A.26}$$

A.9 Gas formation volume factor

Gas formation volume factor B_{g} is calculated by

$$B_{\mathrm{g}} = \rho_{\mathrm{g}}/\rho_{gst} \tag{A.27}$$

A.10 Surface tension

Surface tension is calculated by pure empirical correlation [119]:

$$\sigma_{oD} = 39.2\,(1 - \gamma_{API}/148) - 0.0438(T - 68) \tag{A.28}$$

For different pressure, the surface tension is further corrected by:

$$\sigma = \sigma_{oD} \exp(-0.0007307P) \tag{A.29}$$

Appendix B

Economics model

NPV is one of the most important economic indicators for evaluating the profitability of a project. It is calculated as

$$NPV = \sum_{t} \frac{CF_t}{(1+r)^{t-1}} \tag{B.1}$$

where, cash flow is formulated without tax:

$$CF_t = RE_t - CP_t - OP_t - RO_t \tag{B.2}$$

Revenue comes at the end of each month and is discounted by the effective monthly discount rate to represent the equivalent revenue at the beginning of each year t:

$$RE_t = \sum_{n=12(t-1)+1}^{12t} \frac{30 C_{\text{oil}} Q_t (1+R_{\text{inflation}})^n}{12(1+r)^{[n-12(t-1)]/12}} \tag{B.3}$$

Capital expenditure for each year includes the investment on FPSO, drilling, pipelines and risers, manifolds and subsea separators, if applicable. It is assumed that the construction of the subsea architecture lasts for three years before the first oil and the total capital expenditure is evenly distributed in these three years. The expenditure on subsea separator is included for the specific year that it is introduced.

$$CP = C_{\text{fpso}} N_{\text{fpso}} + C_{\text{s}} N_{\text{s}} + C_{\text{m}} N_{\text{m}} + C_{\text{well}} L_{\text{well}} + C_{\text{pipe}} L_{\text{pipe}} \tag{B.4}$$

FPSO price is modeled as a linear function of FPSO capacities:

$$C_{\text{fpso}} = aQ_{\max} + bW_{\max} + cWI_{\max} + d \tag{B.5}$$

where, $Q_{\max}$, $W_{\max}$ and $WI_{\max}$ represent maximum oil production, water production, and water injection rates on the FPSO, respectively.

Similarly, the price for a subsea separator is modeled as a linear function of water separation capacity $WS_{\max}$:

$$C_{\mathrm{s}} = eWS_{\max} \tag{B.6}$$

Operating expenditure is modeled by a fixed part related to the number of wells, FPSOs and subsea separators on site and a variable part related to production, water separation and injection rates. Opex is viewed as an equivalent investment at the beginning of year t:

$$OP_t = O_{\mathrm{fpso}} + O_{\mathrm{well}} + O_{\mathrm{s}} + O_{\mathrm{op}} \cdot Q_t + O_{\mathrm{wp}} \cdot W_t + O_{\mathrm{ws}} \cdot WS_t + O_{\mathrm{wi}} \cdot WI_t \tag{B.7}$$

where, Q_t, W_t, WS_t, and WI_t are the oil production rate, water production rate, subsea water separation rate and water injection rate in year t, respectively.

Royalty is a fixed fraction of revenue and should be paid monthly. Therefore, royalty is directly calculated:

$$RO_t = RE_t \cdot R_{\mathrm{royalty}} \tag{B.8}$$

Economic parameters used in the study are as listed in Table B.1 to B.4, based on the built-in procurement repository in software Que$tor [120]. An example of the cash flow calculation by this economic model is shown in Figure B.1.

Table B.1: Economic parameters

parameter	value	unit	description
r	0.1	–	discount rate
$R_{\mathrm{inflation}}$	0.0025	–	monthly inflation rate
R_{royalty}	0.1	–	royalty rate
C_{oil}	50	\$/bbl	base oil price
a	1120	\$/bbl	coefficient for FPSO oil capacity
b	229	\$/bbl	coefficient for FPSO water capacity
c	229	\$/bbl	coefficient for FPSO injection capacity
d	700	\$ million	base FPSO tanker price
e	1000	\$/bbl	coefficient for subsea separator capacity
O_{op}	1	\$/bbl	opex on unit oil production
O_{wp}	3	\$/bbl	opex on unit water production
O_{ws}	1	\$/bbl	opex on unit subsea separation
O_{wi}	1	\$/bbl	opex on unit water injection
O_{fpso}	50	\$ million/year	fixed opex on FPSOs
O_{well}	3	\$ million/year	fixed opex on wells
O_{s}	2	\$ million/year	fixed opex on subsea separators

Table B.2: Pipeline cost C_{pipe}

diameter, inch	price, $ million/km
4	2.0
5	2.3
8	3.0
10	3.5

Table B.3: Manifold cost C_{m}

number of slots	price, $ million
4	2.5
6	2.9
8	3.3

Table B.4: Drilling cost C_{well}

well type	cost, $ million/km
vertical	10
deviated	16

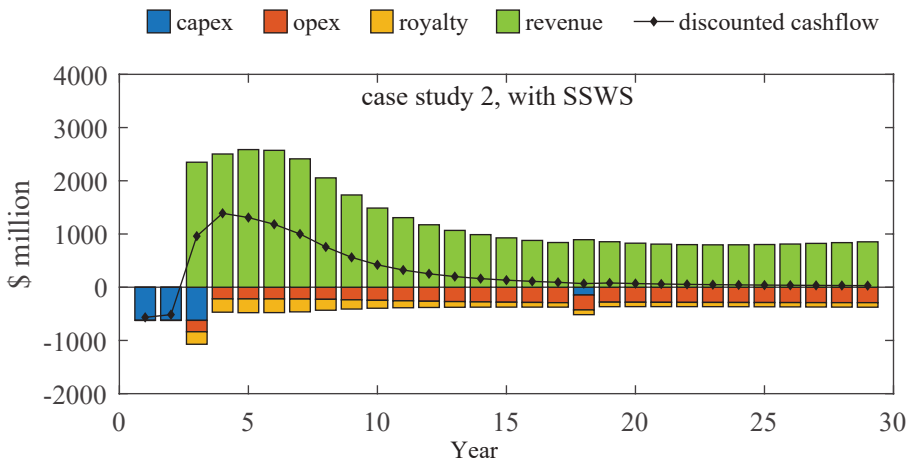

Figure B.1: Cashflow of case study 2, with subsea water separation.

Appendix C

Statistics

Information on the modeling statistics for each case study presented in chapter 6 is summarized below for direct comparison.

Table C.1: Statistics for the numerical models in the studied cases

	case study 1		case study 2		case study 3	
apply SSWS or not	N	Y	N	Y	N	Y
number of network paths	7	9	15	17	22	26
number of network nodes	8	10	16	18	23	27
number of segments	359	373	1021	1032	1799	1968
number of augmented nodes	366	382	1036	1049	1821	1994
number of injectors	–	–	6	6	6	6
number of producers	5	5	11	11	11	11
number of manifolds	1	1	2	2	0	0
number of separators	0	1	0	1	0	2
number of production risers	1	1	2	2	11	11
number of reservoirs	2	2	1	1	1	1
number of reservoir nodes	0	0	22044	22044	22044	22044
number of reservoir cells	2	2	17250	17250	17250	17250
number of timesteps	360	360	54	54	54	54
timestep length, days	30	30	180	180	180	180
convergence tolerance	1E-04	1E-04	1E-04	1E-04	1E-04	1E-04
total CPU time, min	15.7	9.5	23.0	24.2	27.6	26.9
average number of iterations per timestep	8	7.8	9.6	10.1	11.5	11.8

Notes: All the simulations performed with Inter®Core™i7-4790 (3.6 GHz). The total CPU time is the sum of the computational time needed to solve the nonlinear equations in each timestep.